

UCSF

UC San Francisco Electronic Theses and Dissertations

Title

Molecular Mechanisms Governing Synaptic Strength at Hippocampal Synapses

Permalink

<https://escholarship.org/uc/item/5xt3045w>

Author

Adesnik, Hillel

Publication Date

2007-08-09

Peer reviewed|Thesis/dissertation

Molecular Mechanisms Governing Synaptic Strength at Hippocampal Synapses

by

Hillel Adesnik

DISSERTATION

Submitted in partial satisfaction of the requirements for the degree of

DOCTOR OF PHILOSOPHY

in

Neuroscience

in the

GRADUATE DIVISION

of the

*To my uncle Philip, a doctor himself, who
tirelessly pursued knowledge and the well-being of others*

Acknowledgements

I would not have become a scientist if it were not for my mother and father – both on material and intellectual grounds. As early as I can remember, my father has explained the natural universe to me in detailed scientific terms, particularly the hidden world of molecular biology. Although a description of, say, the invention of the polyacrylamide gel, was a bit over the head of a nine year old, I usually listened in awe of such wonders of modern science. Now I have the joy of explaining to my father the subtleties of neuroscience while he listens, hopefully, in rapt attention as well. My mother, likewise, in her own tireless pursuit of knowledge, has been a particular inspiration to me. Her never-ending journey into the intricacies of Jewish law, and her very recent ordination as a Rabbi has highlighted to me that the process one is in as a learner is never over. I take from this that my graduate education is merely a beginning. Now if a love of knowledge were all my parents had given me, it would have been enough. But their true driving force, and one that they have indelibly instilled in me is that an intellectual contribution is not sufficient. Rather, we must also make some measurable, definite contribution to the advancement of our society and local community. This I hope to maintain as a real goal and motivation for the future.

In my graduate career and in becoming a true scientist I owe much of the rest to my graduate advisor and mentor, Roger Nicoll. His infectious passion for biology and insatiable hunger to query the wonders of neural function would have been enough to keep me going during this Ph.D., but his equal delight in the proper training of a graduate student is really what made working in his lab so invaluable. Roger's door was always open, and I usually felt it that was not a satisfying day if I did not have the chance to

discuss data, a publication, or some finer point of the history of neurophysiology, at length, in his office. Working for and with Roger will no doubt leave a permanent imprint on how I think and do science. I will probably always measure any of my future work against how it could have been done in Roger's lab, but I know that even when I am long gone from here he will still gladly take the time to discuss my newest findings.

Working in Roger's lab would not have been nearly as fun and exciting were it not for the many colleagues with which I constantly shared new ideas, commiserated with about failed experiments, and ceaselessly discussed the functioning of the synapse and the brain. My initial training in the actual workings of neurophysiology I owe largely to the matchless Kaiwen Kam. From the beginning Kaiwen, in his unsurpassed patience, helped me through the trying times of learning the hands-on part of electrophysiology, and in his equally unmatched knowledge and intellect he imparted to me a solid understanding of generally how to conceive of and conduct scientific experiments. The three post-docs who were present when I started, Kim Moore, Valentin Stein, and Nathalie Rouache were also indispensable sources of help and answers. Later Tasso Tzingounis, with his encyclopedic knowledge, and Sandip Panicker, with his experience and unending excitement, were unrivaled sounding boards for ideas and sources of inspiration. Recently, Wei Lu and Camille Belone have added a new element of fun to the lab, each with their own unique brand of passion and determination in the pursuit of secrets of synaptic function and plasticity. My colleagues in this Ph.D. program, Karen Menuz, Guillermo Elias, and Aaron Milstein have all been essential sources of ideas and discussion throughout my Ph.D. Of course, the expert technical help provided by David

House, Keith Brown, and now, Pierre Apostolides not only eased the burden, but their assistance even came often with an interest in what I was doing.

I owe an incalculable amount to my collaborators throughout my graduate career. As they were all experts in techniques or fields in which I was rather naïve, I learned a great deal from my interaction with them. I spent much time with David Bredt, Susumu Tomita, Masaki and Yuko Fukata, Pamela England, James Chambers, and more recently, Grant Li. Our collaborations were much more than a marriage of convenience, as we all gained by seeing how we each approached scientific questions differently, but with the common goal of seeing a line of experiments to the finish.

Throughout my graduate training I owe a significant debt to my thesis committee, Grae Davis, David Copenhagen, and David Julius. They have always listened to me explain my recent findings with great interest, and have frequently suggested important experiments and given advice on how to proceed with a line of work. I owe my first cellular physiology experience to work I conducted in Grae's lab as a rotation student, and it was there that I fell in love with the electrical currents generating all our thoughts and movements. I also must thank by external committee member, Robert Malenka, for inspiration in his work and his passion towards science.

Graduate school, as a whole, wouldn't have been a fraction of the fun were it not for the many great friends I found in my classmates – many with whom I'm sure I will be discussing both science, and other things, for many years to come. I must also thank my two brothers; my older brother, Ariel, and my twin brother, Moshe. Both have been potent forces in my intellectual growth from the get-go, whether discussing politics, science, music, or really anything that came to mind. Finally, no doubt I owe a particular

debt to my girlfriend Helen, who has been with me for the majority of this Ph.D., and has always supported me in my work and has been a constant source of inspiration.

Contributions

The work in Chapters 2, 3, 4, 5, and 7 were conducted in collaboration with other authors.

The initial idea of a photo-activatable antagonist of AMPA receptors, as described in Chapter 3, was conceived of by Pamela England. The antagonist was designed and synthesized by Pamela England and James Chambers. Hillel Adesnik collected all the data. Reprinted with permission from Adesnik et al (2005).

The data presented in Chapter 4 was largely collected by Susumu Tomita, with contributions by Masayuki Sekiguchi from Keiji Wada's laboratory, and Wei Zhang from James Howe's laboratory. Specifically, Susumu Tomita began the project, constructed all plasmids, and performed all the initial experiments with stargazin and stargazin chimeras in oocytes. Masayuki Sekiguchi performed the fast-application of glutamate experiments to oocytes patches, and Wei Zhang conducted the fast-application and single-channel recording experiments on HEK cells. Hillel Adesnik performed all electrophysiological experiments on neurons as well as some of the preliminary experiments on HEK cells. Reprinted with permission from Tomita et al (2005).

The data presented in Chapter 7 was largely collected by Masaki and Yuko Fukata. Masaki and Yuko Fukata conceived of the study, and performed all the biochemistry, cloning of Lgi1 and ADAM22, histology in brain slices, constructed all plasmids, and purified all protein reagents. Hillel Adesnik performed all electrophysiological experiments on neurons. Reprinted with permission from Fukata et al (2006).

Abstract

The speed and reliability of computation in neural circuits depends on fast chemical transmission between neurons in the brain. Excitatory transmission in the central nervous system relies on the activity-dependent release of glutamate onto ionotropic receptors clustered at the postsynaptic membrane. AMPA receptors mediate the majority of synaptic communication in the mature central nervous system, but NMDA receptors play a critical role under conditions of strong or correlated activity. The precise mechanisms governing the number and subtype of AMPA receptor at synapses are essential for the proper regulation of synaptic strength. Recent work has identified many neuronal proteins involved in the trafficking and scaffolding of AMPA receptors at synaptic sites and has begun to clarify how these proteins interact to support excitatory synaptic transmission, though several fundamental questions remain.

To assess directly the trafficking of AMPA receptors in real time, we used a novel, photo-activatable, irreversible AMPA receptor antagonist. Inactivation of surface receptors reveals that AMPA receptors cycle rapidly between an intracellular domain and the extrasynaptic somatic membrane. The total surface pool at synaptic sites is exchanged with intracellular receptors every 18 hours. Following insertion to the extrasynaptic domain, AMPA receptors can also move laterally within the plasma membrane where they can ultimately stabilize at postsynaptic densities.

Trafficking of AMPA receptors to the neural surface requires isoforms of the protein stargazin. Stargazin controls AMPA receptor trafficking by an interaction involving its intracellular c-terminus. Surprisingly, stargazin also modulates AMPA receptor gating through its first extracellular domain, which acts to stabilize the open

state of the AMPA receptor channel. Overexpression of a stargazin with a mutated first extracellular domain reduces charge movement during transmission by accelerating the decay of postsynaptic quantal events. This suggests that stargazin acts as an AMPA receptor auxiliary subunit and is necessary for the normal function of AMPA receptors during ongoing synaptic transmission.

Stargazin recruits AMPA receptors to synapses by its interaction with the postsynaptic scaffolding protein, PSD-95. Through an additional interaction, PSD-95 binds to the transmembrane protein ADAM22, which forms a receptor/ligand complex with the secreted factor Lgi1. Binding of Lgi1 to ADAM22 results in an increase in AMPA-receptor mediated synaptic transmission. This newly identified signaling complex may represent an alternate pathway of AMPA receptor recruitment to synapses.

Long-term potentiation (LTP) at the CA3 to CA1 synapse is thought to rely on the rapid insertion of AMPA receptors into the synaptic membrane following strong NMDA receptor activation. However, LTP does not involve the insertion of calcium permeable AMPA receptors that lack the GluR2 subunit, nor does LTP require ongoing activity to be maintained.

LTP-like processes are believed to play a major role in wiring neural circuitry during development by recruiting AMPA receptors to nascent synapses allowing them to sense glutamate. Although LTP is critically dependent on activation of the NMDA receptor, deletion of the essential NMDA subunit, NR1, in pyramidal neurons results in a net increase in AMPA-receptor mediated transmission. When the deletion occurs embryonically, synapses form in normal number but exhibit increased quantal strength. When NR1 is deleted postnatally in organotypic culture, synapses exhibit normal quantal

strength, but increase dramatically in number. Reintroduction of NR1 to the knockout results in a net loss of synapse number. Thus NMDA receptor activity limits rather than promotes synaptic maturation during brain ontogeny.

Table of Contents

Acknowledgements	iii
Contributions.....	vii
Abstract.....	viii
List of figures.....	xiv
<u>CHAPTER 1: General Introduction</u>	<u>1</u>
Glutamate receptors mediate excitatory transmission in the central nervous system...2	
Proteins involved in the trafficking of AMPA receptors to synapses.....4	
Biophysical determinants of AMPA receptor gating.....6	
AMPA receptor cycling in transmission and plasticity7	
Synaptic plasticity at the hippocampal Schaeffer-Collateral synapse8	
Role of NMDA receptors in synaptic maturation.....11	
<u>CHAPTER 2: Methods</u>	<u>13</u>
Primary hippocampal cell culture	14
Primary culture electrophysiology.....	14
Photoactivation of light-activated molecules.....	15
Oocyte electrophysiology	17
Chemiluminescence Assays.....	17
Glutamate fast application	17
Organotypic slice electrophysiology.....	18
Single channel recording.....	19
Acute hippocampal slice electrophysiology	21
Antibodies.....	23
Cloning an plasmid construction	23
Cell surface binding assay	25

Immunofluorescence analysis of hippocampal neuron culture.....	25
Preparation of AP fusions	26
Immunohistochemistry	27
Generation of conditional NR1 knockouts	27
Biolistic transfection of mouse slice culture.....	28
<u>CHAPTER 3: Photo-inactivation of native AMPA receptors reveals their real time</u>	
<u>trafficking</u>	<u>29</u>
Introduction.....	30
Results	32
Discussion	38
Supplemental discussion.....	44
<u>CHAPTER 4: Stargazin modulates AMPA receptors gating and trafficking by distinct</u>	
<u>domains</u>	<u>66</u>
Introduction.....	67
Results	68
Discussion	75
<u>CHAPTER 5: Epilepsy-related ligand/receptor complex Lgi1 and ADAM22 regulates</u>	
<u>synaptic transmission</u>	<u>98</u>
Introduction.....	99
Results	99
Discussion	105
<u>CHAPTER 6: Conservation of GluR2-containing AMPA receptors during long-term</u>	
<u>potentiation</u>	<u>133</u>

Introduction.....	134
Results	135
Discussion.....	140
<u>CHAPTER 7: NMDA receptor activity limits synaptic strength and number during brain development</u>	<u>153</u>
Introduction.....	154
Results	157
Discussion.....	164
<u>CHAPTER 8: General Conclusions</u>	<u>187</u>
<u>CHAPTER 9: References</u>	<u>196</u>

List of Figures

CHAPTER 3

- Figure 1. ANQX is a photoreactive, specific, irreversible inhibitor of native, surface-exposed AMPA receptors49
- Figure 2. Synaptic AMPA receptors do not rapidly cycle with an intracellular pool of receptors on the timescale of minutes.....51
- Figure 3. Synaptic AMPA receptors cycle with an intracellular pool of receptors on the timescale of hours53
- Figure 4. Extrasynaptic AMPA receptor currents initially recover more quickly than synaptic currents from photoinactivation. Cycling of AMPA receptors is independent of protein synthesis55
- Figure 5. Somatic AMPA receptors rapidly cycle with an intracellular pool of receptors on the timescale of minutes57
- Figure 6. Somatic AMPA receptors laterally diffuse on the surface of the neuron on the timescale of seconds.....59
- Figure 7. A model of basal AMPA receptor trafficking.....61
- Figure S1. Following inactivation with ANQX, AMPA receptor-mediated mEPSCs are reduced in amplitude and in frequency and do not rapidly recover..63
- Figure S2. Representative mEPSC traces, recorded in 100 μ M cyclothiazide, at different time points after ANQX-mediated photoinactivation of total surface AMPA receptors.....65

CHAPTER 4

- Figure 1. Stargazin enhances glutamate-evoked currents from oocytes injected with limiting amounts of GluR180
- Figure 2. Stargazin not only mediates AMPA receptor trafficking, but also modulates AMPA receptor agonist efficacy82

Figure 3.	Stargazin regulates AMPA receptor trafficking and agonist efficacy by distinct mechanisms	84
Figure 4.	Stargazin slows AMPA receptor desensitization and deactivation.....	86
Figure 5.	Stargazin modulates AMPA receptor single-channel properties	88
Figure 6.	Stargazin regulates AMPA receptor gating during transmission.....	91
Figure S1.	Stargazin does not change the I-V relationship for homomeric GluR1 flip (GluR1i) or heteromeric (GluR1i/GluR2i) AMPA receptors.....	93
Figure S2.	Overexpression of wild-type stargazin does not affect the decay kinetics or amplitude of hippocampal mEPSCs	95
Figure S3.	The ectodomain of stargazin is necessary to properly restore the time course and amplitude of synaptic currents in stg (-/-) cerebellar granules cells	97

CHAPTER 5

Figure 1.	Identification of a PSD-95-associated protein complex containing ADAM22 and LGI1	108
Figure 2.	Tripartite complex formation of PSD-95, ADAM22, and LGI1	110
Figure 3.	ADAM22 is a neuronal receptor for secreted LGI1	112
Figure 4.	LGI1 selectively enhances AMPAR-mediated synaptic currents.....	114
Figure S1.	PSD-95 and Lgi1 co-immunoprecipitate with ADAM22	116
Figure S2.	Developmental change and regional distribution of the PSD-95 precipitates	188
Figure S3.	ADAM22 and stargazin bind different PDZ domains on PSD-95	120
Figure S4.	Lgi1 is secreted as an oligomer from transfected HEK293 cells and binds to ADAM22.....	122
Figure S5.	Specific interaction of Lgi1 with ADAM subfamily on the cell surface	124
Figure S6.	Interaction of ADAM22 and Lgi1 in brain is stoichiometric and constitutive.....	126
Figure S7.	ADAM22 is a neuronal receptor for Lgi1 in brain	128

Figure S8. Lgi1 increases AMPA receptors surfaces expression in hippocampal neurons.....	130
Figure S9. Lgi1 regulates AMPA receptor-mediated synaptic transmission	132

CHAPTER 6

Figure 1. LTP is not associated with a change in the rectification of synaptic AMPAR currents	144
Figure 2. LTP does not involve the recruitment of calcium-permeable AMPA receptors even in the first few minutes after induction.....	146
Figure 3. Philanthotoxin 433 does not block synaptic currents after LTP	148
Figure 4. LTP does not require activity to be maintained	150
Figure S1. Philanthotoxin antagonizes synaptic NMDARs, GluR2-lacking receptors on outside out patches from GluR2 ^{-/-} cells, and native GluR2-lacking receptors on cerebellar Bergmann Glial cells	152

CHAPTER 7

Figure 1. Embryonic deletion of NR1 in NEX-CRE;NR1 ^{fl/fl} mice does not impede the functional maturation of synapses in CA1	168
Figure 2. Mosaic deletion of NR1 in organotypic slice culture increases AMPA receptor-mediated synaptic transmission by large increase in synapse number	170
Figure 3. Incubating slice cultures in an NMDA receptor antagonist cocktail occludes the effect of CRE-mediated NR1 deletion	172
Figure 4. Reintroduction of NR1 to slice cultures from NEX-CRE;NR1 ^{fl/fl} mice drives a net loss in synapse number	174
Figure S1. LTP and heterosynaptic LTD are absent from NEX-CRE:NR1 ^{fl/fl} mice.....	176
Figure S2. Effects of NR1 deletion in forebrain interneurons in Dlx5/6-CRE; NR1 ^{fl/fl} mice	178

Figure S3. CRE-expression in slice cultures from wild-type NR1^{+/+} mice does not affect AMPA or NMDA EPSCs180

Figure S4. Molecular replacement of native NMDA receptors with those containing the pore mutant NR1(R).....182

Figure S5. Normal AMPA receptor-mediated synaptic transmission in T29.1-CRE:NR1^{fl/fl} mice184

Figure S6. Acute blockade of NMDA receptors in hippocampal slices does not rapidly affect quantal strength or synapse number186

Chapter 1
General Introduction

In central excitatory pathways action potentials invading axon terminals drive the release of the amino acid glutamate. Within a millisecond following the presynaptic nerve impulse a bolus of glutamate fills the synaptic cleft and binds to glutamate receptors on the postsynaptic cell. Several types of ionotropic glutamate receptors are clustered at or near postsynaptic sites, including the AMPA, NMDA and Kainate types. Though activity through NMDA receptors can rapidly trigger synaptic plasticity, the majority of transmission is mediated by AMPA receptors. The number and gating properties of synaptic AMPA receptors primarily determine the time-course and amplitude of the postsynaptic response to a fixed amount of neurotransmitter. Accumulating evidence suggests that activity-driven regulation of synaptic AMPA receptor density and channel properties following activation of NMDA receptors underlies rapid changes in synaptic strength necessary for the functional wiring of neural circuits during learning and brain development. Here I present data characterizing the process of AMPA receptor trafficking to the surface and synapses of neurons under basal activity and following the induction of synaptic plasticity.

Glutamate receptors mediate excitatory transmission in the central nervous system

Though much of our understanding of fast chemical transmission derives from exploration of the neuromuscular synapse that uses acetylcholine as a transmitter, most excitatory transmission at central synapses in vertebrates relies on the amino acid glutamate. Initially, subtypes of glutamate receptors in neurons were discriminated based upon specific agonists. This analysis suggested three types of ionotropic glutamate receptors: those most sensitive to Kainate, AMPA, and NMDA (Jahr and Stevens, 1987;

Watkins and Jane, 2006). Discovery and use of quinoxalinediones as specific antagonists of AMPA/Kainate receptors revealed that most fast glutamate transmission is mediated by AMPA or Kainate receptors, while the NMDA receptor antagonist, D-APV, had little affect on synaptic EPSPs, but could completely block induction of synaptic plasticity (Collingridge et al., 1983; Honore et al., 1988). Our understanding of the molecular architecture of glutamate receptors took a great leap forward with cloning of the various receptor subtypes (Boulter et al., 1990; Hollmann et al., 1989; Planells-Cases et al., 1993). Glutamate receptors were found to be heteromers of subunits specific to each subtype, and the receptor's biophysical properties strongly depended on the subunits making up each channel (Geiger et al., 1995; Verdoorn et al., 1991). Recently, studies on knockout mice of many of the glutamate receptor subunits have generally confirmed the insight gained from heterologous expression of the glutamate receptors in oocytes and in cultured cell lines (Jia et al., 1996; Zamanillo et al., 1999).

Sequence analysis indicates that all ionotropic glutamate receptors are multiple transmembrane domain proteins with a large extracellular N-terminus, a cytoplasmic C-terminus and a reentrant loop between the first and second transmembrane domains that forms the pore of the channel (Gouaux, 2004). Glutamate binds to an interface between the proximal part of the N-terminus and a large extracellular loop between transmembrane domains two and three termed the S1 and S2 domains (Armstrong and Gouaux, 2000a). Functional assays strongly suggests that these receptors are heterotetramers, though a pentameric structure has not been entirely ruled out (Ferrer-Montiel and Montal, 1996; Rosenmund et al., 1998). AMPA receptors are made up of four possible gene products, termed GluR1-4. GluR2 plays a key role in determining

AMPA receptor characteristics by reducing calcium permeability and voltage-dependent block by cytoplasmic polyamines (Verdoorn et al., 1991). These properties of GluR2 rely on the post-transcriptional editing of its mRNA to alter the codon of a pore residue, exchanging a neutral glutamine for a charged arginine (Lomeli et al., 1994). NMDA receptors are composed of the obligatory NR1 subunit and a mix of NR2(A-D) and possibly NR3 subunits (Erreger et al., 2004). NMDA receptors are unique among the iGluR family in requiring the co-agonist glycine to activate the channel, and are also generally blocked by extracellular Mg^{2+} at membrane potentials close to rest (Clements and Westbrook, 1991; Mayer et al., 1984). GluR5-7 and KA1-2 make up Kainate receptors which play particularly important roles at the hippocampal mossy fiber synapse, and at other sites in the forebrain and spinal cord (Lerma, 2006).

Proteins involved in trafficking AMPA receptors to synapses

Following the cloning of the AMPA receptor genes it became possible to systematically identify other gene products that could interact with the receptor using a variety of techniques. Yeast-two hybrid assays, using the c-termini of AMPA receptor subunits detected a group of cytosolic proteins that are co-localized to excitatory synapses such as GRIP/ABP, PICK1, SAP97, NARP, and NSF (Dong et al., 1997; Leonard et al., 1998; O'Brien et al., 1999; Osten and Ziff, 1999; Srivastava et al., 1998; Xia et al., 1999). Overexpression, knockdown, or ablation of some of these genes has been shown to have modest effects on the number of synaptic AMPA receptors, but a

clear model for the actual function of these proteins remains to be described.

Surprisingly, spontaneous mutant mice lacking the four transmembrane domain protein, stargazin, originally considered a calcium channel subunit by sequence analysis, exhibit a complete loss of surface AMPA receptors in cerebellar granule cells (Chen et al., 2000b; Yamazaki et al., 2004). Despite this, over-expression of stargazin has no effect on synaptic AMPA currents. Overexpression of the well-known synaptic protein PSD-95, a member of the MAGUK family of synaptic scaffolds, however, massively potentiates AMPA receptor-mediated transmission (El-Husseini et al., 2000a). PSD-95 binds to stargazin in vitro and expression of a mutant PSD-95 that does not interact with stargazin has no effect on the synaptic AMPA current unless a complementary mutation was introduced to stargazin that allows their interaction (Schnell et al., 2002b). Thus one prevailing model for the trafficking of AMPA receptors to synapses invokes a two-stage process: first, stargazin chaperones AMPA receptors to the extrasynaptic, plasma membrane of neurons; then stargazin binds through its c-terminal PDZ-binding domain to PSD-95 which stably integrates the complex into the postsynaptic density (Armstrong et al., 1998; Bredt and Nicoll, 2003). Both stargazin and PSD-95 are members of a larger family of similar proteins, and the actual targeting mechanism will likely rely on a more complex interaction between TARP isoforms and MAGUK family members. Additionally, many proteins can bind to PSD-95 in vitro, including the NMDA receptor itself, and perhaps secondary interactions between MAGUKs and some of these proteins may influence stargazin-dependent AMPA receptor trafficking to synapses (Kornau et al., 1995).

Biophysical determinants of AMPA receptor gating

Though a complete, high-resolution crystal structure of the AMPA receptor has been elusive, functional and some structural analysis has led to a detailed model of AMPA receptor activation, deactivation, and desensitization. The tetrameric AMPA receptor is likely to exist as a dimer of dimers, with two molecules of glutamate binding to the interface between pairs of ligand-binding domains on opposite-facing subunits (Armstrong et al., 1998). Glutamate binding triggers conformational changes in the receptor that stabilizes an open state of the channel to allow for ion flow (Armstrong and Gouaux, 2000a). At most central synapses glutamate is thought to exist only briefly at high concentrations in the synaptic cleft before it diffuses away and is actively transported out of the synapse region by plasma membrane glutamate transporters located largely on astrocytes (Bergles and Jahr, 1998). Thus channel closure is most often caused by unbinding of glutamate from the receptor, but under conditions of prolonged glutamate exposure, the AMPA receptor can shift into a third conformation where glutamate remains bound, but the channel is closed (Jonas, 2000). The various kinetics of glutamate binding, channel opening, glutamate unbinding, or receptor desensitization depend on the subunits and splice variants of subunits composing the channel (Jonas and Sakmann, 1992). Most notably, all four AMPA receptor subunits come in two alternate splice variants (termed flip and flop) with the difference being a short sequence near the ligand-binding domain (Sommer et al., 1990). The identity of the sequence influences channel gating as studied in heterologous systems, but it is still unclear how these splice variants differentially regulate transmission in distinct neurons in the brain. The precise mechanisms governing the gating of AMPA receptors are crucial to understanding

synaptic transmission, because even slight differences in the kinetics of channel opening or closing can profoundly alter the net amount of charge transferred by a single quantum of glutamate.

AMPA receptor cycling in transmission and plasticity

Data from several studies suggested that AMPA receptors rapidly cycle between surface and internal pools of receptors, akin to the well-characterized cycling of the transferrin receptor (Bredt and Nicoll, 2003). This constant cycling might allow for rapid and precise changes in synaptic AMPA receptor number to fine tune the strength of ongoing synaptic transmission at individual synapses. Evidence for the fast cycling of AMPA receptors stems from three basic lines of research. In biochemical studies, surface receptors can be labeled with biotin, and the endocytosis can be subsequently followed by separating the surface pool from the intracellular pool of receptors by fractionation and immunodetection (Ehlers, 2000). This procedure suggested that surface AMPA receptors cycle rapidly with an internal pool on the timescale of minutes, and that the process depends on neuronal activity. This technique, however, lacks the ability to separate between synaptic and extrasynaptic pools. By dialyzing drugs that interfere with endocytosis and exocytosis into single cells under electrophysiological control, another study suggested that even synaptic AMPA receptors cycle quickly, with up to half of the pool cycling in under half an hour (Luscher et al., 1999). Although this study could conclusively study synaptic AMPA receptors, the drugs are known to have multiple targets and may have resulted in non-specific effects. A third study engineered a cleavable epitope into the extracellular domain of the AMPA receptor, expressed these

tagged receptors in cultured neurons, and quantified exocytosis of new receptors by immunodetection following cleavage of the epitope from all surface receptors (Passafaro et al., 2001). This line of work supported the idea that receptors cycle rapidly, but suffered from the need to overexpress AMPA receptors subunits which is known to alter the normal trafficking of receptors.

The most conclusive studies of ionotropic receptor trafficking have used irreversible antagonists to permanently block receptors on the cell surfaces permitting the direct observation of the insertion of new receptors to the blocked sites. Using the high-affinity irreversible antagonist MK-801, one study demonstrated that NMDA receptors rapidly exchange with extrasynaptic surface receptors but not those from intracellular stores (Tovar and Westbrook, 2002). The same was found for the GABA receptor by the clever use of an altered receptor subunit that was made sensitive to irreversible block by covalent addition of a thiol-reactive compound (Thomas et al., 2005). Another group described the membrane dynamics of the nicotinic acetylcholine receptor on muscle cells with the well known paralytic agent, bungarotoxin (Akaaboune et al., 1999). Until recently there was no known naturally occurring irreversible antagonist for AMPA receptors.

Synaptic Plasticity at the hippocampal Schaeffer-collateral synapse

Though various forms of activity-dependent plasticity were characterized earlier, Long-Term Potentiation (LTP) at the hippocampal CA3-CA1 synapse is inarguably the best-studied form at the present day. Initially, John Eccles demonstrated that tetanizing an afferent pathway in the spinal cord could profoundly increase synaptic strength,

although the potentiation was only short-lived, lasting at most two hours (Eccles and Rall, 1950). In 1973 Bliss and Lomo showed that brief tetanization of the hippocampal perforant path could result in large increases in synaptic strength that could last for a day or more (Bliss and Lomo, 1973). Ultimately, with the advent of the hippocampal slice preparation, LTP could easily be studied in a dish and its mechanism thoroughly explored. Our current view is that strong homosynaptic activation of CA3 axons results in an envelope of postsynaptic depolarization of CA1 cells that allows for unblocking of synaptic NMDA receptors by extracellular magnesium ions that normally plug the NMDA receptor pore near resting membrane potential (Nicoll and Malenka, 1999). Coincident presynaptic glutamate release with postsynaptic depolarization by backpropagating action potentials or activation of nearby synapses can also allow for NMDA receptor activation to trigger plasticity (Magee and Johnston, 1997). When NMDA channels open they pass a substantial calcium flux into the postsynaptic spine; calcium rapidly binds to calmodulin, which in turn activates calcium-calmodulin-dependent protein kinase II (CaMKII). The kinase then phosphorylates several target proteins (while also phosphorylating itself) driving one or more signaling cascades that ultimately results in the insertion of more AMPA receptors to the synaptic membrane (Malenka and Nicoll, 1999). Because LTP has been shown to occur in some cases in less than ten seconds, all these processes must be extremely fast (Petersen et al., 1998).

Initially there was considerable controversy over whether the expression of LTP relied on changes in pre- or postsynaptic function. On one hand LTP results in a change in the relative strength of AMPA and NMDA currents without a change in the paired pulsed ratio, arguing against an increase in presynaptic release probability (Kauer et al.,

1988). On the other hand, LTP also results in a reduction in release failures observed under conditions of minimal stimulation in which one or only a few fibers are stimulated (Malinow and Tsien, 1990). This seeming contradiction was ultimately resolved when two studies demonstrated that a reduction in apparent failures could be due to an insertion of AMPA receptors to a synapse that had previously only contained NMDA receptors, so-called 'silent' synapses (Isaac et al., 1995; Liao et al., 1995). This mechanism also neatly accounts for the observed increase in the AMPA to NMDA ratio of synaptic currents.

With this paradox solved, the current debate on LTP shifted focus to the downstream signals that convert CaMKII activity into an increased number of postsynaptic AMPA receptors. Some work suggests that the AMPA receptor is itself phosphorylated, enhancing its rate of insertion to synapses or even directly increasing its pore conductance (Barria et al., 1997; Lee et al., 2000). Other evidence suggests that the target could be accessory proteins, small GTPases, auxiliary subunits of the AMPA receptor, such as stargazin, or even other kinases (Bredt and Nicoll, 2003). One study proposed that LTP involves the transient insertion of calcium-permeable AMPA receptors to the synapse, a process previously demonstrated only at non-hippocampal synapses (Plant et al., 2006). Although much of this data could conceivably be fit into a single model, some results are directly conflicting. The next decade should hopefully resolve the remaining questions of this well-studied phenomenon.

Role of NMDA receptors in synaptic maturation

While it remains uncertain whether and how AMPA receptors are inserted to synapses during LTP, it is inarguable that synaptogenesis during brain development necessarily involves the recruitment of AMPA receptors to nascent synapses (Hsia et al., 1998). In the first few postnatal days the total number of synapses in the hippocampus is small and glutamatergic transmission at hippocampal synapses is almost entirely mediated by NMDA receptors. Because NMDA receptors are largely inactive at the resting potential of neurons, these synapses are essentially ‘silent’ in that glutamate under most conditions will not evoke postsynaptic depolarization. Over the course of the next few weeks of development there is a dramatic increase both in the number of morphological synaptic contacts and the prevalence of AMPA receptors at postsynaptic sites (Hsia et al., 1998). Thus central synapses seem to undergo a progressive process of ‘unsilencing’ as AMPA receptors join NMDA receptors at synapses to allow for ongoing transmission near resting potential (Durand et al., 1996). Experience-driven activity through hippocampus and cortex is thought to be the trigger for this process, essentially eliciting punctuated LTP-like events that wire up neural circuits.

Multiple lines of research utilizing pharmacological blockade of NMDA receptors during development support this model. One study reported that chronic blockade of NMDA receptors in dissociated hippocampal cultures prevented the developmental unsilencing of synapses (Liao et al., 1999). Upon removal of the antagonist, AMPA receptors are rapidly recruited to synaptic sites. Separate work found that culturing organotypic hippocampal slice cultures in NMDA antagonist delayed, but did not

ultimately block the relative increase in AMPA to NMDA synaptic currents that is observed during normal development (Zhu and Malinow, 2002). Although consistent with an NMDA receptor activity-dependent model of synaptic development, these results are complicated by conflicting data that NMDA receptor blockade can actually increase synapse number in culture, and dissociated neurons from the NR1 $-/-$ mouse (which dies perinatally) can cluster AMPA receptors on their dendritic membrane (Cottrell et al., 2000; Li et al., 1994; Luthi et al., 2001). Despite this unresolved issue, conditional ablation of NR1 using a floxed NR1 mouse is helping to define the role of NMDA receptors in development. Deletion of NR1 embryonically in forebrain excitatory neurons drastically alters patterning in somatosensory cortex, disrupting the somatotopic cytoarchitectural arrangement in the whisker-to-barrel system probably as a result of improperly targeted thalamic axons (Iwasato et al., 2000). Whether glutamatergic synapses on pyramidal cells mature normally in this mouse model remains to be explored.

Chapter 2

Methods

Primary hippocampal cell culture

Dissociated hippocampal cultures were prepared from P0 sprague-dawley rat pups. Hippocampi were dissected and the dentate gyrus was carefully removed. The tissue was enzymatically digested with papain (Worthington) mechanically triturated and plated on poly-D-lysine coated coverslips at a density of 100,000 cells/well. Cells were cultured in Neurobasal-A media (Gibco) supplemented with B27, FBS and penicillin/streptomycin for three to five days, then half the media was replaced with serum-free media containing the mitotic inhibitor FUDR (10 μ M). Cultures were used for physiology between 12-24 DIV.

Electrophysiology of dissociated neuronal culture

Recordings were performed at room temperature with an Axopatch-1B or 1D amplifier and patch pipettes of 3–5 M Ω . Series resistances ranged between 10 and 25 M Ω . Cells were visualized by IR-DIC on an upright BX50WI or BX51WI Olympus microscope fitted with a 40x objective (LumplanFl). The external solutions contained (in mM) 140 NaCl, 2.4 KCl, 10 HEPES, 10 glucose, 2-4 CaCl₂, 0-4 MgCl₂, 0.01 glycine, 0.1 picrotoxin (pH 7.27). TTX (500 nM) was included for analysis of mEPSCs, sucrose EPSCs, outside-out patches, and all caged glutamate experiments. The internal solution contained (in mM) CsMeSO₄ 115, CsCl₂ 20, HEPES 10, MgCl₂ 2.5, NaATP 4, NaGTP 0.4, NaCreatine 10, EGTA 0.6, QX314 5 (pH 7.2). For recording of autaptic EPSCs K-gluconate was substituted for CsMeSO₄. For perforated-patch recording, 100 μ g/ml gramicidin and 10 μ M Alexa-fluor 488 were included in the internal solution. mEPSCs (about 100 events per cell) were automatically detected using in-house software.

Picrotoxin and TTX were from Sigma, MNI-caged glutamate, AMPA, AP-V, and QX-314 were from Tocris. ANQX was synthesized in-house according to Chambers et. al (2004). Drugs were dissolved in HEPES buffer or DMSO and concentrated stocks were stored at -20° C. Glutamate, AMPA, ANQX, hypertonic sucrose (1M) and MNI-glutamate were delivered by a local flow-pipe (350 μ m tip) connected to a manifold fed by four reservoirs (Automate Scientific). Solutions were switched by alternately opening and closing valves attached to each reservoir, and solutions could be completely exchanged in 1-2 s. Student's t-test was used for all statistical analysis, except for analysis of mEPSC cumulative distributions, for which the Kolmogorov-Smirnov test was used. Sucrose-evoked responses in a given experiment were normalized to an average of responses in at least 8 control cells in that same experiment to account for variability of the amplitude of this response between different sets of cultures, presumably due to different survival densities of cells. Each data point presented for serially sampled experiments (Figs. 3 and 4) represent the averaged response of at least eight cells or patches recorded in 15-minute bins. Extracellularly-evoked EPSCs were induced by placing a glass monopolar pipette within 100 μ m of the recorded cell. This form of stimulation frequently yielded a measurable monosynaptic EPSC.

Photolysis of ANQX and Caged Glutamate:

For continuous recordings ANQX (10-50 μ M) was locally applied for 5-10 seconds at a flow of 1 ml/minute and activated by 0.5-3 seconds of continuous UV light (as indicated) from a mercury arc lamp (100 W Olympus) filtered by a 330-385 nm bandpass UV filter (Olympus). This always gave reliable irreversible block of AMPA

currents, and minimal reduction in NMDA currents. Additionally, UV exposure of these durations alone had no lasting effect on the amplitude of AMPA or NMDA currents. More prolonged inactivation with focused UV illumination often resulted in increases in holding current, decreases in input resistance, and non-specific reductions in NMDA currents. For inactivation of a complete coverslip of cultured neurons ANQX (100 μ M) was bath applied for 2-3 minutes at 5 ml/min with continuous unfocused UV illumination (no objective). Under these conditions we observed no detectable phototoxicity as evidenced by no decrement in the averaged response to exogenously applied glutamate when UV light was applied alone. Additionally, there was no change in the average input resistance, or basic morphological features of the cells. For focal activation of ANQX and glutamate uncaging a pulsed UV laser (UVILA, 355 nm, Rapp Optics) was used coupled to a 25 or 50 μ m quartz fiber and launched into a spot illumination adaptor (Rapp Optics) housed in the epifluorescence port of the microscope. The beam was focused through a 40x objective to \sim 5 or \sim 20 μ m spot measured with a red He/Ne laser also coupled to the same fiber. UV laser activation of ANQX required between 15 and 30 pulses, given at 1 Hz. Caged glutamate was locally applied from an alternate valve at a concentration of 0.2-0.5 mM in the presence of TTX to reduce spontaneous activity. Cyclothiazide (100 μ M) was sometimes included to increase the amplitude of the response, but no difference in recovery rate in CTZ was observed so the data were pooled. Although we generally did not observe any movement of the preparation during recordings, to ensure that drift of the preparation did not lead to artifactual changes in uncaged glutamate responses, we compared photographs of each cell before and at the end of each recording. Any experiments in which drift was apparent were excluded from

analysis. We ensured that UV photolysis of ANQX and MNI-glutamate occurred at the same spot for experiments in Fig. 6 by, in some cases, moving the laser laterally across the cell body after photoinactivation of the receptors in the first spot. Uncaged glutamate current was always observed at the lateral site (at comparable amplitudes to the first site) indicating that photo-crosslinking was limited to the region being irradiated.

Electrophysiology using *Xenopus laevis* oocytes

Two electrode voltage clamp recordings were performed as described (Tomita et al., 2004). Briefly, GluR1, stargazin and γ -5 constructs were subcloned into pGEM-HE vector and cRNAs were transcribed in vitro using T7 mMessage mMachine (Ambion, Austin, Texas). Two-electrode voltage-clamp analysis ($E_H = -70$ mV) was performed 2 days post-injection at room temperature in recording solution containing (in mM) 90 NaCl, 1.0 KCl, 1.5 CaCl₂, and 10 HEPES (pH = 7.4).

Surface labelling of oocytes

Oocytes three days post-injection were incubated for 1hr with 0.25 μ g/ml rat anti-HA antibody (3F10, Roche) followed by 30 min with HRP conjugated anti-Rat Ig. Individual oocytes were then placed into 50 μ l SuperSignal ELISA Femto Maximum Sensitivity Substrate (Pierce) and chemiluminescence quantified using a TD20/20 Luminometer (Turner Designs).

Outside-out patch recordings from oocytes

Outside-out patch recording was carried out using an EPC-8 amplifier (HEKA) under continuous perfusion with frog Ringer's solution (115 mM NaCl, 2 mM KCl, 2

mM CaCl₂ and 10 mM HEPES, adjusted to pH 7.2 with NaOH). The patch pipette was prepared from borosilicate glass capillaries (WPI) and had 4-7 M Ω input resistance when filled with 100 mM KCl, 2 mM MgCl₂, 10 mM EGTA, and 10 mM HEPES, adjusted to pH 7.2 with KOH. Responses were filtered at 10 kHz and digitized at 26 μ sec/point. The holding potential was maintained at -60 mV. Glutamate (10 mM) was applied by perfusion of the patch membrane with θ tubes driven by a piezo manipulator (Burleigh PZ-150M). After recording, the patch membrane was blown off, and the junction current between the control solution and 10% frog Ringer's solution was measured to monitor solution exchange without moving the patch pipette and the θ tube. Responses to glutamate having a 20-80 % rise time less than 400 μ sec were used for analysis. The decay phase of the response was fitted to single exponential functions using Igor Pro (WaveMetrics). The decay time constant was calculated by fitting the decay of the response with a single-exponential function.

Patch clamp recording from rat slice culture and virus infection

Hippocampal slice cultures were prepared from 6- to 11-day-old rats and culture on Millicell inserts. Infection with Semliki forest virus containing stargazin-Ex1 IRES GFP or wild type stargazin was carried out 4-6 days later. Recordings were made from infected cells 1-2 days after infection, using 2-3 M Ω glass electrodes filled with an internal solution consisting of 115 mM CsMeSO₃, 20 mM CsCl, 10 mM HEPES, 2.5 mM MgCl₂, 4 mM Na₂-ATP, 0.4 mM Na-GTP, 10 mM Na-phosphocreatine, 0.6 mM EGTA, and 0.1 mM spermine, pH 7.2. External perfusion medium consisted of 119 mM NaCl, 2.5 mM KCl, 4 mM CaCl₂, 4 mM MgSO₄, 1 mM NaH₂PO₄, 26.2 mM NaHCO₃, and 11

mM glucose, saturated with 95% O₂ and 5% CO₂, and included 100 μM picrotoxin and 0.5 μM TTX. Infected pyramidal cells were identified by using fluorescence microscopy. mEPSCs were automatically detected with custom software, and each event fitted with a mono-exponential decay function. Cumulative frequency distributions were analyzed by Kolmogorov-Smirnov tests. For evoked EPSCs, TTX was excluded and 10 μM 2-chloro-adenosine was added to reduce polysynaptic activity. A monopolar electrode placed in the CA3 region was used for fiber stimulation. Evoked EPSCs were recorded serially from an infected cell and then from a neighboring, uninfected control cell. NMDA currents were measured 100 ms after the stimulus artifact at +40 mV, and the AMPA peak was measured at -60 mV. Paired recordings were analyzed using paired Student's t-test. For all other statistical analysis unpaired Student's t-test was used.

Single channel recording and data analysis

Patch-clamp recordings were performed 12 to 24 hr post-transfection at room temperature with an EPC 9 amplifier. All recordings were from excised outside-out patches held at -100 mV. The external solution contained (in mM): 150 NaCl, 3 KCl, 2 CaCl₂, 1 MgCl₂, and 5 glucose, buffered with 10 mM HEPES (pH adjusted to 7.4 with NaOH). Patch pipettes (open tip resistance 2 to 4 MΩ) were filled with a solution containing (in mM): 120 KF, 33 KOH, 2 MgCl₂, 1 CaCl₂, 0.1 spermine, and 11 EGTA (pH adjusted to 7.4 with CsOH). Glutamate (10mM) was added to the external solution and was applied with theta pipettes mounted on a piezoelectric bimorph. The rate of solution exchange estimated from open-tip potentials was 100 to 200 μs.

Glutamate-evoked currents were analog low-pass filtered at 10 kHz, sampled at 40 kHz, and written directly to the hard-drive of two computers. One computer stored the records in PULSE format (the software used to run the EPC 9), and the other stored the data in QuB format (the software used for single-channel analysis). For analysis of macroscopic current decays, the PULSE records were exported to IGOR, averaged, and fitted with single- or bi-exponential functions. For analysis of unitary currents, the data were digitally low-pass filtered at 2 kHz. The data were edited manually in QuB to isolate unitary events that occurred late in the glutamate applications and the resulting record was idealized with the SKM algorithm in QuB (using hidden Markov models) to identify single-channel transitions and estimate conductance levels. Given the multiple open levels present, there was no single time resolution that applied to all possible types of transitions. The resolution was set to 100 μ s to avoid missing brief large amplitude events. After inspecting the idealized record and removing dubious events, mean open and shut times were obtained with log-binned fitting of the dwell-time distributions for each conductance level (using Maximum Interval Likelihood subroutines in QuB). The shut time distributions with and without stargazin were similar and bursts of openings were defined as a series of openings separated by shittings shorter than a critical time (2.5 to 3 ms for the six patches). Distributions of the durations of bursts were fitted in QuB with two exponential components. In each stargazin record, there was an excess of brief bursts (presumably single openings) that represented less than 10% of the total number of bursts. Because of the small number and brevity of these bursts, the time constant and relative area of this additional component were poorly defined, and they were not included in the results reported here.

Acute slice preparation and recording

300-400 μm thick transverse hippocampal slices were cut from 2-4 week old Sprague-Dawley rats or mice (various transgenic strains) as indicated on a Leica vibratome in normal ACSF. After 1-2 h incubation at room temperature slices were transferred to a submersion chamber on an upright Olympus BX51 microscope, and CA1 pyramidal cells were visualized by infrared-differential interference contrast optics. The extracellular solution contained (in mM): NaCl 119, KCl 2.5, NaHCO₃ 26, Na₂PO₄ 1, Glucose 11, CaCl₂ 2.5, MgCl₂ 1.3, 0.1 picrotoxin, 0.02 bicuculline methiodide or 0.01 GABA_Azine, and saturated with 95% O₂/5% CO₂. The intracellular solution contained (in mM): 135 CsMeSO₄, 8 NaCl, 10 HEPES, 0.3 Na₃GTP, 4 MgATP, 0.3 EGTA, 5 QX-314. For measurement of I-V relations of synaptic currents 0.1 mM spermine was added to this solution. For recovery of cell morphology 0.1% Lucifer yellow, or 500 μM Alexafluor 488 or 555 were added. CA3 axons were stimulated with low resistance monopolar glass pipettes containing ACSF and placed on either side of the recording electrode in stratum radiatum. A cut was made between CA1 and CA3 to prevent epileptiform activity. Stimulus artifacts were blanked or digitally subtracted with traces after the application of the AMPAR antagonist CNQX (10 μM). Whole cell and fEPSPs were recorded with 3-5 M Ω borosilicate glass pipettes. fEPSP recording pipettes were filled with ACSF. Series resistance ranged between 8 and 25 M Ω and was not compensated for. Experiments in which series resistance changed by more than 20% were excluded from analysis. For whole cell experiments responses were evoked at 0.2 Hz, and for field experiments at 0.05 Hz.

LTP was induced in whole-cell by pairing the cell at 0 to -10 mV for 60 s while stimulating at 2 Hz. LTP was induced in field recordings by four 100 Hz trains consisting of 100 pulses given every 20 seconds at test stimulus intensity. For experiments in Chapter 6, Fig 2A,B APV was rapidly applied and removed from the vicinity of the recorded cell with a local flow pipe (350 μ m diameter) fed by two reservoirs with computer-controlled solenoid driven valves (AutoMate Scientific). In control experiments (not shown) APV reached saturation in less than 15 s and could be completely removed in 2-3 minutes.

Rectification indices were calculated by plotting the magnitude of the average EPSC at -60 , 0, and $+40$ mV and taking the ratio of the slope of the lines connecting values at 0-40 mV and at -60 -0 mV. We prefer this calculation rather than simply a ratio of EPSC amplitude at $+40$ / -60 mV because it takes into account the variable AMPAR reversal potential of each recording. In LTP experiments, the IV relation was measured 10 minutes after pairing. The cell was immediately depolarized to $+40$ mV for 90 s, then to 0 mV for 60 s. Picrotoxin, bicuculline, and kynurenatate were from Sigma, D-APV and CPP from Tocris Biosciences, GABAzine and MK-801 from Ascent scientific, and Philanthoxin 433 was custom synthesized in bulk by Chiralix (The Netherlands). Student's t-test was used for all statistical analyses.

For experiments in Chapter 5, AMPA/NMDA ratios were quantified by holding the cell at $+40$ mV and by subtracting the EPSC recorded after wash-in of D-APV (50 μ M) from the EPSC in control solution. In the NR1 knockouts in Chapter 7, NMDA currents were quantified by measuring the amplitude of the EPSC at $+40$ mV holding

potential, 150 ms after stimulation. AMPA currents were quantified by taking the peak at -60 mV holding potential.

Antibodies

The following antibodies were used: rabbit polyclonal antibodies to GluR1 (Chemicon and albiochem), stargazin (Upstate), HA (Santa Cruz Biotechnology), PSD-95 and SAP102 *SI*); and mouse monoclonal antibodies to PSD-95 (MA1-046, Affinity Bioreagents), FLAG (M2, SIGMA), HA (Covans), Neuroligin (Synaptic System), NR1 and β -catenin (BD Biosciences); and goat polyclonal antibodies to LGI1 and ADAM22 (Santa Cruz Biotechnology). Rabbit polyclonal antibodies to ADAM22 were raised against GSTADAM22 (aa 757-857) or (aa 451-526) and affinity-purified.

Cloning and plasmid constructions

The following cDNAs were cloned from brain total RNA by RT-PCR using primers based on the GenBank databases: rat LGI1 (accession number AJ487517), mouse ADAM23 (AB009673), mouse ADAM9 (AK122188) and mouse Mass1 EPTP repeat domain (aa 3194-3530) (NM_054053). Mouse ADAM22 splicing variant encoding C-terminal PDZ binding motif (-ETSI) was isolated based on accession numbers AB009674 for the forward primer and AB179842 for the reverse primer; F(5'-ATGCAGGCAGCGGCGGCCGCG-3') and R(5'-TTAAATGGATGTCTCCCATAGCCTG-3'). The cDNAs of mouse Slit2 (mKIAA4141, accession number AK220505) and human Robo2 (KIAA1568, accession number AB046788) were provided by Kazusa DNA Research Institute (Chiba, Japan). All PCR

products were analyzed by DNA sequencing. The cDNAs were subcloned into cytomegalovirus promoter-driven vectors and pAP5 (AP, myc, and His x 6-tags fused; GenHunter, Nashville). pGW-PSD-95-GFP constructs and pcDNA-HA-stargazin were described previously (SI). Immunoprecipitation and mass spectrometry A rat brain was homogenized in STE buffer (320 mM sucrose, 20 mM Tris, pH 8.0, and 2 mM EDTA) containing 200 µg/ml PMSF. Homogenates were spun at 20,000 g for 1 h and pellets were resuspended in TET buffer (20 mM Tris, pH 8.0, 1 mM EDTA, and 1.3% Triton X-100). The lysates were spun at 100,000 g for 1 h. Precleared lysates (5 mg protein) were immunoprecipitated with 5 µg of antibodies. Immunoprecipitates were separated by SDS-PAGE and gels subjected to silver staining. The specific protein bands were excised, reduced with 10 mM dithiothreitol and alkylated with iodoacetamide. Band slices were digested with trypsin (12 µg/ml) overnight and desalted with ZipTip C18 (Millipore). The extracted peptides were then separated via nano flow liquid chromatography (LC) (Paradigm MS4, AMR) using a reverse phase C18 column (Magic C18). The LC eluent was coupled to a micro-ionspray source attached to a LCQ Advantage MAX mass spectrometer (Thermo Electron Corporation). The stoichiometry of LGI1 to ADAM22 was determined by Coomassie blue staining and by quantitative western blotting. For quantitative western blot analysis, LGI1-AP or ADAM22-ED-AP was expressed in HEK cells, and secreted LGI1-AP and ADAM22-ED-AP were concentrated by Centriprep (YM-30, Amicon). Concentrated proteins were quantitated by Coomassie blue staining using bovine serum albumin (BSA) for calibration. Scanned signals were analyzed by NIH Image software.

Cell-surface binding assay

COS7 cells were seeded onto three 12-mm cover slips in each well of a six-well cell culture plate (3×10^5 cells/well) and co-transfected with LGI1-Flag and ADAM22-HA. 24 h after transfection, cells were fixed with 4% paraformaldehyde at room temperature for 10 min and blocked with PBS containing 2 mg/ml BSA for 10 min on ice. The fixed cells were stained with anti-Flag antibody, followed by Cy3-conjugated secondary antibody. Then, the cells were permeabilized with 0.1% Triton X-100 for 10 min, blocked with PBS containing 2 mg/ml BSA, and stained with anti-HA polyclonal antibody, followed by Alexa488- conjugated secondary antibody. Fluorescent images were taken with a confocal laser microscopy system (Carl Zeiss LSM 510; Carl Zeiss, Oberkochen, Germany).

Immunofluorescence analysis of hippocampal neuron culture

Rat hippocampal neurons (0.5×10^5 cells) were seeded onto 12-mm cover slips. The neurons were transfected (Nucleofector; Amaxa) before plating with LGI1-Flag and ADAM22-GFP. For surface LGI1-Flag or surface AMPAR staining, cells (DIV 20 – 30) were fixed with 4% paraformaldehyde at room temperature for 10 min and blocked with PBS containing 2 mg/ml BSA for 10 min on ice. The fixed cells were stained with anti-Flag antibody or an antibody to an extracellular epitope of GluR1 (Calbiochem), followed by Cy3-conjugated secondary antibody. Fluorescent images of surface LGI1 and ADAM22 were taken with an inverted research microscope (IX81; Olympus) equipped with a DP30 digital camera. The out-of focus information was removed by three dimensional deconvolution (AutoQuant X). Fluorescent images of surface

AMPA receptors labeled by GluR1 antibody were taken with confocal laser microscopy system (Carl Zeiss LSM 510). To quantify changes in the surface GluR1 intensity, fields were randomly chosen from two independent hippocampal cultures and were taken under the identical conditions (gain and offset). All pixel intensities were measured by Histogram analysis of LSM510 ver3.2 software. For cumulative distributions, data were analyzed by the Kolmogorov-Smirnov test.

Preparation of AP Fusions

AP, LGI1-AP, LGI1, and ADAM22-ED-AP were expressed in HEK293 cells. Cells were cultured for 24 h in growth medium and then cultured in serum-free medium for 72 h. The media containing secreted proteins were harvested and concentrated about 25-fold by Centriprep (YM-30, Amicon). Protein expression and concentration were determined by Coomassie staining. Staining with AP Fusions COS7 cells were stained with AP-tagged fusion proteins as described (S2, S3). Briefly, cells were washed with Hank's balanced salt solution containing 0.5 mg/ml BSA and 20 mM HEPES, pH7.4 (HBH) and incubated for 90 min at 25°C with the AP-fusion protein (1:25 dilution in DMEM). The cells were then washed with HBH, fixed with 4% paraformaldehyde for 15 min and incubated for 100 min at 65°C to inactivate endogenous phosphatase activity. Bound AP activity was visualized by 5-bromo-4-chloro-3-indolyl phosphate (BCIP) and nitroblue tetrazolium (NBT) solution (DAKO cytometry) for several hours. The reaction was stopped by addition of PBS. Fresh frozen mouse brain was serially sectioned (thickness, 10 µm) on cryostat (Leica) and subjected to *in situ* AP analysis (S3) and

immunohistochemistry. Sections were treated with LGI1-AP or AP containing supernatant (1:25 dilution) for 2 hr, followed by staining in BCIP and NBT overnight.

Immunohistochemistry

Serially sectioned brain specimens (10 μm) were fixed with 4% paraformaldehyde. Endogenous peroxidase activity was inactivated by incubating brain sections in 0.5% H₂O₂ for 10 min. Sections were blocked for 1 h in PBS containing 3% normal goat serum and then incubated in the same buffer containing diluted 2 $\mu\text{g}/\text{ml}$ rabbit ADAM22 antibody. Immunoreactivity was visualized with an avidin/biotin/peroxidase system (Vector Laboratories). *In situ* hybridization *In situ* hybridization on 7- μm paraffin-embedded mouse brain sections was carried out using digoxigenin (DIG)-labeled RNA probes (Roche). cDNAs of rat LGI1 (nucleotides 11-284 from initiating ATG), mouse ADAM22 (nucleotides 1351-1960), and rat PSD-95 (nucleotides 1212-1444) were used for probe templates. A section for PSD-95 was counterstained with Nuclear Fast Red.

Generation of NR1 conditional knockout mice

NR1^{fl/fl} mice were bred to NEX-CRE^{+/-}, T29.1-CRE^{+/-}, Dlx5/6-CRE^{+/-}, or Dlx1/2-CRE^{+/-} mice to generate four genotypes, of which NR1^{fl/fl} and NR1^{fl/fl};CRE^{+/-}; were used. All experiments were performed on conditional knockouts and their littermates lacking the CRE allele.

Biolistic Transfection of mouse slice culture

DNA-coated gold particles were prepared according to the manufacturer's directions (BioRad) at 50-100 μ g DNA to 1 mg gold and pressure-ejected onto mouse slice culture 3-5 days in vitro. Slices were used for physiology 6-17 days post-transfection as indicated. Vectors used were CRE-IRES-GFP in pCSCG, GFP-NR1 and GFP-NR1(R) in pCI.

Chapter 3

Photo-inactivation Reveals the Real-Time Trafficking of Native AMPA Receptors

Introduction

Ionotropic neurotransmitter receptors mediate all fast chemical transmission in muscle and nerve. The rapid trafficking of these proteins to and from synapses is the subject of intense research, but remains incompletely understood. AMPA (α -amino-3-hydroxy-5-methyl-4-isoxazolepropionic acid) receptors, a major subtype of ionotropic glutamate receptors, mediate fast excitatory synaptic transmission in the brain. These receptors, while expressed throughout neurons, are highly clustered at the postsynaptic density ensuring rapid responses to synaptically released glutamate. Glutamatergic synapses undergo activity-dependent long lasting changes in synaptic strength, a process considered to underlie aspects of learning and memory (Malenka and Nicoll, 1999). Changes in synaptic strength are thought to involve rapid movement of AMPA receptors into and out of synapses, depending on the frequency of synaptic activity.

A number of studies have suggested that AMPA receptors, unlike NMDA, GABA, and nicotinic acetylcholine receptors, rapidly and constitutively cycle between intracellular stores and the cell surface (Bredt and Nicoll, 2003; Collingridge et al., 2004; Malinow and Malenka, 2002; Sheng and Kim, 2002). This cycling may allow for rapid, regulated changes in synaptic AMPA receptor number and thus provide a mechanism for synaptic plasticity. A variety of optical, biochemical, and electrophysiological approaches have been used to investigate AMPA receptor trafficking. For example, one study tracked AMPA receptors optically by tagging them with either Green Fluorescent Protein (GFP) (Shi et al., 1999), an α -bungarotoxin-binding site (Sekine-Aizawa and Huganir, 2004) or receptor-specific antibodies conjugated to fluorophores. Another group studied AMPA receptor trafficking biochemically by bulk biotinylation of surface

proteins and subsequent immuno-purification (Ehlers, 2000) or by exogenous introduction of receptor subunits containing an extracellular protease cleavage site (Passafaro et al., 2001). Finally, a third line of research has monitored AMPA receptors electrophysiologically by pharmacologically blocking either exocytosis or endocytosis and following the changes in AMPA receptor-mediated synaptic currents (Luscher et al., 1999; Luthi et al., 1999). The general conclusion from these studies is that AMPA receptors are remarkably dynamic, constitutively trafficking between intracellular stores on the time scale of 10-20 minutes.

The real-time lateral diffusion of receptors has also been investigated optically by monitoring the movement of fluorescently tagged surface receptors (via receptor antibodies attached to fluorophores or quantum dots) across the membrane surface (Borgdorff and Choquet, 2002; Tardin et al., 2003). These studies suggested that, whereas extrasynaptic receptors appear to be highly mobile, synaptic receptors represent a comparatively immobile pool under basal conditions.

These approaches have provided valuable insight into the trafficking of receptors, but they have a number of limitations. Most importantly, optical and biochemical studies cannot unequivocally distinguish between synaptic and extrasynaptic receptors. Further, many of these studies relied on the use of antibodies, which are large divalent proteins that have been shown to affect the trafficking of receptors (Grunfeld, 1984; Weissman et al., 1986); or they required the use of over-expressed AMPA receptor subunits, which may perturb normal trafficking. To permit the direct, quantitative, real-time measurement of native AMPA receptor trafficking in live neurons we have used a membrane-impermeable, photoreactive AMPA receptor antagonist to photoinactivate

surface receptors. The photoreactive antagonist, 6-azido-7-nitro-1,4-dihydroquinoxaline-2,3-dione (ANQX), is an aryl azide that, when irradiated with ultraviolet light, becomes a highly reactive nitrene that can covalently cross link to and, as a result, irreversibly antagonize AMPA receptors. Thus, ANQX provides a means of rapidly silencing surface-exposed AMPA receptors, permitting the real-time monitoring of AMPA receptor *insertion* from intracellular stores to the cell surface as well as the *lateral diffusion* of receptors across the plasma membrane (see Figure 1A). Specifically, by recording the ‘recovery’ of AMPA receptor-mediated currents electrophysiologically immediately following the global or focal photoinactivation of surface receptors, we present a direct and quantitative measurement of the exocytosis and lateral diffusion of native AMPA receptors on live neurons. In agreement with previous reports, we observed rapid trafficking of AMPA receptors from internal stores to the cell surface. Surprisingly, however, this fast exocytosis occurred only at non-synaptic sites. Synaptic receptors did exchange with intracellular receptors, but on a much longer timescale, and this cycling did not require activity or protein synthesis. Finally, the most rapid form of AMPA receptor trafficking was through the lateral movement of receptors across the neural surface.

Results

Previous work described the design, synthesis and preliminary characterization of 6-azido-7-nitro-1,4-dihydroquinoxaline-2,3-dione (ANQX), a photoreactive analog of the high affinity AMPA receptor antagonist, DNQX. When ANQX is irradiated with ultraviolet light it becomes a highly reactive nitrene that covalently cross links to and,

thereby, irreversibly antagonizes AMPA receptors. Here we characterize the effect of ANQX on native neuronal synaptic and extrasynaptic AMPA receptors in cultured hippocampal neurons. First, we tested ANQX on AMPA receptor responses from outside-out patches (Fig. 1B). Brief exposure (3 s) to UV light (330-385 nm, Hg⁺ arc lamp) alone had no effect on glutamate-evoked currents and in the absence of UV light the antagonizing effects of ANQX (100 μ M, 2 s) were rapidly reversible. Only in the presence of UV light does ANQX become an irreversible antagonist, permanently reducing the evoked current in the patch for the duration of the recording (n = 8). To examine the selectivity of ANQX and its effect on synaptic currents, we recorded extracellularly evoked EPSCs in dissociated culture and rapidly applied ANQX from a local flowpipe (Fig. 1C). Two seconds of UV irradiation in the presence of ANQX (100 μ M, 10 s application) irreversibly blocked AMPA currents without altering postsynaptic NMDA receptors (n = 7, AMPA block 66 \pm 5%, NMDA block 0 \pm 6%). The fact that ANQX did not affect NMDA currents indicates that ANQX is selective for AMPA receptors and that it has no presynaptic effect on transmitter release.

Next, we tested whether ANQX has an additional feature expected of a photoreactive irreversible antagonist when in great excess of its target: namely, that the amount of irreversible block depends primarily on the time of exposure to UV light. Indeed, serial applications of ANQX (100 μ M, 10 s) with UV light (1 s) caused stepwise reductions in the evoked current (Fig. 1D), and continuous application of *sub-saturating* concentrations of ANQX (2 μ M) in the presence of UV light progressively reduced the evoked current beyond the level of steady-state block (Fig. 1E). These results also highlight the fact that while the photoinactivation of AMPA receptors is quite robust, the

photocrosslinking requires repeated application of ‘fresh’ non-photolyzed ANQX (for a complete analysis see supplemental discussion). These findings demonstrate that ANQX can be used to rapidly, selectively and irreversibly block surface-exposed native neuronal AMPA receptors and, thereby, provides a means of monitoring the rates of insertion or lateral diffusion of these receptors in real time.

To examine the rate of delivery of native AMPA receptors from internal stores to the neuronal surface we photoinactivated all surface-exposed AMPA receptors on dissociated cultured hippocampal neurons with ANQX and full-field UV illumination and monitored the recovery of AMPA currents over time. The insertion of synaptic receptors was monitored selectively by recording evoked AMPA EPSCs in autapses (Fig. 2A and B). The NMDA EPSCs were monitored simultaneously (in 0 mM extracellular Mg^{+2}), providing a measure of the stability of the recording. Immediately following the application of a saturating dose of ANQX (10 μ M) and brief (2 s) irradiation with UV light the synaptic AMPA EPSC (isolated by briefly washing in extracellular Mg^{+2}) was strongly and irreversibly reduced whereas the NMDA EPSC was unchanged (after washout of Mg^{+2}). Unexpectedly, the synaptic AMPA current did not recover from photoinactivation during the recording, indicating that intracellular AMPA receptors are not trafficked to synapses on the minute timescale, even when synaptic NMDA receptors are repetitively activated (Fig. 2C). We noted that the application of this high dose of ANQX with UV light *reversibly* antagonized the synaptic NMDA EPSC, presumably due to the low affinity of quinoxalinediones for the glycine binding-site on the NMDA receptor (Kleckner and Dingledine, 1989). We repeated this experiment on evoked EPSCs in standard dissociated culture in perforated-patch mode to rule out any

consequences of whole-cell dialysis or peculiarities unique to autaptic cultures. Again, we found no rapid recovery of AMPA receptor-mediated synaptic currents after photoinactivation of surface AMPA receptors (Fig. 2D). It is conceivable that the recycling of inactivated receptors could slow any apparent recovery of the synaptic EPSC. However, since we observed no significant recovery whatsoever during these continuous recordings, there cannot be any considerable internal pool of AMPA receptors available at or near synapses for rapid cycling. Consistent with these observations, mEPSCs in all of these experiments were numerous prior to the photoinactivation of surface AMPA receptors and largely absent afterwards (not shown).

Since our results unexpectedly indicated that synaptic AMPA receptors do not exchange with an internal pool on the minute timescale, we next investigated if these receptors cycle on the hour timescale. To address this question we inactivated all surface AMPA receptors on entire cover slips of neurons (100 μ M ANQX, 2-3 min application, see methods) and returned the cultures to a 34°C incubator for various periods of time before assaying the extent of recovery of synaptic AMPA receptor responses. To avoid the problem with signal-to-noise associated with recording mEPSCs, EPSCs were evoked by a brief application of hypertonic sucrose, a reliable method for simultaneously activating all synaptic AMPA receptors (Rosenmund and Stevens, 1996). We observed a 33 \pm 5% (n = 14) recovery in sucrose-evoked EPSCs at 6 h and 79 \pm 12% (n = 12) recovery at 16 hours (Fig. 3A). It should be noted that while sucrose-evoked EPSCs were evident at 6 h, mEPSCs did not become readily apparent until 16 h, presumably due to the difficulty of resolving these miniature currents from baseline noise, unless cyclothiazide was included to increase the amplitude of the events (Fig. 3B and supplemental Fig. 2).

Interestingly, incubating the cultures in tetrodotoxin to block action-potential driven network function had no effect on the recovery of AMPA receptors at synapses, indicating that this cycling is independent of activity (Fig. 3C).

Having established that the time course of synaptic AMPA receptor cycling is slow, we next examined the cycling of extrasynaptic receptors. Toward this end, we repeated the previous serial sampling experiments, and instead examined specifically the recovery of extrasynaptic AMPA receptors by recording AMPA receptor currents from outside-out somatic patches. In striking contrast to the slow recovery observed for synaptic AMPA currents, the extrasynaptic currents exhibited fast recovery following photoinactivation, regaining about $36\pm 8\%$ ($n = 25$) of their initial value within 0.5 h, and ultimately showing $79\pm 19\%$ ($n = 9$) recovery in 18 h (Fig. 4A). As would be expected, if the cultures were maintained at room temperature instead of at 34°C , the extent of recovery at 0.75 h was moderately decreased ($23\pm 3\%$, $n = 11$, instead of $44\pm 5\%$, $n = 9$, $p < 0.05$).

To determine if the apparent recovery of synaptic and extrasynaptic AMPA receptors is due to the synthesis of new receptors or to the trafficking of a preexisting pool of receptors, we examined the effect of the protein synthesis inhibitor cycloheximide over an 18-hour period on the size of mEPSCs and glutamate-evoked currents in outside-out patches. Cycloheximide had no effect on either synaptic (Fig. 4B) or extrasynaptic currents (Fig. 4C), indicating that a pool of preexisting receptors is the sole source of AMPA receptors inserted into the plasma membrane in an 18 h period.

To measure the dynamics of the fast cycling of extrasynaptic receptors in real time, we uniformly inactivated all surface AMPA receptors with full-field UV

illumination (1 s, Hg⁺ arcclamp, ANQX 50 μM) (Fig. 5A, see graphic) while we simultaneously uncaged glutamate focally at the cell body with a UV laser (pulse width = 20 ns) to monitor the cycling of somatic receptors. Although UV light is used to both activate ANQX and uncage glutamate, these photolysis processes were separated in time by alternate application of these drugs from a local flowpipe. Consistent with the serial sampling result, we observed a rapid recovery of the uncaged glutamate response indicating that somatic receptors cycle with an internal pool of AMPA receptors on the minute timescale. To test if dendritic AMPA receptors, like somatic receptors, undergo cycling on the minute timescale, we repeated the previous experiment but uncaged glutamate on dendrites of neurons 75-100 μm from the soma, instead of at the cell body itself. When we photoinactivated dendritic receptors no significant recovery was observed during the duration of the recording (up to 25 minutes, Fig. 5B). Although in this experiment the evoked current was not mediated exclusively by extrasynaptic receptors, this result indicates that there is no significant pool of AMPA receptors on dendrites that cycles on this timescale. Thus the primary source of new functional AMPA receptors is likely to come from exocytosis at the cell body.

Recently, optical tagging of AMPA receptors has revealed that these proteins laterally diffuse within the plane of the membrane at relatively high rates (Borgdorff and Choquet, 2002; Tardin et al., 2003). To test this idea electrophysiologically, we photoinactivated a small patch (~5 μm diameter) of AMPA receptors on the soma of neurons with focused irradiation from a UV laser in the presence of ANQX (50 μM) and then monitored the recovery of AMPA-mediated currents in the same region using focal uncaging of glutamate with the same UV laser spot to ensure that both photochemical

reactions accessed the same receptors (Fig 6, see graphic). These experiments were intentionally performed in whole-cell mode to minimize the insertion of receptors from internal stores at the cell body (see above) so that any recovery must be due to the lateral movement of surface receptors into the photo-inactivated zone. In this recording scheme the focally activated AMPA current began recovering within tens of seconds ($\tau = 35.4$ s for an exponential fit). As expected, when the same experiment was repeated with a larger diameter spot ($\sim 20 \mu\text{m}$) to deplete the cell body surface of much more of its functional receptors, the recovery was slowed ($\tau = 82.8$ s, Fig. 6B). Additionally, none of the lateral diffusion required activity, as these experiments were conducted in the presence of tetrodotoxin. These results confirm the idea that AMPA receptors are moving extremely rapidly across the surface of neurons.

Discussion

In the present study we employed a photochemical approach to characterize directly the trafficking of native AMPA receptors in live neurons. We used the photoreactive AMPA receptor antagonist, ANQX, to specifically and irreversibly antagonize surface AMPA receptors, permitting the real-time monitoring of the *insertion* of AMPA receptor from intracellular stores to the cell surface, as well as the *lateral diffusion* of receptors across the plasma membrane. Owing to the improved spatial and temporal resolution of this approach, we found that the cycling rate of surface AMPA receptors depends primarily on their location: the insertion of receptors at synaptic sites is slow, occurring on the timescale of hours, whereas the insertion of receptors to extrasynaptic somatic sites is rapid, occurring on the timescale of minutes. Lateral

diffusion of receptors across the cell surface occurred on the timescale of seconds, in agreement with previous reports using antibody tagged receptors. Importantly, neither receptor insertion nor lateral diffusion required network activity, as both were unaffected by the application of tetrodotoxin.

Notably, our finding that the inhibition of protein synthesis had no effect on the stability of either synaptic or extrasynaptic AMPA currents suggests that the intracellular pool of AMPA receptors is much larger than the total surface pool. That is, if the number of intracellular receptors were small compared to the number of surface receptors, the observed recovery after photoinactivation would have been much more incomplete due to the recycling of photoinactivated receptors. However, we observed near total recovery of surface currents ($79\pm 12\%$) in the same time period that protein synthesis inhibition had no effect.

Our results highlight the power of using an irreversible antagonist to study receptor trafficking. Along the same lines, a number of previous studies have used irreversible antagonists of NMDA receptors (Tovar and Westbrook, 2002), nicotinic acetylcholine receptors (Akaaboune et al., 1999), and modified GABA receptors (Thomas et al., 2005), to study the dynamics of those classes of ion channels, and their results have proven invaluable to our understanding of how these other types of neurotransmitter receptors traffic in neurons. We were able to take advantage of the photoreactivity of ANQX to determine the contributions of both receptor insertion and lateral diffusion to AMPA receptor trafficking.

Although the use of a photoreactive receptor antagonist to irreversibly silence surface AMPA receptors has several advantages over previous approaches used to study

AMPA receptor trafficking, a number of potential limitations should be considered. One possible problem is that irreversibly antagonized AMPA receptors could traffic differently than unblocked, but closed receptors. However, given the evidence that antagonizing AMPA receptors does not alter receptor trafficking under basal conditions or during synaptic plasticity, this concern seems unjustified (Kauer et al., 1988). It should be pointed out that because we only studied receptor trafficking on a comparatively short timescale (<18 h) the homeostatic compensatory insertion of AMPA receptors observed after more prolonged activity blockade (~48 h) is unlikely to have influenced our results (Tardin et al., 2003). Indeed, under our conditions incubation of neurons with saturating NBQX for 18 h did not significantly enhance mEPSC amplitude (data not shown).

Another potential limitation arises if receptor cycling at synapses is both extremely rapid and involves a very small pool of intracellular receptors. If this were the case, we might underestimate the rate of receptor trafficking at synapses due to the eventual recycling of inactivated receptors. However, since we did not see *any* recovery of synaptic currents immediately following photoinactivation of surface receptors there cannot be any considerable pool of internal receptors at or near synapses available for cycling. Rather, new receptors must be coming from a more distant location. It is possible that the recycling of inactivated receptors slowed the observed recovery of synaptic and extrasynaptic currents at much longer time points. Nonetheless, the minimal recovery of synaptic currents observed in the first hour after photoinactivation and the significant recovery observed at 16 hours provides upper and lower limits for the rate of replacement of AMPA receptors at synapses.

Why is the rate of AMPA receptor insertion to synapses that we measure with photoinactivation so much slower than that suggested by previous studies? There are a variety of potential factors. First it is possible that the recovery of surface AMPA receptors observed in previous studies, which could not unequivocally distinguish between trafficking of receptors to synaptic and extrasynaptic sites, was actually due to the cycling of extrasynaptic receptors. Alternatively, studies using over-expressed AMPA receptor subunits may have led to overestimates of receptor trafficking rates. Finally, the rapid changes in synaptic AMPA currents observed in studies using peptides thought to specifically disrupt endo- and exocytosis of AMPA receptors has recently been called into question by another study that demonstrated that one of the drugs, the NSF-binding fragment, may also inhibit the lateral movement of receptors into synapses (Gardner et al., 2005). Thus it is possible that the selectivity of some of these drugs for disrupting vesicular traffic has been overestimated. In fact, another study found that blockade of endosomal trafficking had no effect on basal synaptic transmission, although it did reduce the ability to induce LTP (Park et al., 2004).

Our data is best compared with the results from the study by Passafaro *et. al.*, which used over-expressed tagged receptors with an extracellular thrombin cleavage tag to directly address the rate of exocytosis of AMPA receptors from internal stores. This study found that the exocytosis rate differed depending on the AMPA receptor subunit over-expressed. While over-expressed GluR2 was rapidly trafficked to the membrane, over-expressed GluR1 was exocytosed more slowly (about 25% in 60 minutes). Interestingly, when GluR1 and GluR2 were co-expressed the trafficking rate was slow, akin to that when GluR1 was expressed alone. Since we studied native receptors, which

are thought to be heteromers of GluR1/2 and GluR2/3 subunits (Wenthold et al., 1996), our data is best compared to this last result with GluR1/2 co-expression. Since we find ~35% recovery of extrasynaptic currents in 30 minutes, and ~25% recovery of synaptic currents in 3 hours (see Figs. 3 and 4) we argue that our data is relatively in line with that from Passafaro *et. al.*, and the faster recovery rates observed there may be due to substantial over-production of AMPA receptor subunits under conditions of over-expression. An additional study from Shi *et. al.* demonstrated that insertion of AMPA receptors to synapses depends on the subunit composition. Although this study could conclusively show that receptors are inserted to synapses as their assay was electrophysiological, they made no direct measurement of synaptic cycling on the short timescale, because their manipulation involved viral-mediated expression of recombinant AMPA receptor subunits which minimally takes 16 hours to express.

An obvious experiment to conduct with ANQX is to irreversibly antagonize surface AMPA receptors and then induce long-term potentiation, (LTP), since LTP is thought to involve the rapid insertion of AMPA receptors into synapses, possibly from an intracellular pool. Unfortunately, despite considerable effort, we were unable to obtain a reliable induction protocol for LTP in cultured neurons. Conducting such an experiment in acute hippocampal slices, where LTP is a robust phenomenon, also was not possible because of several technical limitations of this system (for a full discussion see supplementary material).

A fundamental question in molecular neuroscience is how neurotransmitter receptors synthesized within the cell body are targeted to synapses. Are receptors first exocytosed at the cell body and then trafficked along the cell surface to synapses, or are

they trafficked intracellularly to dendrites and then exocytosed directly at synapses? Our data support the former model (Figure 7). First, we established that there is a large intracellular pool of AMPA receptors that are mostly inserted at the cell body. Second, this pool of receptors rapidly supplies the neuronal surface with functional receptors at the cell body but not at dendrites or synapses—suggesting that the bulk of the cycling intracellular pool is restricted to the soma. Third, the lateral diffusion of receptors at the cell body is rapid, and according to previously published reports, the lateral diffusion at distal dendrites is also rapid, although it will be restricted by the constrained geometry of dendrites compared to the cell body (Tardin et al., 2003). This observation supports the idea that diffusion along the surface is a primary route for targeting receptors to the synapse.

An interesting question is why, given that somatic exocytosis is fast and the mobility of surface receptors is high, it still takes hours to see appreciable recovery of synaptic currents? Based on the measured coefficient of diffusion (D) for extrasynaptic AMPA receptors from optical studies (Tardin et al., 2003) and a simple model of Brownian motion along a one-dimensional surface (where $x^2 = 2Dt$ and $D = 0.45 \mu\text{m}^2/\text{s}$), an AMPA receptor at the cell body could take up to 3 hr to travel 100 μm , the range of most proximal synapses. But even for synapses much closer to the cell body, replacement will be limited by the relative immobility of synaptic receptors observed in the optical study. Thus we suggest that the ultimate rate-limiting factor in exchange of synaptic receptors could be a regulated biochemical process in which accessory proteins ‘free’ a synaptic receptor, making the site available for a new receptor to diffuse inward and become fixed. Future studies will be required to quantitatively determine the rate at

which laterally diffusing dendritic AMPA receptors supply synapses with functional receptors.

The present study highlights the power of using a photoreactive antagonist to study AMPA receptor trafficking. By irreversibly inactivating all surface AMPA receptors, we were able to track the movement of receptors from internal stores to the cell surface. By irreversibly inactivating AMPA receptors focally, we were able to monitor the rapid movement of receptors across the membrane surface. We anticipate that future work with ANQX, as well as other classes of photoreactive receptor ligands, will help answer fundamental questions in neuroscience related to receptor trafficking, synaptic plasticity, and neural circuit function.

Supplemental Discussion

The example trace in Figure 1D demonstrates that sub-saturating concentrations of ANQX can knock out nearly all of the evoked AMPA current, presumably because irreversible photo-crosslinking quantitatively removes functional AMPA receptors, making the apparent block independent of the steady-state affinity. In an additional series of experiment not shown we determined that the rate of progress towards total inactivation is dependent primarily on the rate of perfusion of fresh non-photolyzed ANQX. This was demonstrated by repeating the experiment shown in 1D but in a situation in which the flow of fresh ANQX was stopped during the application of UV light. This resulted in minimal photoinactivation. Restarting the flow then allowed for photoinactivation to continue towards completion. Additionally, the reaction rate was also dependent on the concentration of ANQX perfused, but this is a direct consequence

of the fact that higher concentrations simply deliver more non-photolyzed ANQX per unit time for the same rate of solution flow.

An additional feature of ANQX that is apparent from the trace in 1D is the highly reproducible drop in antagonism at the onset of UV light. This can be explained by the fact that photolyzed ANQX has a measured IC_{50} (~10 μ M) approximately an order of magnitude higher than non-photolyzed ANQX (P.M.E., unpublished observation). Thus, at the onset of UV light the majority of ANQX mediating the steady-state inhibition is rapidly converted to a form that is lower affinity, and only a small fraction actually cross-links to the receptors mediating the evoked current. Over time (in our conditions, on the order of several seconds) irreversible antagonism builds up despite the apparent inefficiency in cross-linking, because each cross-linking event is irreversible.

We attempted in a variety of fashions to activate ANQX in acute hippocampal slices, which offer many advantages over dissociated culture (*viz.*; the possibility of extracellular recordings, the increased stability of intracellular recordings, the ability to reliably induce synaptic plasticity, and a system that better approximates an *in vivo* situation). Unfortunately we had minimal success. This is primarily due to the inability to rapidly introduce ANQX to acute slices, and to rapidly remove it to allow for monitoring of recovery of AMPA currents. As explained above, the ability to efficiently photoinactivate AMPA receptors requires rapid introduction of fresh non-photolyzed ANQX to the receptors being studied because cross-linking is inefficient. Two additional complications are that synapses in hippocampal slices are difficult to localize (compared to synapses in culture which exist in two dimensions) and prolonged UV exposure is necessary to activate ANQX in slices (owing to slower ANQX perfusion rates and light

scattering and/or absorption) and results in appreciable phototoxicity before photoinactivation becomes apparent. Nonetheless, it is possible that rapid micro-perfusion systems in combination with two-photon activation of ANQX could be successful, and may permit not only the analysis of AMPA receptor trafficking in slices, but may also be useful for the function analysis of intact neural circuits in brain tissue.

Long-term potentiation (LTP) of excitatory synaptic transmission is thought to rely on the rapid insertion of AMPA receptors to synapses, presumably from intracellular stores. An obvious experiment to perform with ANQX would be to photoinactivate all surface AMPA receptors and then induce LTP, which is expected to result in an immediate recovery of synaptic responses. Unfortunately, LTP has been notoriously difficult to induce in dissociated cultures for reasons that are not well characterized. Nonetheless, we attempted to induce LTP using a variety of published approaches. First we employed the most common induction procedure: pairing postsynaptic depolarization with presynaptic action potentials. In normal whole-cell mode this never led to potentiation ($n = 6$). Recently, several studies have employed the application of supersaturating glycine to stimulate receptor insertion by activating NMDA receptors (despite the fact that normal culture media already includes supersaturating levels of glycine). Unfortunately, in 0 out of 6 cells did application of glycine (in the absence of external magnesium to unblock NMDA receptors) lead to increases in mEPSC amplitude. Finally, several reports claim that LTP can be induced if the postsynaptic cell is recorded in perforated-patch mode to avoid intracellular dialysis. Interestingly, in 4 out of 11 experiments standard pairing in perforated-patch mode led to significant potentiation, though in 3 out of 11 experiments it led to depression, and in 4 out of 11 it

resulted in no change. Given the unreliability of this LTP induction protocol we did not conduct any photoinactivation experiments because the results would be difficult to interpret. Investigating AMPA receptor trafficking associated with LTP will require future work with an irreversible antagonist that can be used in acute hippocampal slices, where LTP is a robust phenomenon.

Figure 1. ANQX is a photoreactive, specific, irreversible inhibitor of native, surface-exposed AMPA receptors.

(A) ANQX rapidly binds to surface exposed extrasynaptic (1) and synaptic (2) but not intracellular (3) receptors. Global irradiation of ANQX-bound receptors with UV light irreversibly antagonizes surface receptors and permits the real-time monitoring of AMPA receptor insertion from intracellular stores to the cell surface (depicted). Focal illumination of ANQX-bound receptors permits the real-time monitoring of AMPA receptor diffusion across the cell surface. **(B)** Outside-out patch recording from a cultured hippocampal neuron (10 mM glutamate, 100 μ M cyclothiazide) following the indicated treatments. UV light (1 s) alone has no effect on the glutamate-evoked current. ANQX (100 μ M) alone reversibly blocked the glutamate-evoked current. ANQX and UV light applied together irreversibly antagonizes AMPA receptors (n = 8). **(C)** ANQX-mediated irreversible antagonism is selective for AMPA receptors. Following the brief application of ANQX (100 μ M) and UV light (1 s) the synaptic AMPA-mediated EPSC at -60 mV is permanently reduced, but the NMDA EPSC recorded at $+40$ mV is unchanged (n = 7). Stimulus artifacts have been blanked. **(D)** Serial applications of ANQX (100 μ M) and UV light (1 s) reduced the whole-cell AMPA (10 μ M) evoked current in a stepwise fashion (n = 3). **(E)** Continuous application of UV light in the presence of non-saturating doses of ANQX (2 μ M) progressively reduces the whole-cell AMPA current (n = 7).

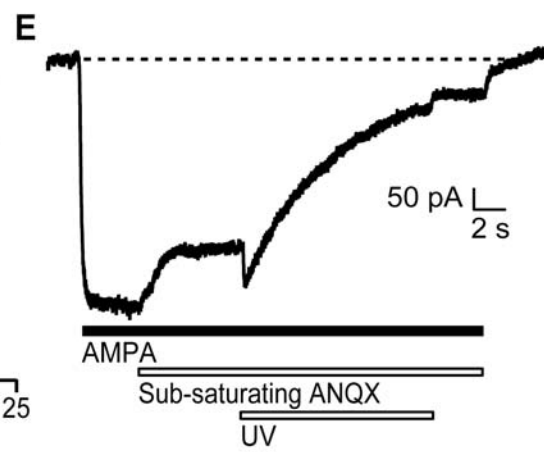
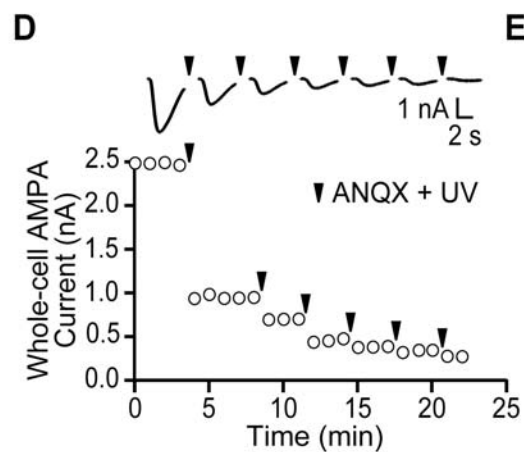
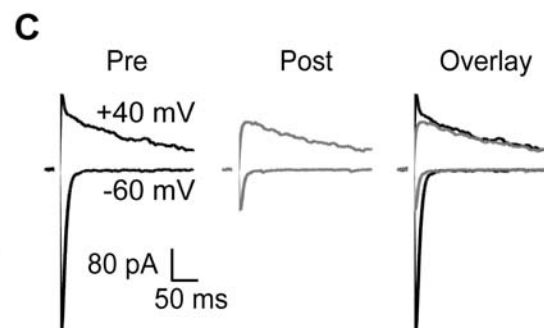
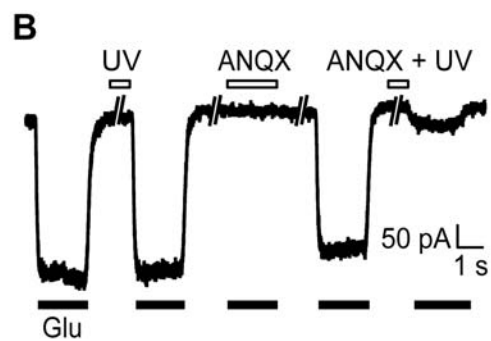
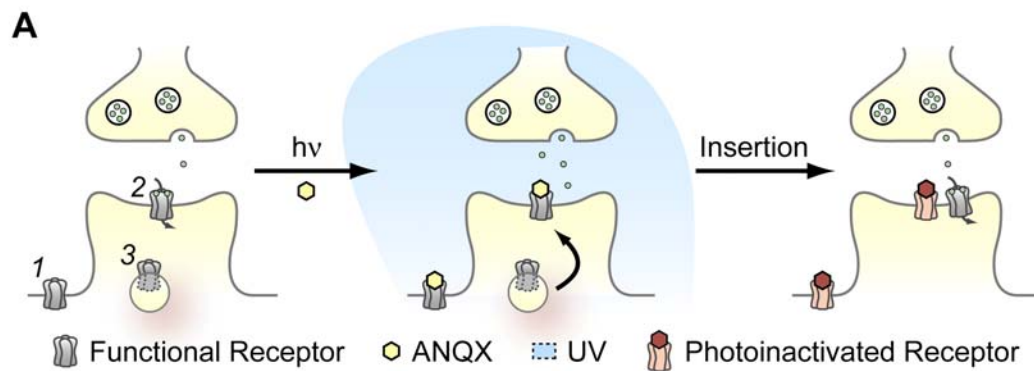


Figure 2. Synaptic AMPA receptors do not rapidly cycle with an intracellular pool of receptors on the timescale of minutes.

(A) Following brief application of ANQX and UV light the synaptic AMPA EPSC in an autaptic cultured hippocampal neuron is permanently reduced. The NMDA EPSC measured at 100 ms after the stimulus is unchanged ($n = 6$). The action potentials in the traces have been blanked and responses have been averaged in one-minute bins. **(B)**

Expansion of minute 6-7 of the recording in (A). Mg^{+2} was rapidly applied for 40 s immediately following inactivation to isolate the AMPA response. No recovery on this timescale is apparent. Traces of each EPSC are plotted above the corresponding point in the expansion. The first trace has been truncated and the action potentials blanked. **(C)**

Following photoinactivation of surface AMPA receptors, synaptic AMPA receptor currents do not recover despite repetitive stimulation (0.5 Hz and 2 Hz) of synaptic NMDA receptors (0 mM Mg^{+2}). APV was present until after photoinactivation to isolate the AMPA receptor current. **(D)**

An average of five similar experiments, but using extracellular evoked EPSCs in standard dissociated cultures and in gramicidin-perforated patch mode ($n = 5$). Stimulus artifacts in the traces have been blanked.

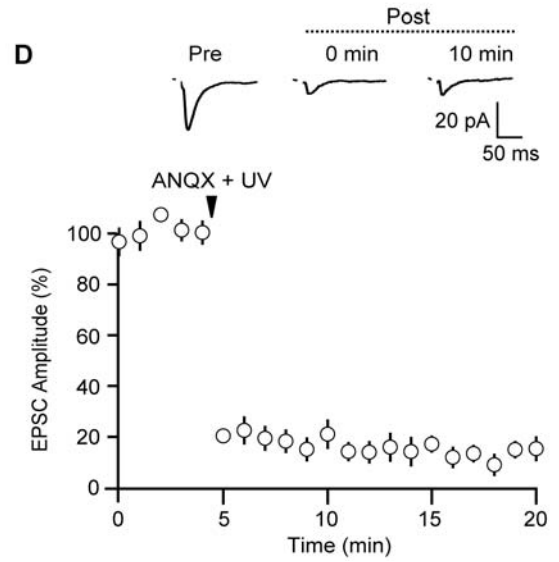
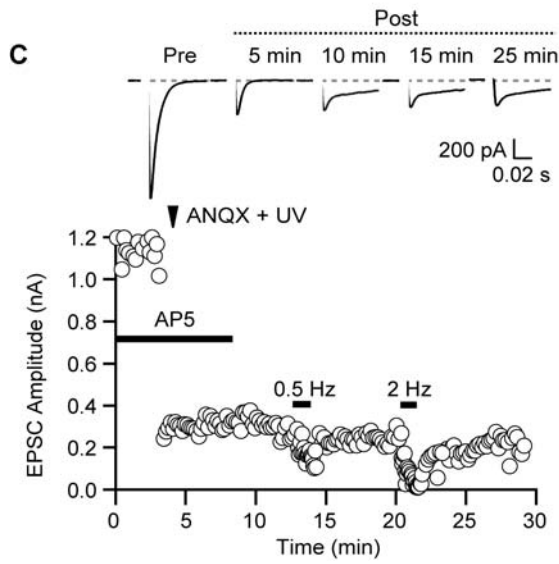
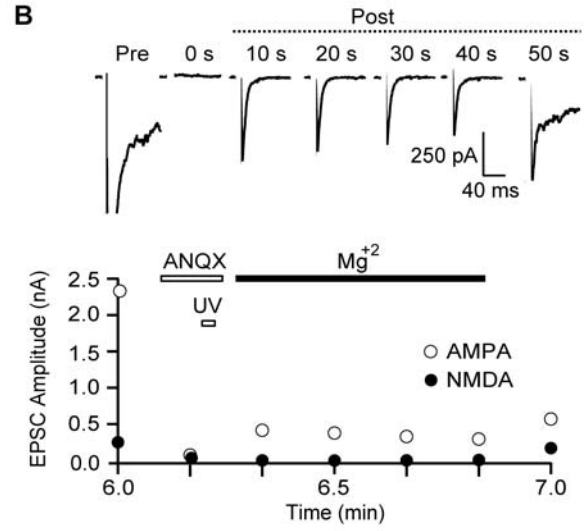
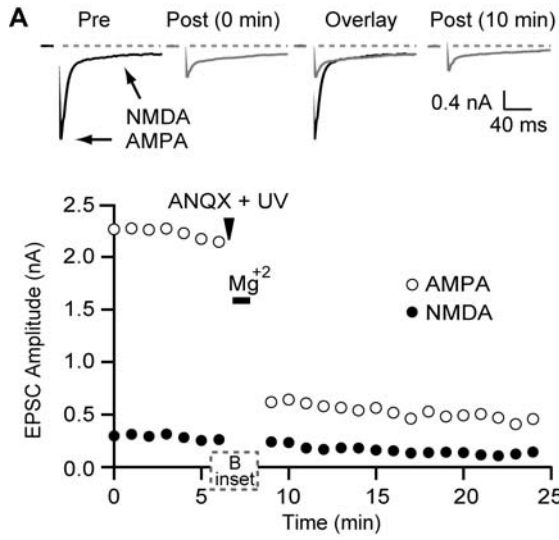


Figure 3. Synaptic AMPA receptors cycle with an intracellular pool of receptors on the timescale of hours.

(A) Average sucrose-evoked EPSCs from neurons at various time points following global photoinactivation of all surface AMPA receptors. Representative traces from the indicated times are presented above the graph. **(B)** Representative recordings of mEPSCs at the indicated times following photoinactivation. **(C)** Cumulative distribution of mEPSC amplitudes before ($n = 6$) and 16 h after ($n = 7$) photoinactivation of total surface AMPA receptors. **(D)** Incubation of neurons with TTX to block action potential driven activity does not affect the recovery of sucrose-evoked EPSCs at the 6 h time point ($n = 11$ in TTX, $n = 9$ control).

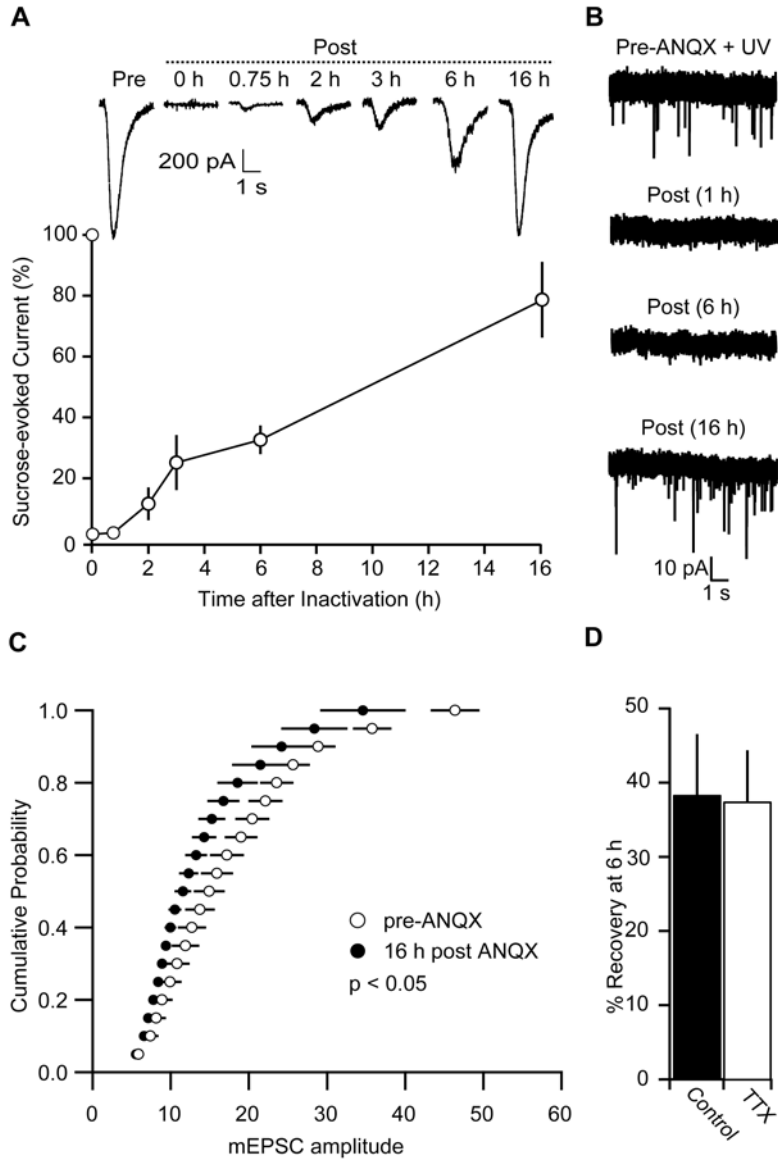


Figure 4. Extrasynaptic AMPA receptor currents initially recover more quickly than synaptic currents from photoinactivation. Cycling of AMPA receptors is independent of protein synthesis.

(A) Average glutamate-evoked (10 mM, 100 μ M cyclothiazide) outside-patch currents measured at various time points following photoinactivation of all surface AMPA receptors. Representative traces from the indicated times are presented above the graph.

(B) The amplitude of AMPA receptor mEPSCs is not affected by incubation of neuronal cultures for 18 h with the protein synthesis inhibitor cycloheximide (100 μ M).

(C) Average response of somatic outside-out patches to glutamate is not affected by incubation of neuronal cultures for 18 h with cycloheximide (100 μ M).

(D) Cumulative distribution of mEPSC amplitudes before ANQX treatment ($n = 7$) and 18 h later with or without incubation in cycloheximide ($n = 8$ each, $p = 0.38$, K-S test).

(E) Average mEPSC amplitudes before ANQX treatment ($n = 7$), and 18 h later with or without incubation in cycloheximide ($n = 8$ each, $p = 0.62$, Student's t -test).

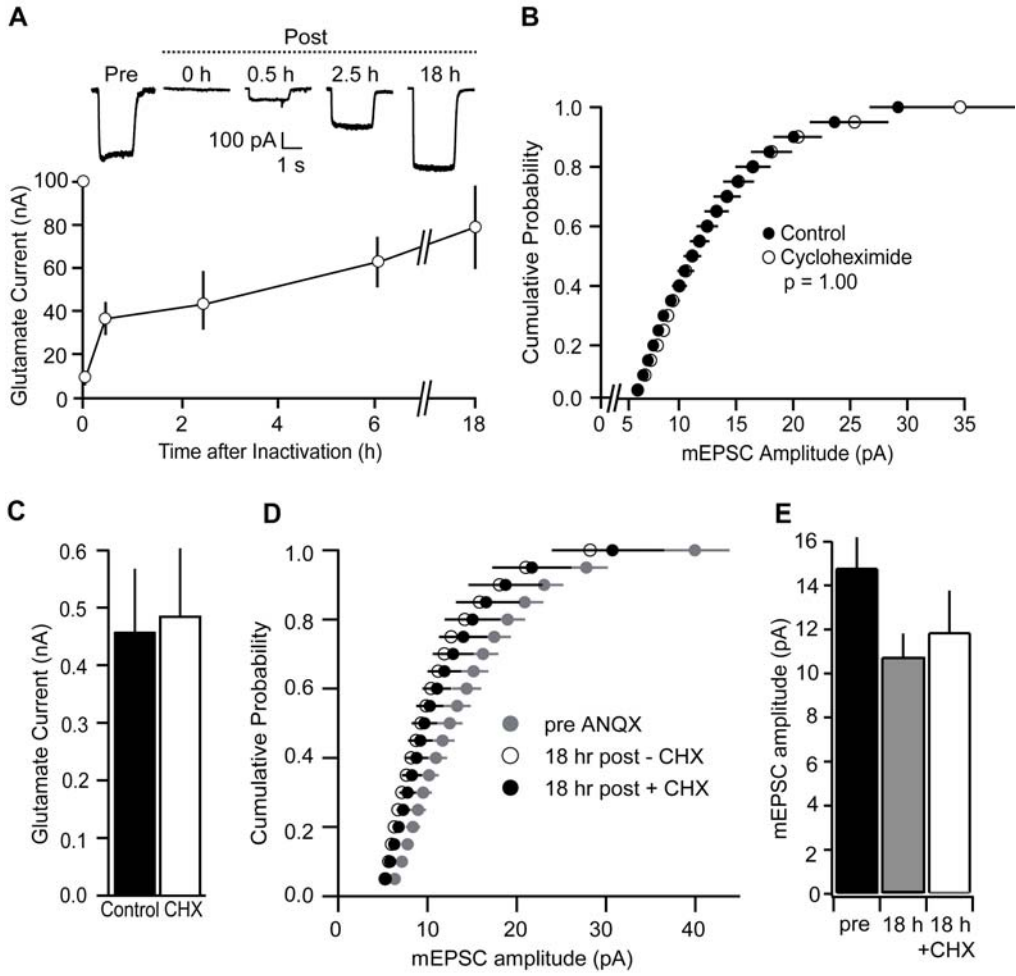


Figure 5. Somatic AMPA receptors rapidly cycle with an intracellular pool of receptors on the timescale of minutes.

(A) Fast recovery of focally evoked uncaged glutamate responses from somatic AMPA receptors is observed on the timescale of minutes following global photoinactivation of all surface AMPA receptors ($n = 6$). Representative traces from the indicated times are presented above the graph. Recording scheme graphic: The cell is recorded in perforated patch mode. Full-field (global) UV irradiation of the entire neuron in the presence of ANQX (yellow) inactivates surface receptors. Focal UV irradiation of the cell body in the presence of caged glutamate (blue) activates somatic AMPA receptors. Overlap of inactivated receptor region (yellow) and uncaged glutamate region (blue) is shown in green. **(B)** When the uncaging spot is moved to a dendritic region 75-100 μm from the soma no fast recovery of current is observed ($n = 6$). Error bars are too small to see.

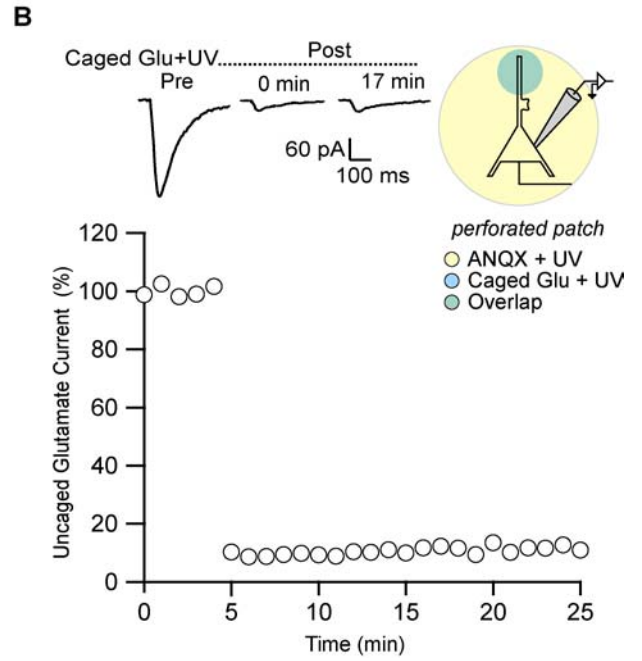
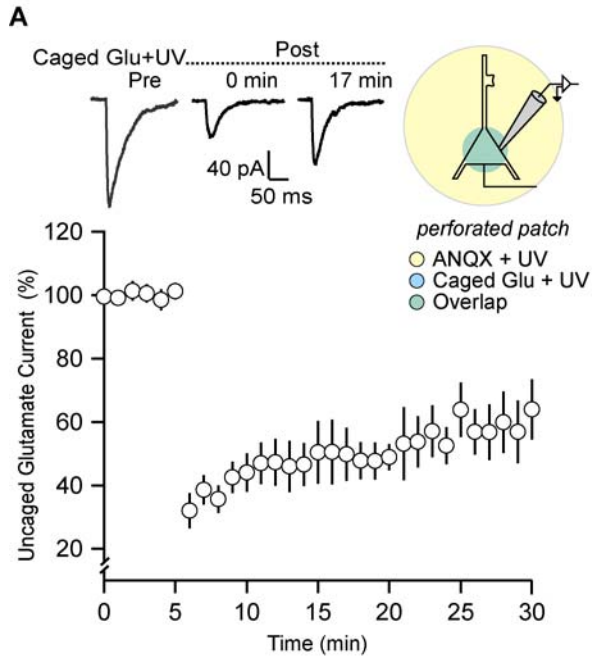


Figure 6. Somatic AMPA receptors laterally diffuse on the surface of the neuron on the timescale of seconds.

(A) Somatic AMPA receptor responses to focally uncaged glutamate rapidly recover following focal photoinactivation of AMPA receptors in a defined ($\sim 5 \mu\text{m}$ spot) region on the cell body. Uncaged glutamate-evoked responses were measured in the identical region (see graphic, $n = 7$). Representative traces from the indicated times are presented above the graph. Recording scheme graphic: The cell is recorded in whole-cell patch mode. Focused UV irradiation of a $5 \mu\text{m}$ spot on the cell body in the presence of ANQX (yellow) inactivates a fraction of the surface receptors. Focused UV irradiation of a $5 \mu\text{m}$ spot on the cell body in the presence of caged glutamate (blue) activates somatic AMPA receptors. Overlap of inactivated receptor region (yellow) and uncaged glutamate region (blue) is shown in green. **(B)** Normalized recovery rate of somatic AMPA receptor responses to focally uncaged glutamate. The rate of recovery following focal photoinactivation is reduced when the diameter of the photolysis region (spot size) is increased from $5 \mu\text{m}$ to $20 \mu\text{m}$ ($n = 10$). The $5 \mu\text{m}$ spot size data is re-plotted from (A).

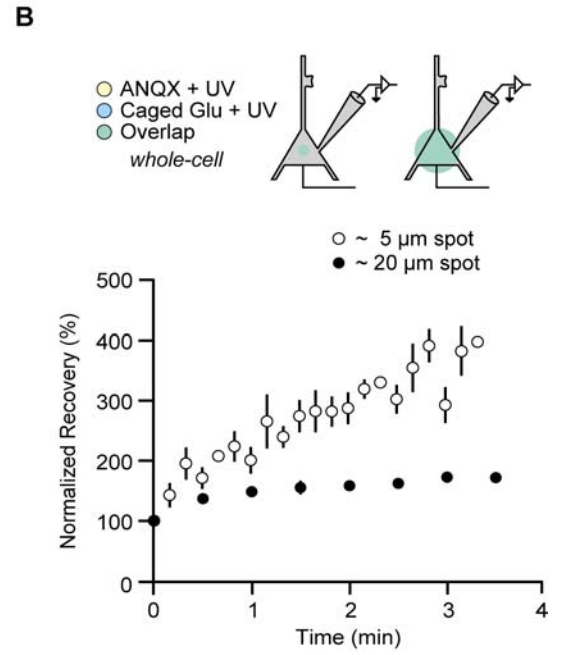
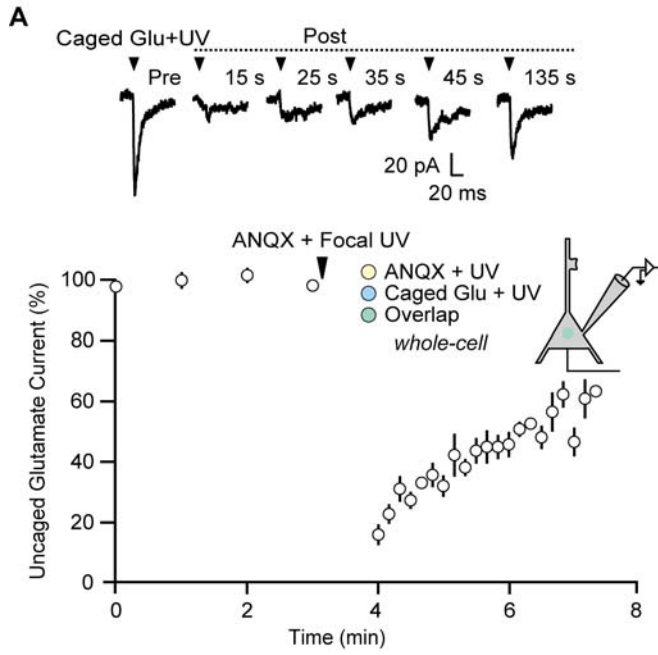
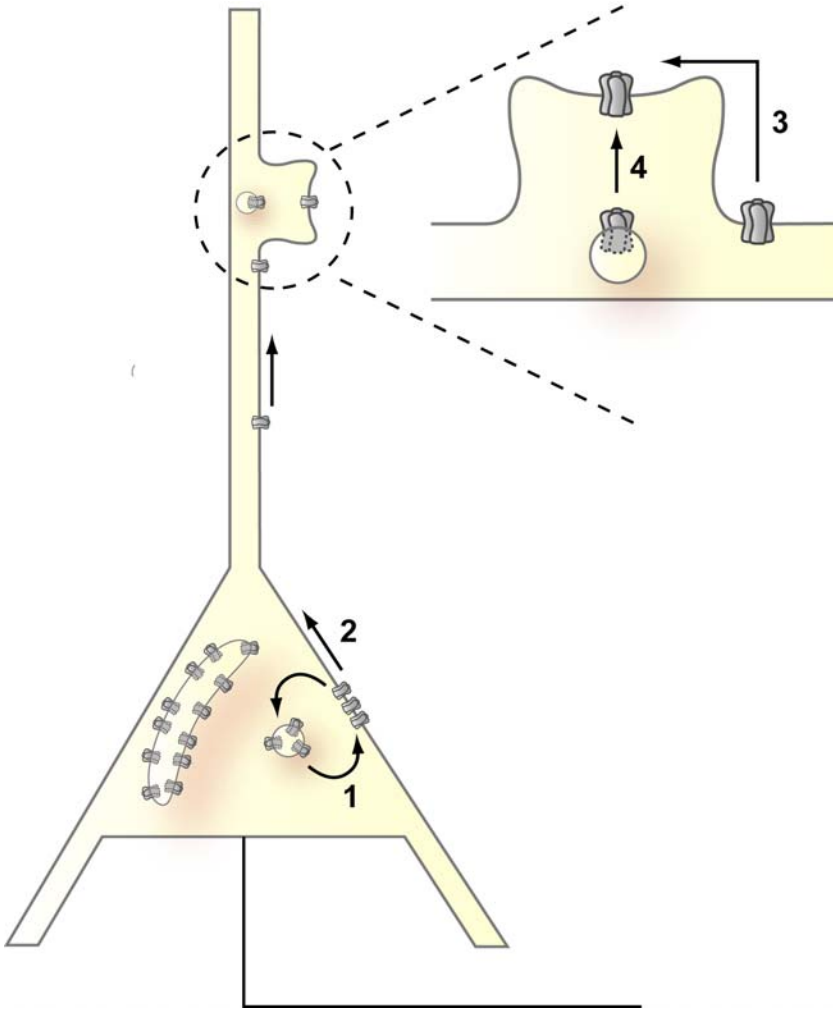


Figure 7. A model of basal AMPA receptor trafficking.

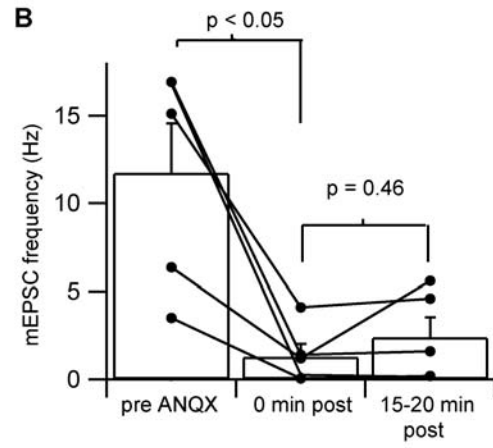
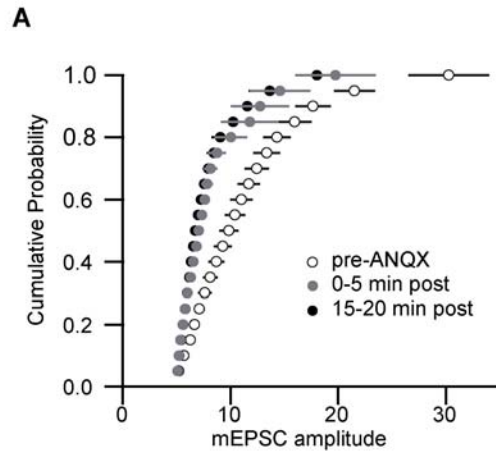
A large intracellular pool of AMPA receptors exchanges rapidly (1) with extrasynaptic somatic AMPA receptors, and these newly inserted AMPA receptors then travel laterally (2) out to dendrites to reside stably at synapses. The lateral diffusion of perisynaptic receptors into the synapse may be regulated by accessory synaptic proteins (3). The exchange of intracellular receptors with synaptic receptors is slow (4).



Supplemental Figure 1: Following inactivation with ANQX, AMPA receptor-mediated mEPSCs are reduced in amplitude and in frequency and do not rapidly recover.

(A) Cumulative distributions of mEPSC amplitudes before and 15-20 minutes after ANQX-mediated photoinactivation of surface AMPA receptors (n = 5).

(B) Average frequency of mEPSCs is significantly reduced after photoinactivation, but does not recover within 20 minutes (n = 5).



Supplemental Figure 2: Representative mEPSC traces, recorded in 100 μ M cyclothiazide, at different time points after ANQX-mediated photoinactivation of total surface AMPA receptors.

Pre-ANQX + UV



Post (1 h)

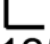


Post (6 h)



Post (16 h)



10 pA  125 ms

Chapter 4

Stargazin Modulates AMPA Receptor Trafficking and Gating by Distinct Domains

Introduction

Most excitatory synapses in brain use glutamate as a neurotransmitter. The three major classes of glutamate-gated ion channel receptors, AMPA, kainate, and NMDA types, subserve distinct functions (Hollmann et al., 1994; Nakanishi, 1992). The AMPA-preferring glutamate receptors – which are also sensitive to kainate – are monovalent cation channels and mediate most of the postsynaptic depolarization that induces neuronal firing. High-affinity kainate-preferring receptors also participate in glutamatergic transmission at a subset of synapses. NMDA receptors are permeable to calcium as well as monovalent cations. Calcium influx through NMDA receptors induces synaptic plasticity by changing the number of synaptic AMPA receptors. Because alterations in synaptic AMPA receptor trafficking underlie synaptic plasticity and provide a mechanism for information storage in brain, intensive studies have addressed protein interactions with AMPA receptors (Barry and Ziff, 2002; Brecht and Nicoll, 2003; Malinow and Malenka, 2002; Sheng and Kim, 2002; Song and Huganir, 2002).

The four pass transmembrane protein stargazin traffics AMPA receptors (Chen et al., 2000b; Hashimoto et al., 1999). Stargazin is mutated in stargazer mice (Letts et al., 1998b), which show absence epilepsy and a lack of functional AMPA receptors in cerebellar granule cells (Chen et al., 1999; Chen et al., 2000b; Hashimoto et al., 1999). Although AMPA receptor function is normal in forebrain of stargazer mice, three related transmembrane AMPA receptor regulatory proteins (TARPs) expressed in forebrain can also traffic AMPA receptors (Tomita et al., 2003). To date, effects of stargazin on AMPA receptor function has been interpreted in terms of trafficking alone. We report

here that stargazin functions akin to auxiliary subunits of voltage-dependent calcium channels(Arikkath and Campbell, 2003; Catterall, 2000) and controls both receptor trafficking and channel properties. By controlling AMPA receptor opening, stargazin shapes the postsynaptic currents that determine excitatory transmission.

Results

Stargazin and related TARPs greatly increase glutamate-evoked currents from oocytes injected with limiting amounts of GluR1 (Chen et al., 2003; Tomita et al., 2004) (Fig. 1a). They do this by greatly increasing the current evoked for a given amount of expressed GluR1, such that GluR1 levels that exhibit no current on their own, evoke near maximal current in the presence of stargazin (Fig. 1a). To further quantify this effect, we measured glutamate-evoked currents in oocytes injected with varying amounts of stargazin and GluR1. Injection of GluR1 cRNA in large amounts (1 or 20 ng) yielded large currents whereas injection of 0.1 ng of GluR1 cRNA produced minimal glutamate-evoked currents (Fig. 1b). Addition of stargazin cRNA increased currents from oocytes co-injected with 0.1 ng GluR1 cRNA yielding currents similar to those observed with 20 ng GluR1 alone (Fig. 1b). To determine whether stargazin influences both receptor trafficking and channel properties, we developed an assay to measure these effects independently. To study trafficking, we engineered an HA epitope into the extracellular region of GluR1-flip and quantified surface expression by chemiluminescence(Zerangue et al., 1999). We detected decreasing GluR1 surface expression and glutamate-evoked currents in oocytes injected with 2, 1 or 0.1 ng GluR1 cRNA (Fig. 2a). As shown above, co-injection of stargazin cRNA greatly potentiated glutamate-evoked currents. Remarkably, the stargazin-mediated increase in glutamate-evoked currents was much

greater than was the increase in GluR1 surface expression (Fig. 2a). This indicated that stargazin increases the steady-state current / surface receptor ratio and has an effect on GluR1 function independent of trafficking.

We next compared the effects of stargazin on responses to the partial agonist, kainate. In oocytes, co-injecting stargazin with 0.1 ng GluR1 cRNA increased receptor surface expression by ~10 fold (Fig. 2b) but increased the kainate-mediated response by ~70 fold (Fig. 2b). In GluR1 injected oocytes, the absolute magnitude of kainate-evoked current was less than that of glutamate-evoked current (Fig. 2c, d). However, co-injection of stargazin with GluR1 greatly increased the efficacy of kainate (Fig. 2c, d). Cyclothiazide potentiates glutamate-induced currents from AMPA receptors by blocking receptor desensitization (Ito et al., 1990). With GluR1 alone, currents elicited by glutamate + cyclothiazide were much greater than those produced by kainate. In oocytes expressing stargazin, kainate-induced currents were almost as large as those generated by glutamate + cyclothiazide (Fig. 1c). Stargazin potentiated kainate responses to both flip and flop alternatively spliced versions of GluR1 and to GluR1 / GluR2 heteromers (Fig. 2d). In outside-out patches from hippocampal neurons, AMPA receptor-mediated steady state currents elicited by kainate were much larger than those by glutamate (Fig. 2d), which resembles the results with stargazin in expression systems.

We asked whether the effects of stargazin might reflect major changes in agonist affinity. However, we did not find a dramatic difference in the EC_{50} for glutamate or kainate by co-injection of stargazin with GluR1 (Fig. 2e). In addition to stargazin, three related TARPs can also traffic AMPA receptors in neurons (Tomita et al., 2003). We

found that these other TARPs, γ -3, γ -4 and γ -8 all increased the relative efficacy of kainate (Fig. 2f) whereas γ -5, a homologue that does not traffic AMPA receptors, was inactive. The effects of stargazin and γ -3 were greater in magnitude than are those of γ -4 and γ -8 (Fig. 2f). We also found that stargazin does not change the I-V relationship for GluR1-flip or GluR1-flip/GluR2 flip AMPA receptors (Supplementary figure).

As our previous work showed that both extracellular and intracellular determinants in stargazin interact with AMPA receptors (Tomita et al., 2004), we asked whether these regions might differentially control AMPA channel properties and trafficking. The ratio of kainate and glutamate-evoked currents (relative kainate sensitivity) now provided a simple assay independent of absolute currents to evaluate the effect of stargazin on AMPA receptor channel properties. To exploit this, we constructed stargazin mutants in which specific domains were replaced by those from γ -5, which is structurally similar to stargazin (Tomita et al., 2003), but does not enhance glutamate-evoked currents (Fig. 3a). We co-injected cRNAs for these chimeras with GluR1-flip and monitored, in parallel, receptor trafficking and relative kainate sensitivity to separate pharmacological change from receptor trafficking (Fig. 3a). AMPA receptor preference for kainate was abolished by mutating the extracellular loop of stargazin even though this change did not interfere with receptor trafficking (Fig. 3a, “Ex1”). Conversely, swapping out the cytoplasmic domain prevented stargazin’s enhancement of receptor trafficking but preserved relative kainate selectivity (Fig. 3a, “Cyto”). These data indicate that stargazin’s effects on AMPA receptor agonist efficacy and trafficking are separable – the first extracellular loop of stargazin controls channel properties, whereas stargazin’s cytoplasmic tail mediates receptor trafficking.

To determine whether these domains are sufficient for stargazin's effects on AMPA receptors, we made the converse chimeras by swapping domains of stargazin into γ -5 (Fig. 3b). Although a chimera containing only the first extracellular loop of stargazin was inactive (Fig. 3b, "2Ex1"), replacing this loop and the flanking transmembrane domains produced currents with relative kainate sensitivity that resembled the influence of wild type stargazin (Fig. 3b, "2TM1Ex1TM2"). This rescue required the first extracellular domain and the second, but not the first, transmembrane domain of stargazin (Fig. 3b, "2Ex1TM2"). On the other hand, we found that swapping in just the cytoplasmic domain of stargazin selectively rescues receptor trafficking but not relative kainate sensitivity (Fig. 3b, "2Cyto"). Finally, combining the first extracellular loop and second transmembrane domain with the cytoplasmic region reconstitutes both receptor trafficking and relative kainate sensitivity (Fig. 3b, "2Ex1TM2Cyto"), which demonstrates that these domains are necessary and sufficient for stargazin's actions.

To evaluate whether stargazin's potentiation of steady-state current / surface AMPA receptor ratio results from changes in desensitization, we employed a fast glutamate perfusion system. We found that stargazin slowed GluR1 desensitization and deactivation of both GluR1 flip and flop forms (Fig. 4a-d). The first extracellular loop of stargazin mediates these effects on receptor kinetics, as the Ex1 chimera had minimal effects on desensitization or deactivation (Fig. 4a-d). Stargazin does not influence AMPA receptor recovery from desensitization (Fig. 4e, f).

Stargazin also slowed desensitization of GluR4 in patches from transfected tsA201 cells (Fig. 5a, b). GluR4 shows larger steady-state currents than GluR1 (Robert and

Howe, 2003) and allowed us to quantify steady state glutamate evoked currents. Consistent with data from figure 2, we found stargazin quadrupled the relative size of the steady-state current (GluR4 alone, $0.8 \pm 0.1\%$; GluR4 + stargazin, $3.3 \pm 0.9\%$ of the peak current amplitude, $n = 6$ and 3 , respectively: $P < 0.05$). Thus stargazin reduces steady state desensitisation. However, our experiments with CTZ (Fig. 1 and 2) indicate that changes in desensitization cannot account for the dramatic enhancement of the steady state current / surface receptor ratio.

To determine the mechanism for stargazin's effects, we recorded single channel activity in patches from GluR4 transfected tsA201 cells. The patches gave peak currents of 20 to 40 pA (at -100 mV) and likely contained 10-20 channels. Single-channel openings could be distinguished late in the applications, and stargazin increased the frequency of these openings (Fig. 5c, d). Conductance levels and apparent open and shut times were analyzed in records containing single-channel currents ($n=6$ patches). Four discrete open levels were seen in all records. Without stargazin, most openings were to conductance levels of 9 and 20 pS (8.7 ± 0.7 pS, 19.5 ± 1.2 pS), with rare openings to larger levels (31 ± 1.2 pS and 44.8 ± 2.6 pS). Stargazin did not significantly alter the conductance levels but dramatically increased the frequency of openings to larger levels (Fig. 5e). Stargazin increased the occupancy of the largest conductance level ~ 7 fold (Fig. 5e). The two smallest levels seen here are similar to the largest levels seen in some previous work on recombinant AMPA receptors (Banke et al., 2000; Jin et al., 2003; Swanson et al., 1997), and levels close to our third level have been seen for GluR1 and GluR2 channels (Derkach et al., 1999; Mansour et al., 2001). Our largest open level has not been seen in previous studies of recombinant channels lacking stargazin; however, a

similar large level was found in work on native receptors (Smith et al., 2000; Wyllie et al., 1993)

Stargazin did not alter open times or durations of brief shuttings significantly. Mean dwell times for the four open levels were between 0.7 ms to 1.1 ms and did not differ significantly with or without stargazin. However, stargazin prolonged channel activations. To quantify this, bursts were defined as a series of openings (to any level) that were separated by shuttings shorter than a critical duration (< 2.5 to 3 ms for the various patches). Distributions of the durations of these bursts were fitted to estimate mean burst length (Fig. 5f). Two exponential components were detected in the distributions, and stargazin prolonged burst length (Table 1). The stargazin-mediated increases in large conductance openings (Fig. 5e) and burst lengths (Table 1) provide an explanation for the potentiation of steady-state currents (Figs. 2, 5a, b).

Several mechanisms might explain the effects of stargazin on channel kinetics. Delayed glutamate dissociation or altered rates of channel gating could account for the slower deactivation. Delayed entry into desensitization would both slow current decay and increase the duration of bursts. Of these possible mechanisms, only an increased rate of channel opening would slow both deactivation and desensitization, increase both burst duration and amplitude of steady-state currents (with no effect on apparent open times), and have no effect on recovery. Therefore, we conclude that stargazin alters AMPA receptor kinetics by increasing the rate constant for channel opening.

To determine whether the stargazin-mediated effects on AMPA receptor biophysics has physiological relevance, we took advantage of the Ex1 stargazin- γ -5 chimera that mediates receptor trafficking but does not slow receptor desensitization and deactivation (Fig. 4c, d). We reasoned that this chimera, when expressed in neurons, would replace the endogenous TARP and disrupt its effects on channel properties. We infected hippocampal pyramidal cells with a virus driving expression of the Ex1 chimera and monitored AMPA-receptor mediated synaptic transmission. The chimera dramatically accelerated the decay of miniature EPSCs (mEPSCs) (Fig. 6a, b) and also decreased the peak amplitude of these currents (Fig. 6a, c), whereas stargazin did not (data not shown). The reduction in mEPSC amplitude is an under-estimate of the true effect because in Ex1 infected cells many more events fell below detection threshold, as demonstrated by the decrease in apparent frequency (average inter-event intervals for uninfected cells = 1.7 ± 0.3 s, $n = 17$; Ex1 infected cells = 4.6 ± 1.1 s, $n = 13$ $p < 0.05$).

To quantify the effect of Ex1 overexpression on AMPA-receptor mediated synaptic currents more accurately, we compared evoked EPSCs in an infected cell and a neighboring control cell. The chimera decreased both the peak amplitude of the AMPA EPSC (Fig. 6d, e) and the charge transfer mediated by AMPA receptors (uninfected = 2.2 ± 0.8 pC, $n = 8$; Ex1 infected = 0.7 ± 0.2 pC, $n = 8$, $p < 0.05$; data not shown). Although we detected no obvious difference in the decay of the evoked EPSCs, in both groups the kinetics of the evoked EPSC (uninfected: rise time = 7.8 ± 1.3 ms, decay = 11.5 ± 1.4 ms, $n = 9$, Ex1 infected: rise time = 8.4 ± 0.8 ms, decay = 11.5 ± 0.9 ms, $n = 9$) were considerably slower than that for the mEPSC (uninfected: rise time = 2.6 ± 0.2 ms, decay = 6.8 ± 0.7 ms, $n = 14$; Ex1 infected: rise time = 2.1 ± 0.2 ms, decay = 5.3 ± 0.3 ms, $n = 10$), presumably

due to asynchronous release, which will obscure the decay kinetics observed with individual quanta. As a control, the Ex1 chimera had no effect on the NMDA receptor component of the EPSC in these experiments (Fig. 6d, f). These results indicate that the ectodomain of stargazin controls the strength and kinetics of synaptic transmission at central synapses.

Discussion

This study demonstrates that stargazin not only mediates AMPA receptor trafficking, but also controls the channel's biophysical properties. Analysis of mutants shows that the stargazin C-terminal tail dictates AMPA receptor trafficking whereas the ectodomain of stargazin influences channel gating. Disrupting stargazin ectodomain interactions alters the size and shape of hippocampal EPSCs indicating that stargazin serves as a functional AMPA receptor auxiliary subunit at the synapse. The discovery of an auxiliary subunit that controls the gating of a mammalian ionotropic receptor is unprecedented; however, the transmembrane protein SOL-1 may similarly function as a necessary subunit for the glutamate-gated channel GLR-1 in *C. elegans* (Zheng et al., 2004).

The role of the stargazin C-terminal tail in trafficking suggest that interactions of stargazin and AMPA receptor subunits with cytoplasmic proteins regulate receptor surface expression. Numerous cytosolic proteins have been shown to bind to AMPA receptors (for reviews see (Barry and Ziff, 2002; Bredt and Nicoll, 2003; Malinow and Malenka, 2002; Sheng and Kim, 2002; Song and Huganir, 2002)). However, these

cytoplasmic partners all show specificity for interaction with specific AMPA receptor subunits. For example, SAP-97 interacts only with GluR1, and PICK1/GRIP1 bind only to GluR2/3. By contrast, stargazin traffics all AMPA receptor subunits (Tomita et al., 2004), so stargazin's actions are likely to be independent of these previously reported proteins.

The mechanism by which stargazin increases the efficacy of kainate on AMPA receptors remains uncertain. Structural studies of the isolated GluR ligand-binding core indicate that agonists induce closure of the clamshell shaped binding site and that this movement gates the channel. Whereas glutamate induces a large conformational change and serves as a full agonist, kainate causes much less movement and acts as a partial agonist (Armstrong and Gouaux, 2000b). Analysis of a series of partial agonists showed that the GluR2 ligand-binding core takes on a range of conformational states that control the probability of opening to discrete sub-conductance states (Jin et al., 2003). That stargazin makes kainate a more efficacious agonist suggests that stargazin's interactions with the ligand-binding core enhances kainate-induced domain closure. This proposal may explain why kainate evokes only small conductance openings on heterologously expressed GluR4 (Swanson et al., 1997), whereas kainate produces much larger openings of GluR4 in cerebellar granule cells, which express stargazin (Wyllie et al., 1993). Structural studies of stargazin / AMPA receptor complexes will be necessary to address this issue directly.

Our finding that stargazin increases glutamate-induced large-conductance openings and burst length suggests that stargazin further increases the efficacy for glutamate.

These single-channel results, together with the effects of stargazin on desensitization and deactivation, indicate that stargazin's augmentation of burst length reflects an increase in the rate constant for channel opening. The modest increase in affinity indicated by the slowed deactivation is presumably within our experimental error for EC_{50} values. However, a small change in affinity cannot explain the massive influences of stargazin on AMPA receptor function. The molecular basis for these effects will also require future structural studies of the stargazin / AMPA receptor complex.

Action potential firing in central neurons is determined by the magnitude and coincidence of synaptic inputs, and depends in large part on synaptic AMPA receptor number and properties. Previously, we found that stargazin's interaction with PSD-95 controls synaptic AMPA receptor number (Schnell et al., 2002b). Here, we demonstrate that stargazin also modulates the channel's biophysical properties, and thereby increases the magnitude and slows the decay of AMPA receptor-mediated synaptic currents. Based on our results with the Ex1 chimera on native synaptic AMPA receptors, these stargazin-mediated effects result in a threefold increase in the net charge movement for a given quantum of synaptically released glutamate. These effects of stargazin, as well as the established effects of distinct AMPA receptor isoforms and splice variants, (Geiger et al., 1995; Jonas, 2000) influence neuronal firing in response to synaptic input. The differential expression of TARP isoforms in discrete neuronal populations (Tomita et al., 2003) may contribute to synapse-specific timing, as different isoforms differ in their ability to modify AMPA receptor function (see Fig. 2e). Future studies of recombinant GluR subunits will require inclusion of appropriate TARPs to model the kinetics of AMPA receptors *in vivo*.

This work also has relevance to the therapeutic pharmacology of AMPA receptors. Over-activation of AMPA receptors may contribute to neurodegenerative diseases(Koh et al., 1990). Modulation of the TARP / AMPA receptor interaction offers a novel target for down regulating the receptors. On the other hand, reagents that limit AMPA receptor desensitization – AMPA receptor potentiators – show promise as cognitive enhancers (Lynch et al., 1997; Staubli et al., 1994) and may also be effective in treating schizophrenia and other mental disorders(Goff et al., 2001; O'Neill et al., 2004). Regulation of the ectodomain interaction of TARPs with AMPA receptors should provide an approach for these neurological disorders.

Figure 1. Stargazin enhances glutamate-evoked currents from oocytes injected with limiting amounts of GluR1. Oocytes were injected with GluR1 flip (GluR1i) and stargazin (STG) cRNAs as indicated and responses to 5 μ M glutamate + 50 μ M cyclothiazide were recorded. **(A)** Addition of stargazin cRNA enhances currents from oocytes co-injected with varying amounts of GluR1 cRNA. **(B)** Injection of GluR1 cRNA in large amounts (1 or 20 ng) yields robust currents whereas injection of 0.1 ng of GluR1 cRNA produces minimal glutamate-evoked currents. Addition of stargazin cRNA dose-dependently increases currents from oocytes co-injected with 0.1 ng GluR1 cRNA.

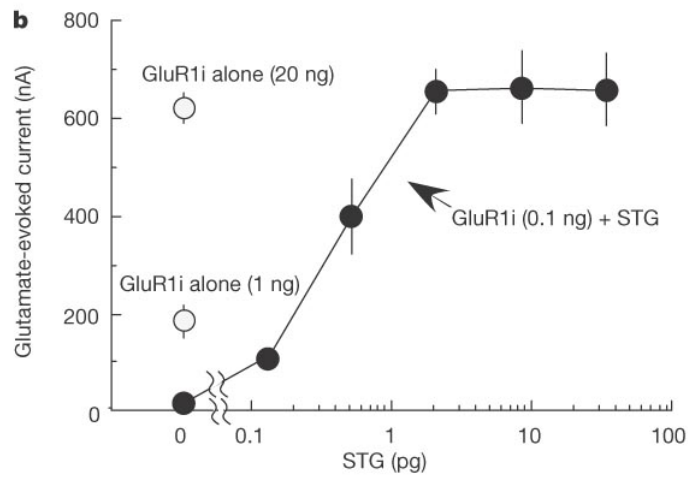
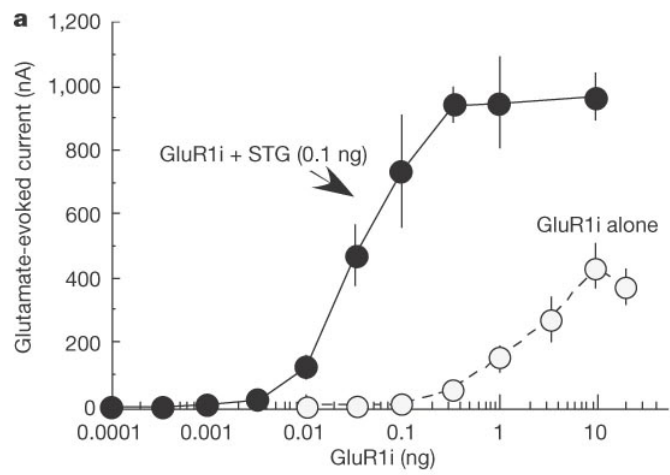


Figure 2. Stargazin not only mediates AMPA receptor trafficking, but also modulates AMPA receptor agonist efficacy. **(A,B)** Oocytes were injected with HA-tagged GluR1-flip (HA-GluR1) and stargazin (STG) or $\gamma 5$ cRNA as indicated. Receptor surface expression and currents evoked by glutamate (10 μM) (I_{Glu}) or kainate (40 μM) (I_{KA}) were quantified in parallel by chemiluminescence ($n = 9$) and two electrode voltage clamp recordings ($n = 5$), respectively. A.U., Arbitrary unit. Stargazin enhances surface expression of limiting amounts (0.1 ng) HA-GluR1 but has a much greater effect on **(A)** glutamate- and **(B)** kainate-evoked currents. **(C,D)** Oocytes injected with GluR1-flip alone (GluR1i) are more sensitive to glutamate (500 μM) than to kainate (500 μM) ($n = 4$). Co-injection of stargazin (STG) with GluR1i enhances kainate sensitivity in oocytes ($n = 4$). With stargazin, the kainate current is nearly as large as that elicited by 500 μM glutamate + 50 μM cyclothiazide (CTZ). **(D)** Stargazin also enhances kainate sensitivity for homomeric GluR1 flop (GluR1o) and heteromeric (GluR1o/GluR2i) AMPA receptors. In outside-out patches from hippocampal neurons, kainate produces larger AMPA receptor mediated (GYKI-53655 sensitive) currents (I_{KA}) than does glutamate (I_{Glu}) ($n = 6$). **(E)** Stargazin does not alter the affinity of GluR1 for glutamate (in presence of CTZ) or kainate. **(F)** Stargazin (STG) and the other TARPs, γ -3, γ -4 and γ -8, all increase kainate efficacy at GluR1 whereas γ -5 does not.

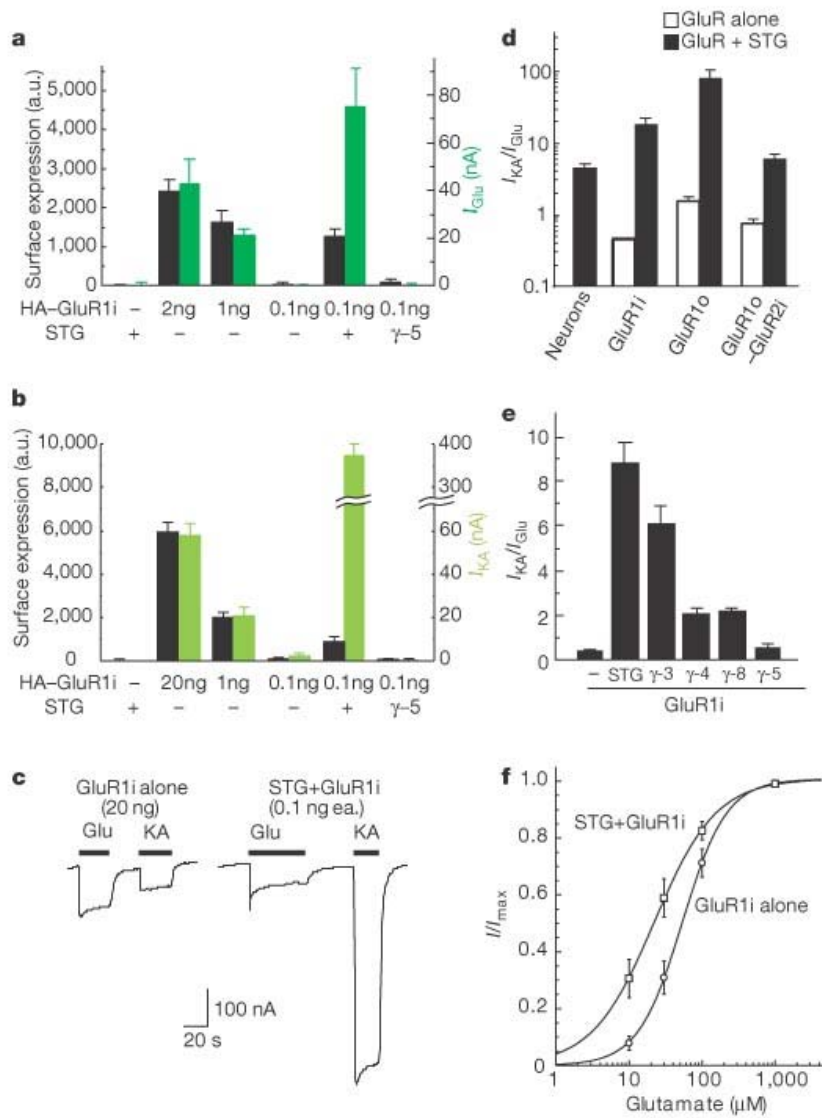
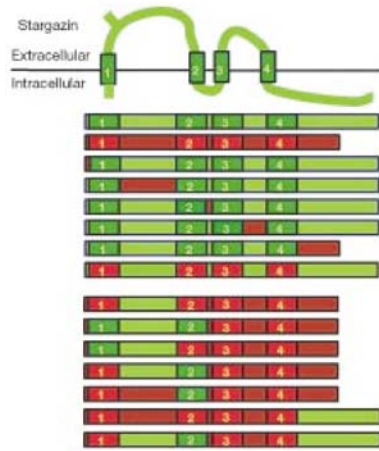


Figure 3. Stargazin regulates AMPA receptor trafficking and agonist efficacy by distinct mechanisms. Oocytes were injected with 1 ng or 0.1 ng GluR1 cRNA and stargazin / γ -5 chimeric constructs as indicated. Receptor surface expression and kainate / glutamate-evoked currents (I_{KA} / I_{Glu}) were quantified in parallel by chemiluminescence and two electrode voltage clamp recordings, respectively. **(A)** Stargazin both enhances receptor trafficking and produces kainate-preferring channels whereas γ -5 is inactive. Replacing the stargazin first extracellular domain with that of γ -5 (Ex1) does not disrupt surface expression but selectively diminishes kainate responses. On the other hand, replacing the cytoplasmic domain of stargazin (Cyto) maintains kainate selectivity but abolishes enhanced receptor trafficking. *(red) different than GluR1+STG, $p < 0.05$). **(B)** Swapping domains into γ -5 shows that the stargazin first extracellular and second transmembrane domains (2Ex1TM2) are sufficient to induce kainate-selective responses. The stargazin cytoplasmic tail (2Cyto) is sufficient to induce receptor trafficking. Combining these regions (2Ex1TM2Cyto) is sufficient to restore both trafficking and pharmacological influences of stargazin. #Kainate induced currents were undetectable. *(green) different than GluR1 alone, $P < 0.05$.

A



B

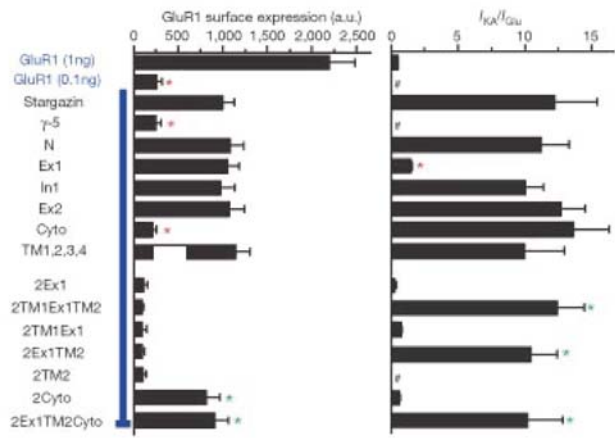


Figure 4. Stargazin slows AMPA receptor desensitization and deactivation.

Superimposed responses of outside-out oocyte patches to 100 ms **(A)** or 1 ms **(B)** applications of glutamate (10 mM) for GluR1 flip alone (GluR1i; black), GluR1i with stargazin (STG/GluR1i; red) or GluR1i with Ex1, $\tilde{\gamma}5$ first extracellular domain in stargazin (Ex1/GluR1i; blue). Open-tip responses recorded at the end of experiments are shown above. Responses are normalized to their peak amplitude to compare their time course. **(C,D)** Stargazin slowed desensitization (τ_{des} ; n = 6) and deactivation (τ_{dea} ; n=5.) for GluR1 flip (GluR1i) and flop (GluR1o), whereas Ex1 did not. (* different than GluR1 alone, $p < 0.01$). All analyzed traces show peak amplitudes between 20 and 400 pA. **(E,F)** Stargazin does not influence recovery from desensitization. Two 1-ms glutamate pulses were applied over varying interpulse intervals to a membrane patch excised from an oocyte expressing GluR1i + STG. **(F)** Recovery from desensitization (τ_{rec}) was determined by plotting the ratios of peak amplitudes for the 1st and 2nd pulses (I_{p2}/I_{p1}) versus the interpulse intervals (n = 4).

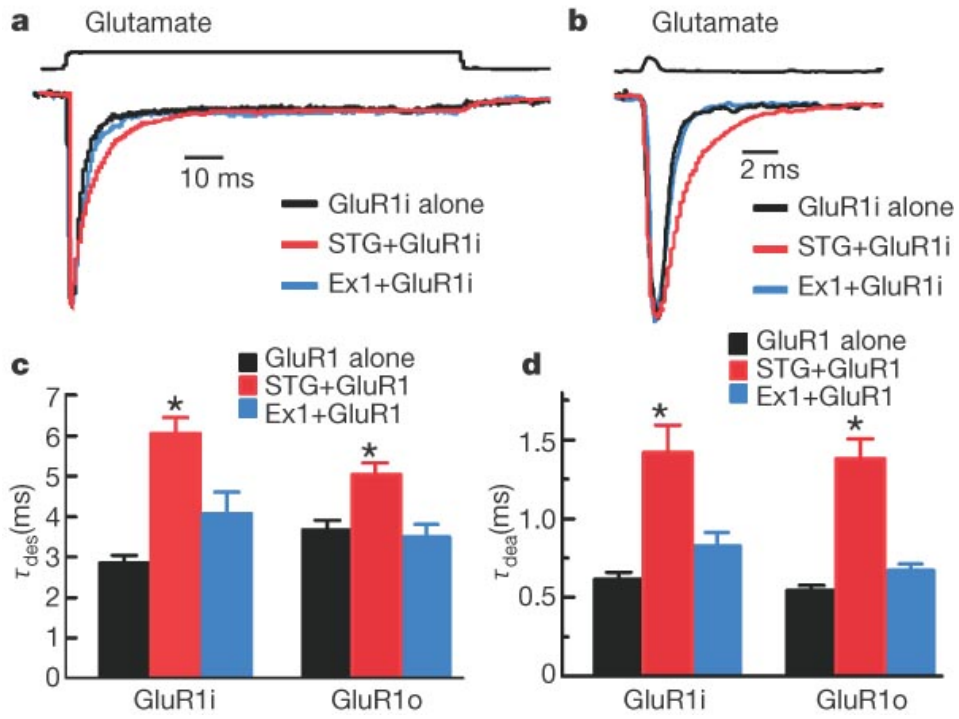


Figure 5. (A,B) Inward currents were averaged from 50 applications of glutamate (10 mM) to patches from transfected cells ($n = 6$ for GluR4 alone; $n = 3$ for STG plus GluR4). The current decay of receptors with stargazin contains two exponential components (dotted lines) with time constants that are slower than the single time constant seen with GluR4 alone. **(C,D)** Examples of unitary inward currents seen during 200-ms applications of glutamate (10 mM) **(C)** 500 applications; **(D)** 1,000 applications). Channel activations are longer in receptors with stargazin. The dotted lines indicate the four open levels detected in each patch. Peak currents were 30–40 pA and are off-scale. **(E)** Plot of the mean percentage of time spent at each of the four open levels for GluR4 alone (open circles; black) and GluR4 with stargazin (filled circles; grey). Error bars indicate s.e.m. for the relative occupancies and conductance levels ($n = 3$). **(F)** Histograms of burst-length distributions from a patch containing GluR4 (left, 610 bursts) and a patch containing GluR4 and stargazin (right, 4,464 bursts). The distributions were fitted (solid line) with two exponential components (dotted lines) (τ_{fast} ; $P < 0.05$, τ_{slow} ; $P < 0.01$). Mean burst length (s.e.m. in parentheses) is indicated for the fast and slow distributions. Note that long bursts are more common with stargazin. The first bin in the stargazin histogram contained 1,012 bursts and is off-scale (see Methods). One burst from the GluR4 patch and 34 bursts from the stargazin patch had durations above 60 ms (off-scale, right).

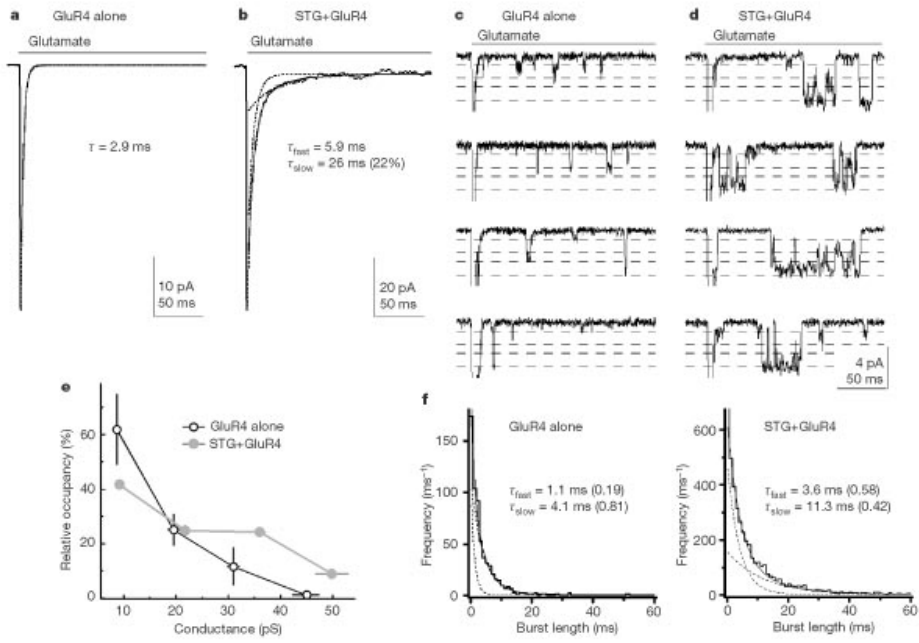
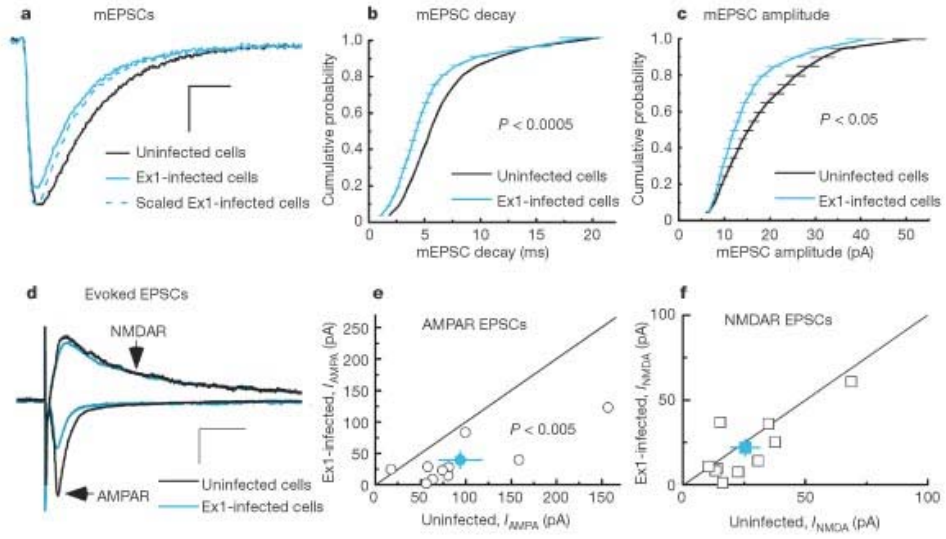


Table 1.

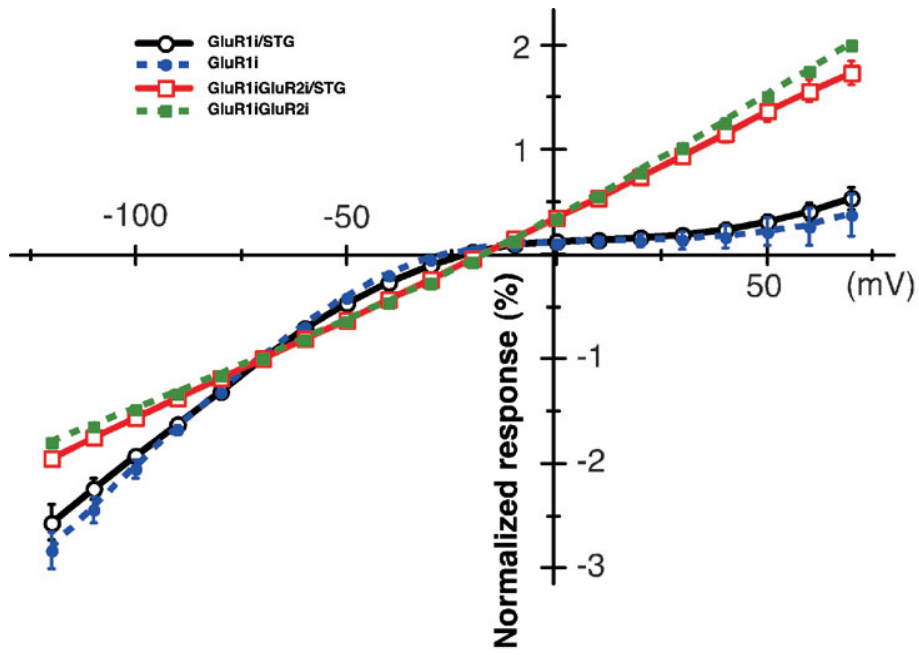
Transfection	τ_{fast} (ms)	Area (%)	τ_{slow} (ms)	Area (%)
GluR4	1.1 ± 0.4	24 ± 10	3.8 ± 0.2	76 ± 10
GluR4 plus STG	3.6 ± 0.3	60 ± 4	12.3 ± 0.5	40 ± 4.0

The results are from three patches each with and without stargazin (STG) (τ_{fast} , $P < 0.05$; τ_{slow} , $P < 0.01$). Bursts were defined and distributions were fitted as described in the Methods.

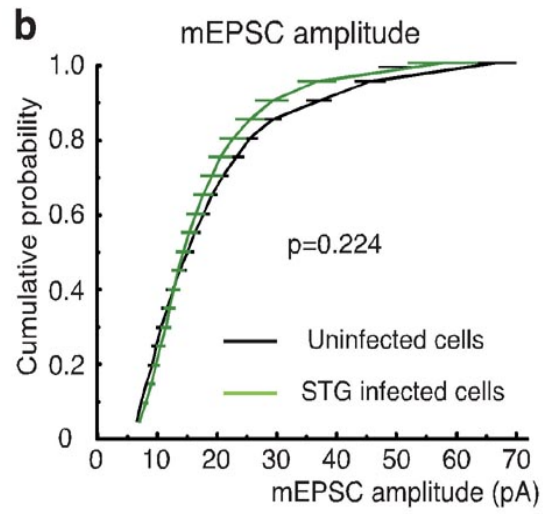
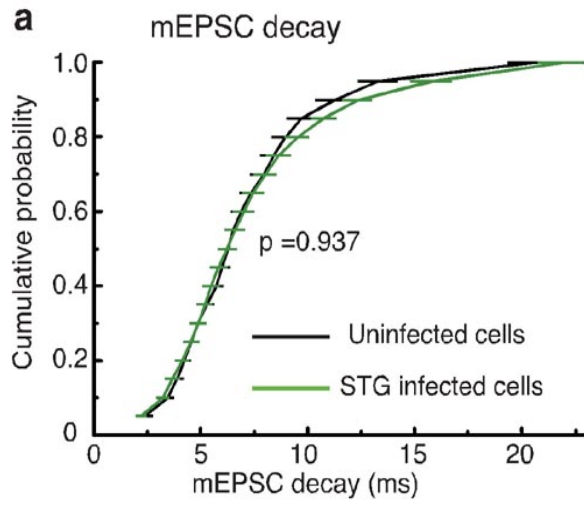
Figure 7. (A) Miniature EPSCs were recorded (in the presence of TTX) from hippocampal CA3 pyramidal cells in slice culture from uninfected (black) or infected (blue) cells expressing the Ex1 chimaera (Ψ -5 first extracellular domain in stargazin). The traces are representative averages of more than 400 individual events in five control and five Ex1-infected cells. Scale bar: 5 pA, 5 ms. (B) Synaptic events were fitted to exponential mEPSC decay times. Cumulative frequency distribution shows that the decay in infected neurons is significantly faster than that in control uninfected cells ($n = 10$ infected and $n = 14$ for control; $P < 0.0005$). (C) Cumulative frequency distribution shows that the amplitude in Ex1-infected neurons is smaller than that in control uninfected neurons ($P < 0.05$). (D) Evoked EPSCs were recorded in hippocampal CA3 pyramidal cells from uninfected (black) and infected (blue) neurons expressing the Ex1 chimaera. Scale bar: 100 pA, 40 ms. (E) The size of the AMPAR EPSC (-60 mV) in uninfected cells was compared with the size of the AMPAR EPSC in neighbouring Ex1-infected cells (ten pairs). Note that all but one of the points falls to the right of the line of unity, indicating a substantial decrease in the AMPAR EPSC in Ex1-infected cells. (F) The NMDAR receptor component was measured at +40 mV and at 100-ms latency, by which time the AMPAR component has decayed to zero. Expression of Ex1 has no effect on the NMDAR EPSC. Points in (E,F) show mean \pm s.e.m. from ten pairs of experiments.



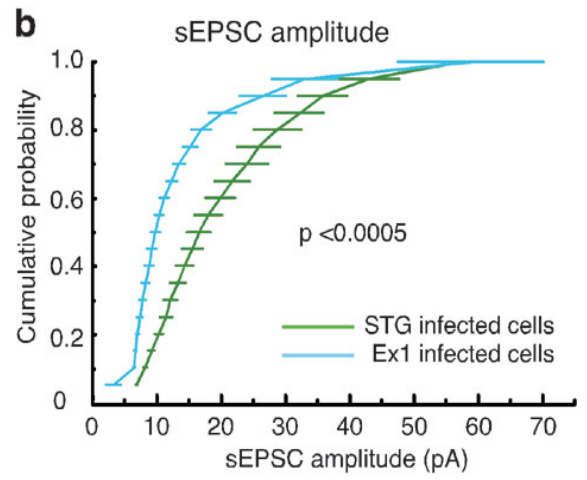
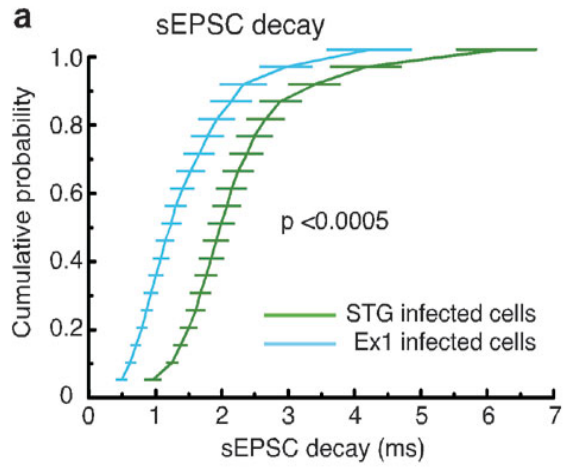
Supplementary figure 1. Stargazin does not change the I-V relationship for homomeric GluR1 flip (GluR1i) or heteromeric (GluR1i/GluR2i) AMPA receptors. Oocytes were injected with GluR1-flip (GluR1i) or GluR1-flip/GluR2-flip (GluR1iGluR2i) with or without stargazin (STG) as indicated. I-V curves for kainate (40 μ M) evoked AMPA receptors currents were recorded (n=5).



Supplementary figure 2. Overexpression of wild-type stargazin does not affect the decay kinetics (**a**) or amplitude (**b**) of hippocampal mEPSCs. Rat hippocampal CA3 pyramidal cells were infected with a Semliki forest virus driving the expression of wild-type stargazin. Infected cells (identified by GFP driven off a separate promoter in the virus construct) had mEPSCs that were indistinguishable from those in nearby uninfected neurons in both peak amplitude ($p = 0.22$) and decay time ($p = 0.94$; $n = 10$ infected, $n = 6$ uninfected).



Supplementary figure 3. The ectodomain of stargazin is necessary to properly restore the time course and amplitude of synaptic currents in *stg* (-/-) cerebellar granules cells. Control, uninfected *stargazer* granule cells exhibited no detectable AMPAR-mediated spontaneous synaptic currents (n = 3, not shown). Expression of either wild-type stargazin (STG) or the mutant Ex1 chimera (Ex1) rescues synaptic currents, but the average decay time (**a**) and amplitude (**b**) of these currents in Ex1 expressing cells are severely reduced compared to those rescued with wild-type stargazin (n = 6 both groups, p < 0.0005).



Chapter 5

Epilepsy-related ligand/receptor complex, Lgi1 and
ADAM22, regulates synaptic transmission

Introduction

Physiological functioning of the mammalian brain involves a finely tuned balance between excitation and inhibition in neural circuits. Upsetting this delicate balance can cause epilepsy, which is a devastating and poorly treated disease. Because many genes that cause epilepsies encode synaptic ion channels, characterization of synaptic protein complexes in rat brain can provide essential insights into molecular mechanisms underlying epilepsy. The postsynaptic density-95 (PSD-95) scaffolding protein at excitatory synapses plays critical roles in synaptogenesis and synaptic plasticity (El-Husseini et al., 2000b; Funke et al., 2005; Kennedy, 2000; Kim and Sheng, 2004; Migaud et al., 1998). PSD-95 contains an array of protein / protein interaction domains, which help organize, AMPA (α -amino-3-hydroxy-5-methyl-4-isoxazole propionic acid) and NMDA (N-methyl-D-aspartate)-type glutamate receptors and cell adhesion molecules at synapses.

Results

Immunoisolation of PSD-95 from rat brain extracts resulted in selective purification of proteins with molecular masses of 95 kDa (p95) and 60 kDa (p60) (Fig. 1A). Mass spectrometry indicated that p95 contained PSD-95 and ADAM22 (Sagane et al., 2005a), and p60 was LGI1 (Chernova et al., 1998; Kalachikov et al., 2002b; Morante-Redolat et al., 2002; Senechal et al., 2005a) (Table S1). Western blotting showed that stargazin (Chen et al., 2000a; Nicoll et al., 2006; Tomita et al., 2005), a transmembrane AMPA receptor (AMPA) regulatory protein, also co-precipitated (Fig. 1B). The recovery of ADAM22, LGI1 and stargazin showed similar efficiency (Fig. 1B, ~10% of

input). In contrast, other reported PSD-95-scaffolding proteins, neuroligin and NR1 were hardly detected under our conditions. The ADAM22 / LGI1 / PSD-95 complex is specific, as PSD-95 and LGI1 quantitatively co-immunoprecipitated with ADAM22 (figs. S1A, 1B and Table S1). Synapse-associated protein 102 (SAP102), another postsynaptic scaffolding protein, did not interact with ADAM22 and LGI1.

We explored the ontogeny of the PSD-95 complex. Silver staining and western blotting showed that the amounts of co-immunoprecipitated ADAM22, LGI1 and stargazin with PSD-95 were very low in embryonic and newborn brain, and increased to reach highest levels in adult (Fig. 1C and 1D). The up regulation of these complexes and the developmental expression of ADAM22 and LGI1 in postnatal week 2-3 (fig. S2A) fit with a role in adult synaptic transmission. This PSD-95 complex containing ADAM22, LGI1 and stargazin was observed in adult cerebral cortex, hippocampus, and cerebellum (figs. S2B and S2C).

All these components of PSD-95 immunoprecipitates are genetically linked to epilepsy. Stargazin is mutated in stargazer mice with absence epilepsy and ataxia (Letts et al., 1998a), and stargazin regulates AMPAR-trafficking and gating as an auxiliary subunit (Chen et al., 2000a; Nicoll et al., 2006; Tomita et al., 2005). LGI1 is a secreted neuronal protein (Senechal et al., 2005a), and its mutations have been found in patients with autosomal dominant partial epilepsy with auditory features (ADPEAF) (Kalachikov et al., 2002b; Morante-Redolat et al., 2002; Steinlein, 2004). ADPEAF is a rare form of familial idiopathic lateral temporal lobe epilepsy characterized by partial seizures with auditory disturbances. ADAM22 shares homology to a large family of transmembrane ADAM metalloproteases but is catalytically inactive (Novak, 2004; Sagane et al., 2005a),

and is considered either a cell adhesion molecule or an orphan receptor (Novak, 2004). ADAM22-deficient mice show cerebellar ataxia and die around two-three weeks after birth because of multiple seizures (Sagane et al., 2005a).

To understand the function of this synaptic complex, we defined the modes for interaction. The C-terminal tail of stargazin binds to the first two PDZ domains of PSD-95 (Schnell et al., 2002a) (figs. S3A and S3B), and we found that one of the ADAM22 splicing variants has a C-terminal PDZ binding motif (-ETSI) that interacts selectively with the C-terminal half containing the third PDZ domain of PSD-95 (fig. S3B). LGI1 has an N-terminal signal sequence (Fig. 2A) and is secreted from transfected hippocampal neurons (fig. S6C) and from transfected HEK293 cells (Bermingham et al., 2006; Senechal et al., 2005a) (fig. S4A) as an oligomer (fig. S4C). As PSD-95 occurs on the inner surfaces of postsynaptic membranes, extracellular LGI1 must interact with a transmembrane protein in the PSD-95 complex. Using cDNA transfection, we found that ADAM22, but not stargazin, specifically interacted with LGI1 (Fig. 2B). Furthermore, we found that transfected LGI1, ADAM22, and PSD-95 form a tripartite complex (Fig. 2C). As further evidence for this interaction, we stained cells without permeabilization, and found that LGI1 interacts specifically with ADAM22 on the cell surface, indicating that secreted LGI1 binds to the ectodomain of ADAM22. As expected, our extracellular domain binding assay readily detects the interaction of Slit2 with its receptor Robo2 (Brose et al., 1999) (Fig. 2D).

LGI1 has two structural domains, LRR (leucine-rich repeat) and EPTP (Epitempin) repeat (Scheel et al., 2002; Staub et al., 2002) (Fig. 2A). The LRR domains show high homology to Slit, a repulsive ligand for the Robo receptor (Brose et al., 1999);

the EPTP repeat domain is shared with Mass1/VLGR/USH2C, genes that cause audiogenic epilepsy in Fringe mice and Usher syndrome in humans (Scheel et al., 2002; Skradski et al., 2001; Staub et al., 2002; Steinlein, 2004; Yagi et al., 2005) (OMIM 602851). We found the EPTP domain (aa 224-557) mediates LGI1 binding to ADAM22 and that the point mutation (E383A) observed in ADPEAF (Kalachikov et al., 2002b) completely prevents binding (Fig. 2E and fig. S4D). ADAM22 did not interact with another EPTP domain (aa 3194-3530) of Mass1/VLGR/USH2C. We also found that LGI1 bound to ADAM23, the closest homologue of ADAM22, but not to the more distantly related ADAM9 (fig. S5A and S5B). The disintegrin domain of ADAM22 is essential for LGI1 binding as ADAM22(D509N) harboring a mutation in disintegrin domain did not bind to LGI1 (fig. S5A).

To demonstrate directly the receptor / ligand relationship of ADAM22 / LGI1, we constructed a secreted alkaline phosphatase (AP) fusion protein of LGI1 (LGI1-AP). LGI1-AP bound to the surface of cells only when transfected with ADAM22 (Fig. 3A). AP alone and Slit2-AP did not bind to ADAM22-transfected cells. Under the conditions, Slit2-AP specifically bound to Robo2-transfected cells (Brose et al., 1999). To test if the interaction of LGI1 with ADAM22 is stoichiometric, the ADAM22 immunoprecipitate from brain was evaluated by Coomassie blue staining and quantitative western blotting. The stoichiometry of LGI1 binding to ADAM22 was at least 1.0 (figs. S6A and S6B). Furthermore, the secreted LGI1 accumulated with ADAM22 at synaptic puncta in hippocampal neurons, where PSD-95 was localized (figs. S6C and S6D). Taken together, these results imply that secreted LGI1 serves as a specific extracellular ligand for ADAM22 and the Lgi1/ADAM22 complex is scaffolded by PSD-95.

LG11 mRNA is co-expressed with ADAM22 and PSD-95 mRNAs in hippocampus, cerebellum and cerebral cortex (Fig. 3B and fig S7A). Immunohistochemical analysis with a specific antibody (Fig. 3C) showed that ADAM22 protein occurs in hippocampus, cerebellum (Fig. 3D) and cerebral cortex (data not shown). We used the LGI1-AP fusion to detect LGI1 receptor activity directly in brain. LGI1-AP detected high receptor activity in the hippocampus, cerebellar cortex (Fig. 3E and fig. S7B) and cerebral cortex (data not shown). In the hippocampus, the molecular layers of dentate gyrus (DG), CA1 and CA3 regions were labeled. In the cerebellar cortex, labeling occurred in neuropil of the molecular layer and synaptic glomeruli of the granular layer. These regions corresponded to the regions where ADAM22 is expressed. Pre-incubation of LGI1-AP with the soluble extracellular domain of ADAM22 (ADAM22-ED, depicted in Fig. 2A) inhibited the LGI1-AP binding (Fig. 3F and fig. S7B), consistent with ADAM22 being a receptor for LGI1.

Because PSD-95 controls synaptic AMPA receptor number (El-Husseini et al., 2000b), we next asked whether application of LGI1 to hippocampal slices would influence glutamatergic transmission. Incubation of hippocampal slices in LGI1-AP significantly increased the synaptic AMPA/NMDA ratio (Fig. 4A) (control = 0.60 ± 0.046 , LGI1 = 0.90 ± 0.10 ; $n = 23$ for each group, $p < 0.05$); non-tagged LGI1 also showed a similar effect, so we pooled the data. The effects of LGI1 on synaptic currents could be prevented by pre-incubation of LGI1 with ADAM22-ED (Fig. 4A) (ADAM22-ED = 0.59 ± 0.06 , LGI1+ADAM22-ED = 0.65 ± 0.07), suggesting that an interaction between LGI1 and ADAM22 was required for the increased AMPA/NMDA ratio. To determine if LGI1 directly affects the number of synaptic AMPARs, we measured AMPAR-mediated

spontaneous miniature excitatory postsynaptic currents (mEPSCs). LGI1 incubation increased the average amplitude of these events ($n = 17$, both groups, $p < 0.005$), and pre-incubation of LGI1 with ADAM22-ED blocked this increase (Fig. 4B and D). The frequency of spontaneous events was also increased, likely due to the increased detection of enlarged events that now reached threshold (Fig. 4C) ($n = 17$, each group, $p < 0.005$). The relation between presynaptic fiber volley amplitude and the field EPSP (fEPSP) slope in LGI1 treated slices tended to be stronger, but was not significantly different from control ($n=17$ slices each $p=0.66$, data not shown), which is most likely due to the inability of the LGI1 protein to penetrate to the depths of the slice where most of fEPSP originates. Supporting the electrophysiological recording, LGI1 expression significantly increased AMPA receptor surface expression in cultured hippocampal neurons (figs. S8A and S8B).

Might the potentiation of synaptic AMPA currents by LGI1 share a mechanism with long-term potentiation (LTP), an activity dependent process that involves synaptic insertion of AMPARs? To address this, we determined whether LGI1 incubation occludes LTP. No significant change in LTP induction was found between control and LGI1-treated slices (Fig. 4E) (control = $295 \pm 27\%$ $n = 10$, LGI1 = $259 \pm 41\%$ $n = 11$ at 20 minutes after LTP induction, $p = 0.47$), suggesting that LGI1 strengthens excitatory synapses by a mechanism distinct from LTP. Finally, we tested whether LGI1 incubation affects presynaptic properties by measuring paired-pulse facilitation. No difference was found between in control and LGI1-treated groups (Fig. 4F) (control = 1.50 ± 0.46 , LGI1 = 1.58 ± 0.05 , ADAM22-ED = 1.45 ± 0.07 , LGI1+ADAM22-ED = 1.56 ± 0.08 , $p = 0.68$).

Taken together, our data indicate that the effects of LGI1 on synaptic transmission are exclusively postsynaptic.

This study establishes a neuronal ligand-receptor interaction between LGI1 and ADAM22, both of which are genetically related to epilepsy. This study also identifies LGI1 as an extracellular factor that controls synaptic strength at excitatory synapses. Stargazin controls the trafficking and gating of AMPARs, and PSD-95 anchors the AMPAR/stargazin complex at postsynaptic sites (Nicoll et al., 2006). As the ADAM22 and stargazin binding sites on PSD-95 do not overlap, the LGI1/ADAM22 complex may stabilize the AMPAR/stargazin complex on the PSD-95-scaffolding platform (fig. S9). Supporting the idea, ADAM22 interacted with stargazin through PSD-95 (fig. S3C). Very recently, LGI1 was reported to be a subunit of Kv1.1-containing voltage-gated potassium channels and to inhibit channel inactivation by a cytoplasmic regulatory protein, Kv β 1 (Schulte et al., 2006a). As LGI1 is secreted, it remains unclear how it might modulate a cytosolic potassium channel mechanism.

Discussion

This study defines a potentially general mode for protein-protein interaction between EPTP domains and the ectodomain of some ADAM family proteins. LGI4, another member of LGI family, is mutated in *claw paw (clp)* mice, which show hypomyelination throughout their peripheral nervous system (Bermingham et al., 2006). Mice lacking ADAM22 display similar hypomyelination of their peripheral nervous system (Sagane et al., 2005a). Knockouts of *Mass1/VLGR/USH2C*, ADAM23 (Mitchell et al., 2001) or ADAM22 (Sagane et al., 2005a) all display a seizure phenotype. These

phenotypes are consistent with EPTP domain interactions with ectodomains of certain ADAM family proteins. Future binding and structural analysis will be needed to clarify the nature of the EPTP domain / ADAM family interaction.

In this study, we show that secreted LGI1 regulates synaptic transmission through ADAM22. A mutation of LGI1 observed in ADPEAF blocks its secretion (Senechal et al., 2005a)(fig. S4B and S4C) and binding to ADAM22 (Fig. 2E and fig. S4D) and could perturb AMPA receptor regulation. By analogy, epileptic stargazer mice have profound AMPA receptor dysfunction. This epileptic ligand/receptor complex LGI1/ADAM22 could become a therapeutic target for synaptic disorders.

Fig. 1. Identification of a PSD-95–associated protein complex containing ADAM22 and LGI1. **(A)** Immunoprecipitation of PSD-95 from adult rat brain extracts showed a series of bands. Specific bands shared by two independent PSD-95 antibodies were identified by mass spectrometry. p95 (by arrows) contained PSD-95 and ADAM22, and p60 (by arrowheads) was LGI1. A PSD-95 degradation product (p75) is shown with asterisks. IP, immunoprecipitation. **(B)** Western blotting showed that ADAM22, LGI1, and stargazin specifically coprecipitated with PSD-95.

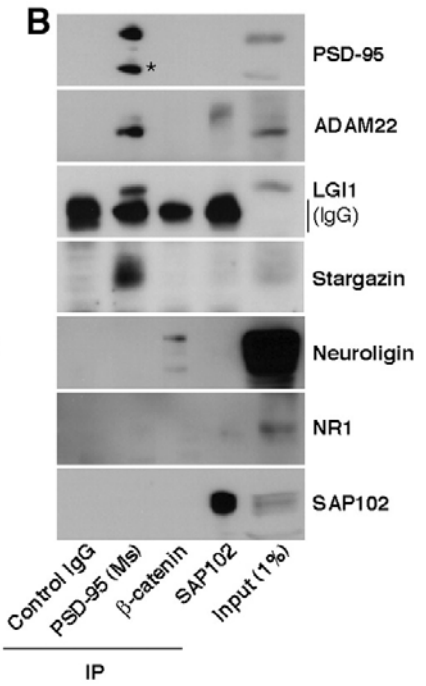
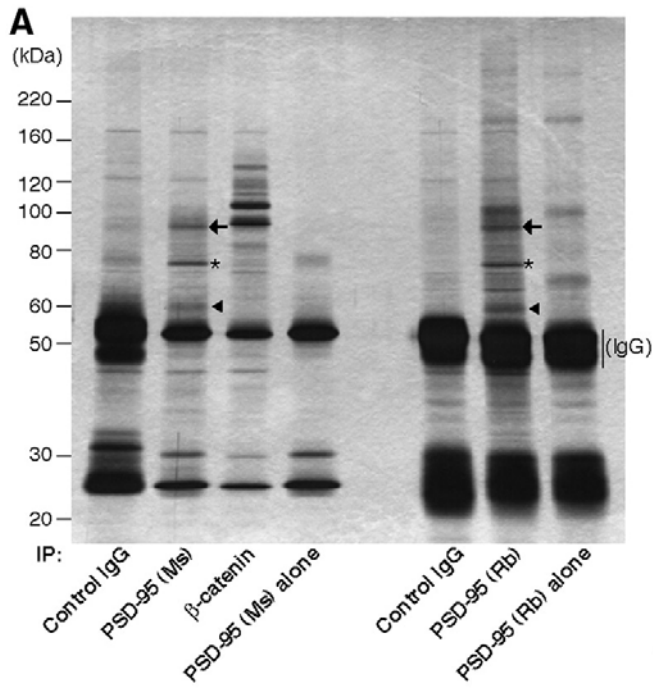


Fig. 2. Tripartite complex formation of PSD-95, ADAM22, and LGI1. **(A)** Domain structures of ADAM22, PSD-95, and LGI1. SS, signal sequence; Pro, prodomain; MP, inactive metalloprotease domain; DI, disintegrin domain; CR, cysteine-rich domain; EGF, EGF-like domain; TM, transmembrane domain. ETSI represents the type I PDZ binding motif of ADAM22. WT, wild type; Δ C4, missing ETSI; ED, extracellular domain; GuK, guanylate kinase domain. LRR, leucine-rich repeat; EPTP, Epitempin repeat; E383A, a point mutant changing Glu (amino acid 383 in the fourth EPTP repeat) to Ala. **(B)** Tripartite complex of PSD-95/ADAM22/LGI1. PSD-95-GFP and ADAM22-HA were cotransfected with or without LGI1-Flag, and PSD-95-GFP was immunoprecipitated (lowest panel, stained by Coomassie brilliant blue). LGI1 indirectly binds to PSD-95 through ADAM22. An arrow and an arrowhead indicate the position of immature and mature ADAM22, respectively. **(C and D)** Interaction between secreted LGI1 and ADAM22 on the cell surface. Indicated cDNAs were cotransfected into COS7 cells. At 24 hours after transfection, surface-bound Flag-tagged proteins (red) were labeled before cell permeabilization, and then HA-tagged proteins were stained (green). The EPTP domain of LGI1 mediates ADAM22 binding. LGI1 E383A, an ADPEAF mutant, failed to bind to ADAM22. Scale bars, 10 μ m.

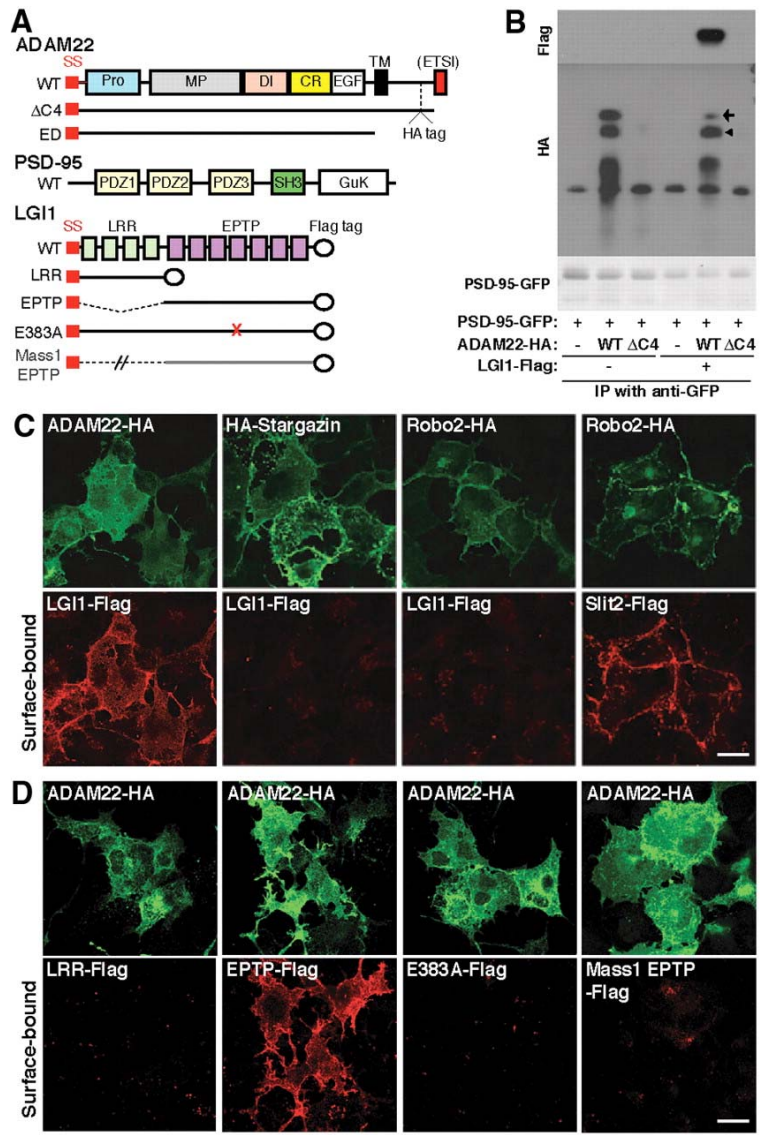


Fig. 3. ADAM22 is a neuronal receptor for secreted LGI1. **(A)** Binding of LGI1-AP to ADAM22-expressing COS7 cells. LGI1-AP or Slit2-AP bound to the cell surface was detected by AP reaction. Scale bar, 20 μm . **(B)** Immunohistochemical staining of ADAM22 in the dentate gyrus (DG) in hippocampus and cerebellar cortex. Mo, molecular layer; Gr, granule cell layer; Pol, polymorphic cell layer; PC, Purkinje cell layer. **(C)** Receptor activity of LGI1 in the hippocampus and cerebellar cortex. Mouse brain sections were treated with conditioned media containing LGI1-AP. LGI1 receptor activity corresponded to the regions where ADAM22 is expressed. **(D)** Preincubation of LGI1-AP with the soluble form of ADAM22 (ADAM22-ED) significantly blocked the LGI1-AP binding in cerebellar cortex. Scale bars in **(B)**, **(C)**, and **(D)**, 50 μm .

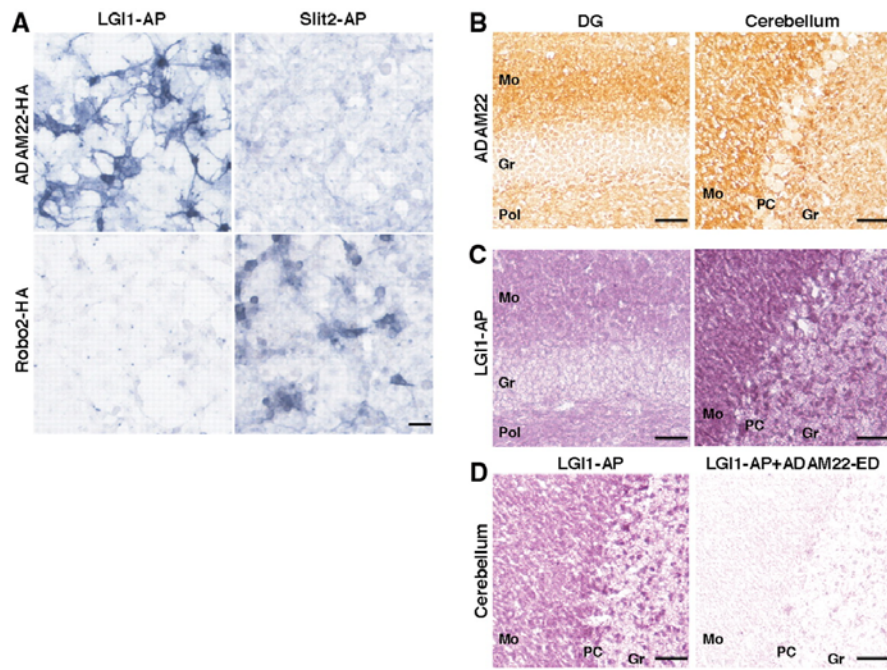


Fig. 4. LGI1 selectively enhances AMPAR-mediated synaptic currents. **(A)** Incubation of slices in buffer containing LGI1 media significantly increased the synaptic AMPA/NMDA ratio ($P < 0.05$), and the effect was blocked by preincubation of LGI1 with the soluble form of ADAM22 (AD22-ED). **(B to D)** Incubation of hippocampal slices with LGI1-containing media increases synaptic AMPA receptor numbers. **(B)** Cumulative distribution plot of mEPSCs from cells in slices incubated in LGI1 as compared with control ($P < 0.005$). **(C)** Cumulative distribution plot of the interevent interval of mEPSCs in the same cells as in **(B)** ($P < 0.005$). **(D)** The increase in mEPSC amplitude by LGI1 was reduced by preincubation with the extracellular domain of ADAM22. **(E)** LGI1 incubation does not alter the magnitude of pairing-induced whole-cell LTP. **(F)** No change in paired-pulse ratio is seen in slices incubated in LGI1, ADAM22-ED, or both ($P = 0.68$).

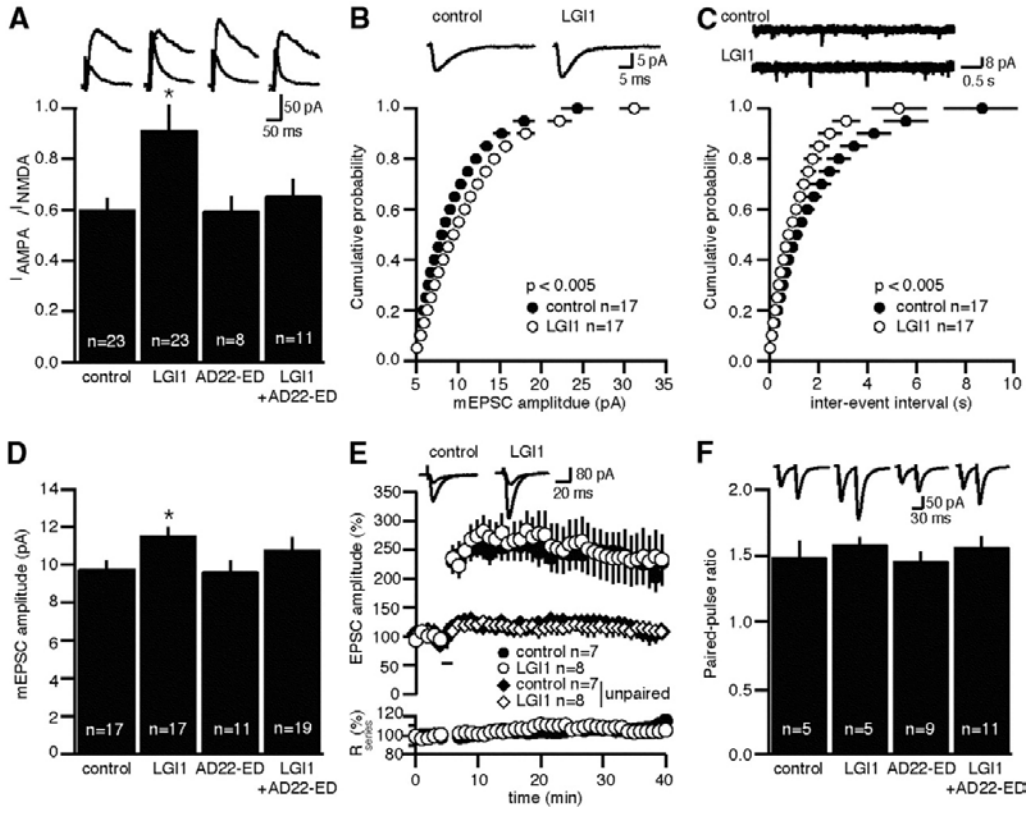


Fig. S1. PSD-95 and LGI1 co-immunoprecipitated with ADAM22. Silver staining with mass spectrometry (A) and western blotting (B) showed that PSD-95 and LGI1, but not SAP102 (**), co-immunoprecipitated with ADAM22. Specific bands shared by anti-ADAM22 and anti-PSD-95 antibodies were identified by mass spectrometry. p95 (by an arrow) contained PSD-95 and ADAM22, and p60 (by an arrowhead) was LGI1. A PSD-95 degradation product (p75) is shown with asterisks (*). IP, immunoprecipitation.

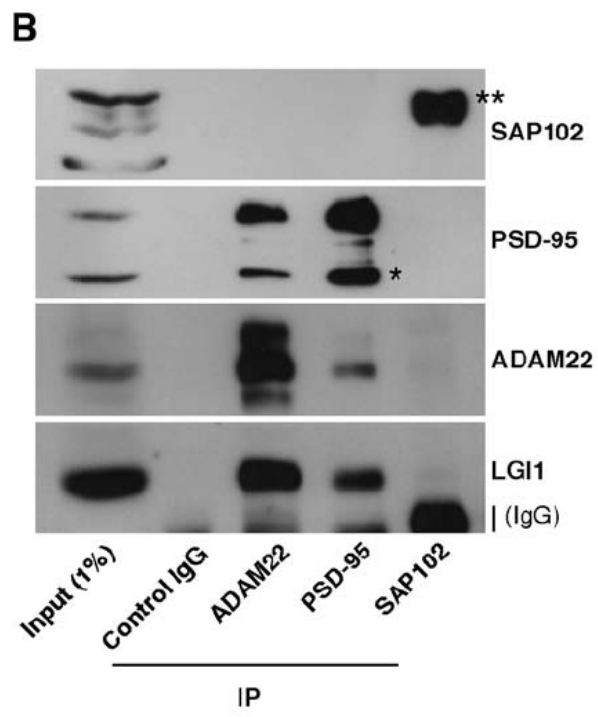
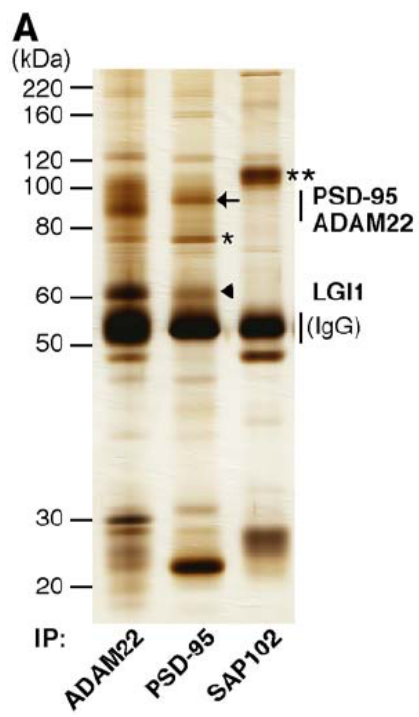


Fig. S2. Developmental change and regional distribution of the PSD-95 immunoprecipitates. (A and B) Developmental change in the PSD-95 immunoprecipitates. Silver staining (A) and western blotting (B) showed that the amounts of ADAM22, LGI1 and stargazin that co-precipitated with PSD-95 progressively increased during animal maturation. (C) Western blotting of various developmental brain extracts (50 μ g total protein each) showed that the amounts of ADAM22 and LGI1 were low in embryonic and neonatal brain, and progressively increased during animal maturation to reach highest levels in adult. E19, embryonic day 19; P2, postnatal day 2; 2W, postnatal week 2. (D and E) ADAM22, LGI1, and stargazin were co-immunoprecipitated with PSD-95 from adult cerebral cortex (Ctx), hippocampus (Hp), and cerebellum (Cb). Whole, whole brain. Arrows, arrowheads and asterisks are as in Fig. S1.

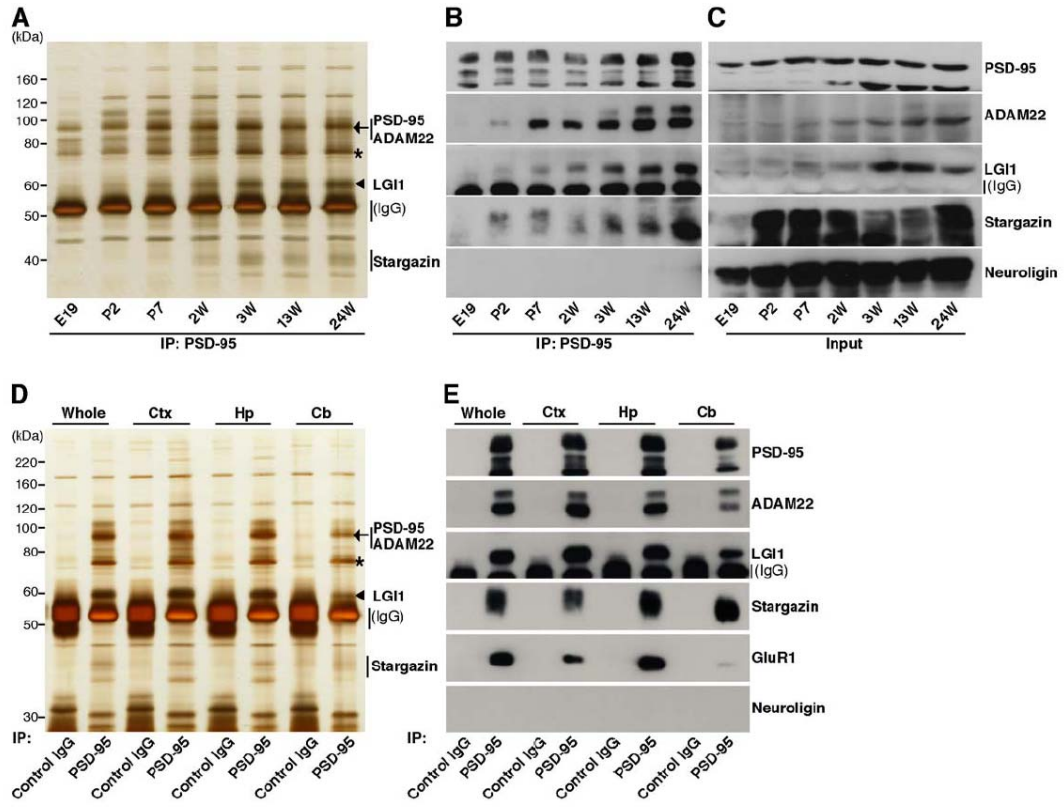
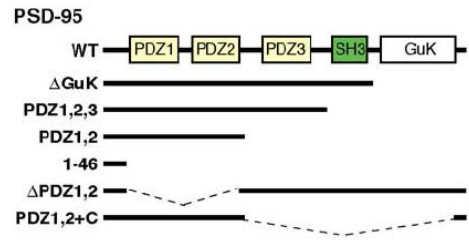
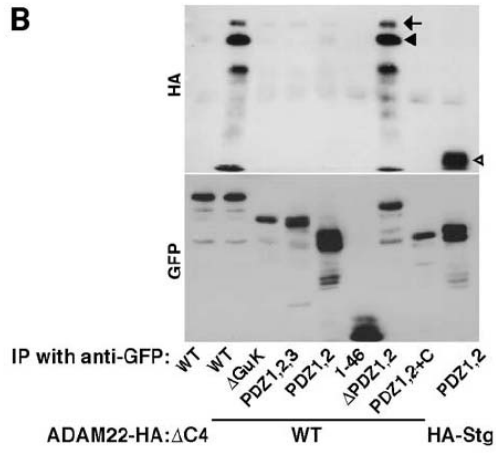


Fig. S3. ADAM22 and stargazin bind different PDZ domains on PSD-95. (A) PSD-95 constructs used are depicted. GuK, guanylate kinase domain. (B) Interaction between ADAM22 and PSD-95. GFP-tagged PSD-95 fragments were co-transfected with HA-tagged ADAM22 or stargazin (Stg) into COS7 cells, and PSD-95-GFP was immunoprecipitated. The immunoprecipitates were analyzed by western blotting with anti-HA and anti-GFP antibodies. An arrow and a closed arrowhead indicate the position of immature and mature ADAM22, respectively. An open arrowhead indicates the position of stargazin. ADAM22 interacted selectively with the C-terminal half containing the third PDZ domain of PSD-95, whereas stargazin bound to the first two PDZ domains of PSD-95. (C) ADAM22-Flag, PSD-95-GFP and HA-stargazin were co-transfected, and ADAM22-Flag was immunoprecipitated. ADAM22 indirectly binds to stargazin through PSD-95.

A



B



C

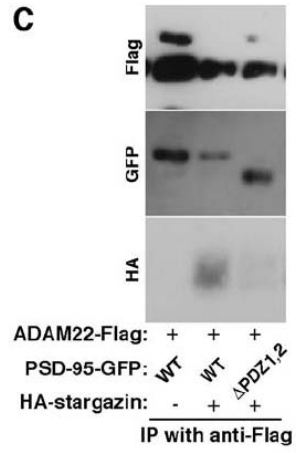


Fig. S4. LGI1 is secreted as an oligomer from transfected HEK293 and binds to ADAM22. (A and B) LGI1, ADAM22 or ADPEAF mutant (E383A) of LGI1 was transfected into HEK293 cells and conditioned media (CM) and cell lysates (Cell) were collected at indicated time. Note that wild type (WT) LGI1, but not ADAM22 and LGI1(E383A), was secreted in the CM. (C) LGI1-HA and LGI1-Flag were co-transfected into HEK293 cells and secreted LGI-Flag was immunoprecipitated from the collected media. Wild-type LGI1-HA was co-immunoprecipitated with LGI1-Flag, indicating that LGI1 is secreted as an oligomer. LGI1(E383A) was not secreted even when wild-type LGI1 was co-expressed. (D) Specific interaction between ADAM22 and LGI1. HA-tagged ADAM22 (AD22) or stargazin (Stg) was co-transfected with LGI1-Flag, and LGI1-Flag was immunoprecipitated. An arrow and an arrowhead indicate the position of immature and mature ADAM22, respectively. (E) The EPTP domain of LGI1 mediates ADAM22-binding, and LGI1(E383A) fails to bind to ADAM22.

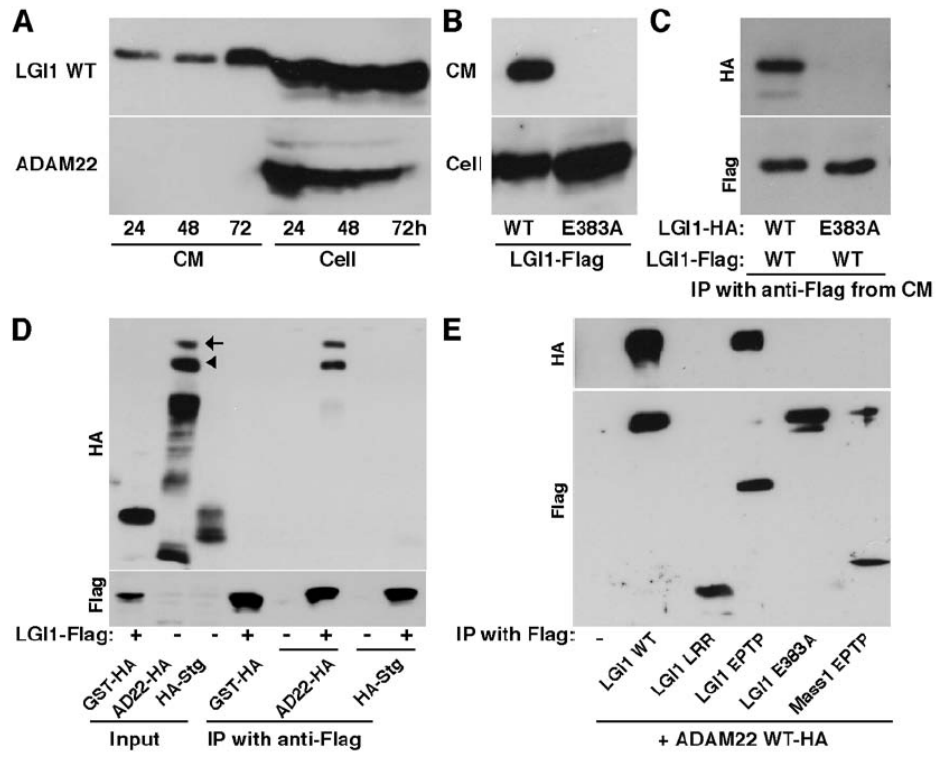


Fig. S5. Specific interaction of LGI1 with ADAM subfamily on the cell surface. (A) Indicated cDNAs were co-transfected into COS7 cells. At 24 h after transfection, the surface-bound LGI1-Flag (red) was labeled before cell permeabilization and then HA-tagged ADAM proteins were stained (green). LGI1 bound to ADAM23, but not ADAM9. ADAM22(D509N) harboring a mutation in disintegrin domain did not bind to LGI1. ADAM22(D509N), a point mutant changing Asp (aa 509) to Asn. Bar: 10 μm . **(B)** Binding of LGI1-AP to ADAM22- and ADAM23-expressing COS7 cells. LGI1-AP bound to the cell surface was detected as described in **Fig. 3A**. Bar: 20 μm .

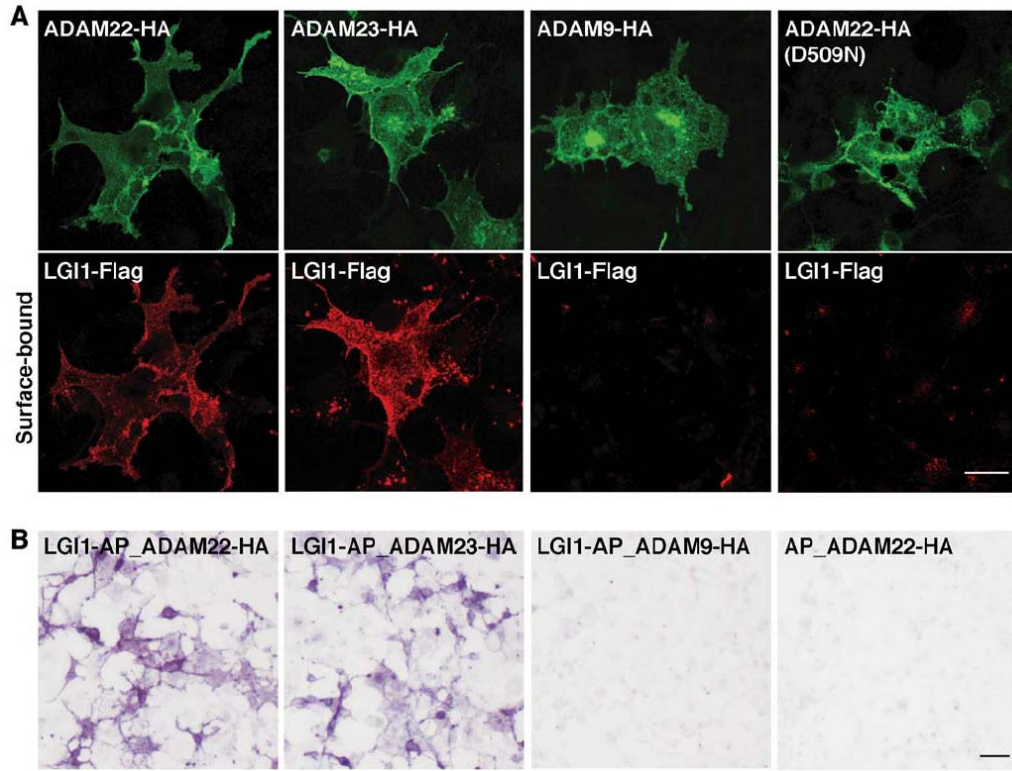


Fig. S6. Interaction of ADAM22 with LGI1 in brain is stoichiometric and constitutive. (A) Immunoprecipitates of brain extracts with an anti-ADAM22 antibody were subjected to SDS-PAGE and stained by Coomassie blue staining. (B) LGI1-AP and ADAM22-ED-AP, which also have 6 x His tags, were normalized by Coomassie blue staining, confirmed by immunoblotting (IB) with anti-His antibody and used as standards. The ADAM22 immunoprecipitates were analyzed with the indicated amounts of ADAM22-ED-AP or LGI1-AP. An arrow and an arrowhead indicate the position of ADAM22 and LGI1, respectively. (C) Interaction between secreted LGI1 and ADAM22 in neurons. Hippocampal neurons transfected with LGI1-Flag and ADAM22-GFP were fixed, and surface-bound LGI1 was stained with anti-Flag antibody. A region of the dendrite is magnified (Right panel). Bars: 10 μ m. (D) ADAM22, but not ADAM22- Δ C4, colocalized with PSD-95 puncta. Bar: 10 μ m.

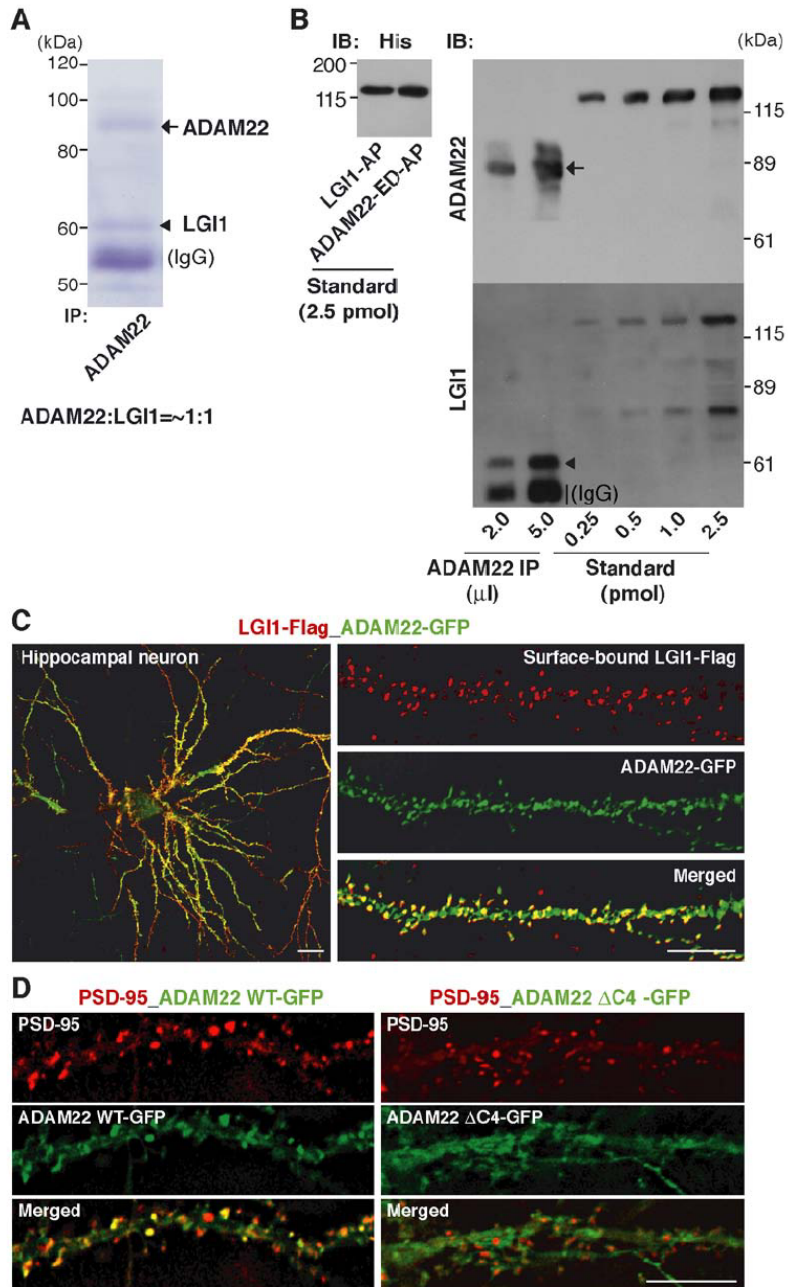


Fig. S7. ADAM22 is a neuronal receptor for LGI1 in brain. (A-C) LGI1, ADAM22 and PSD-95 mRNAs are expressed in overlapping regions of brain. Adult mouse brain parasagittal sections were hybridized with DIG-labeled RNA probes. Regions of hippocampus (B) and cerebellum (C) are magnified. LGI1, ADAM22 and PSD-95 mRNAs were prominent in neuronal populations. Bars: 1 mm in A; 200 μ m in B and C. (D) Antibody to ADAM22 used for immunohistochemistry specifically recognizes a single band in brain tissue. (E) LGI1-AP detected high receptor activity in the CA1 region of hippocampus. Pre-incubation of LGI1-AP with the soluble form of ADAM22 (ADAM22-ED) significantly blocked the LGI1-AP binding. Or, stratum oriens; Py, pyramidal cell layer; Ra, stratum radiatum. Bars: 50 μ m.

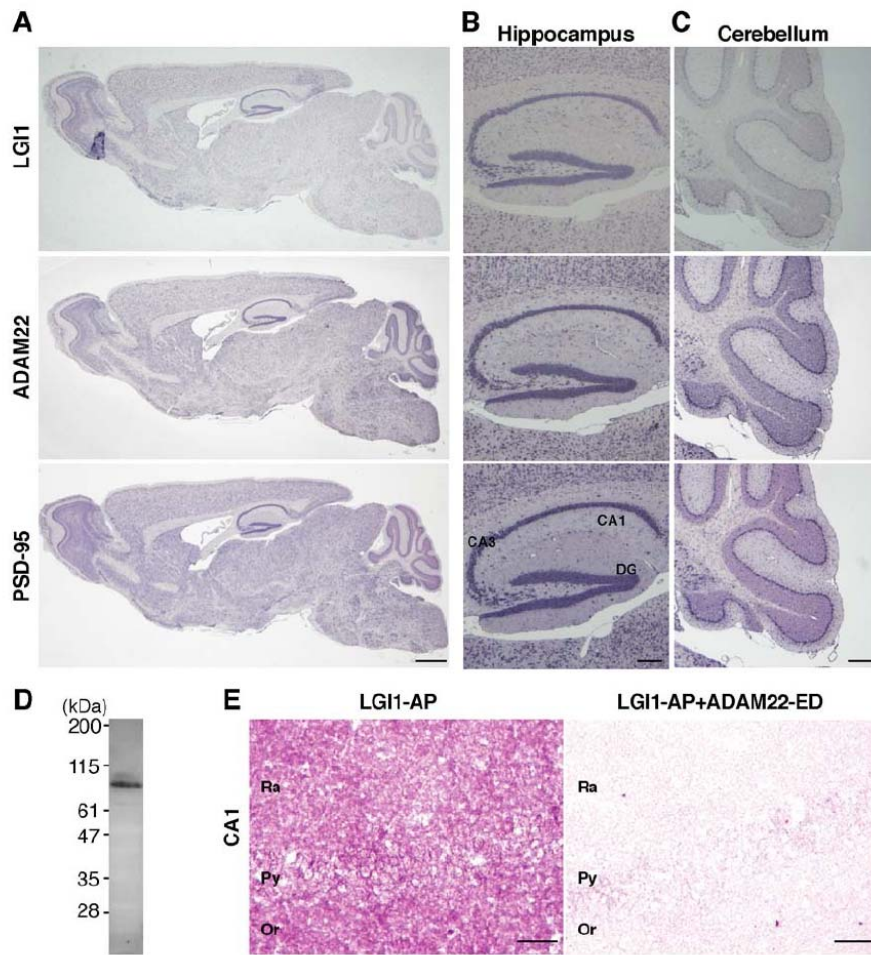


Fig. S8. LGI1 increases AMPA receptor surface expression in hippocampal neurons. (A) Cumulative distribution plot of surface AMPAR (GluR1) intensity from LGI1 expressing cultures was compared to control cultures. N values indicate the number of microscopic fields examined. Each field contained 2 to 4 neurons. (B) Examples of surface AMPAR staining in mock or LGI1-expressed cultures. Bar: 10 μm .

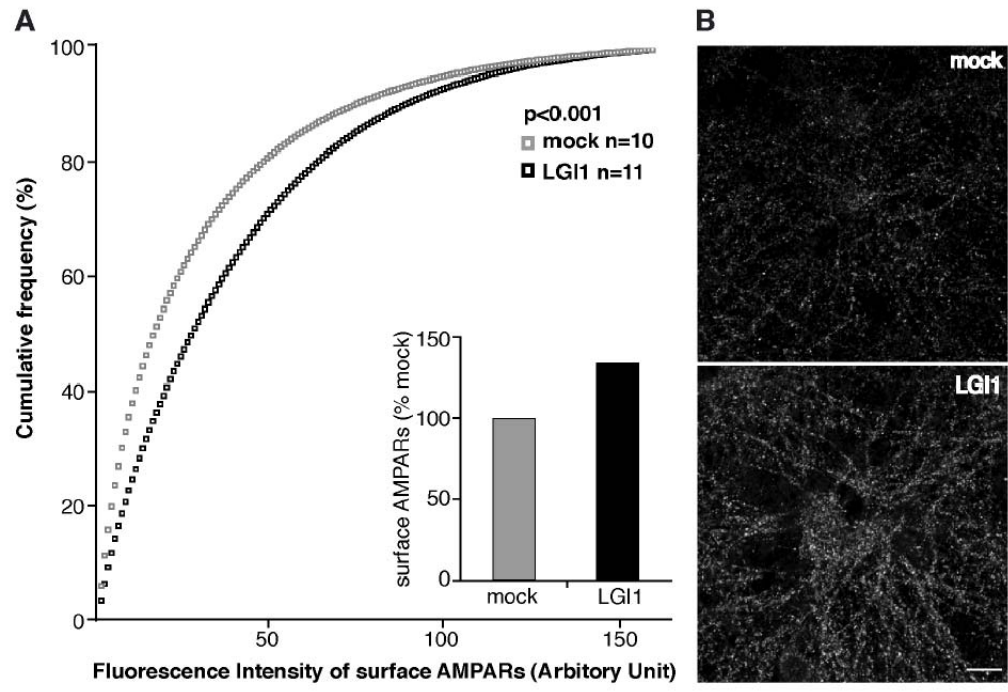
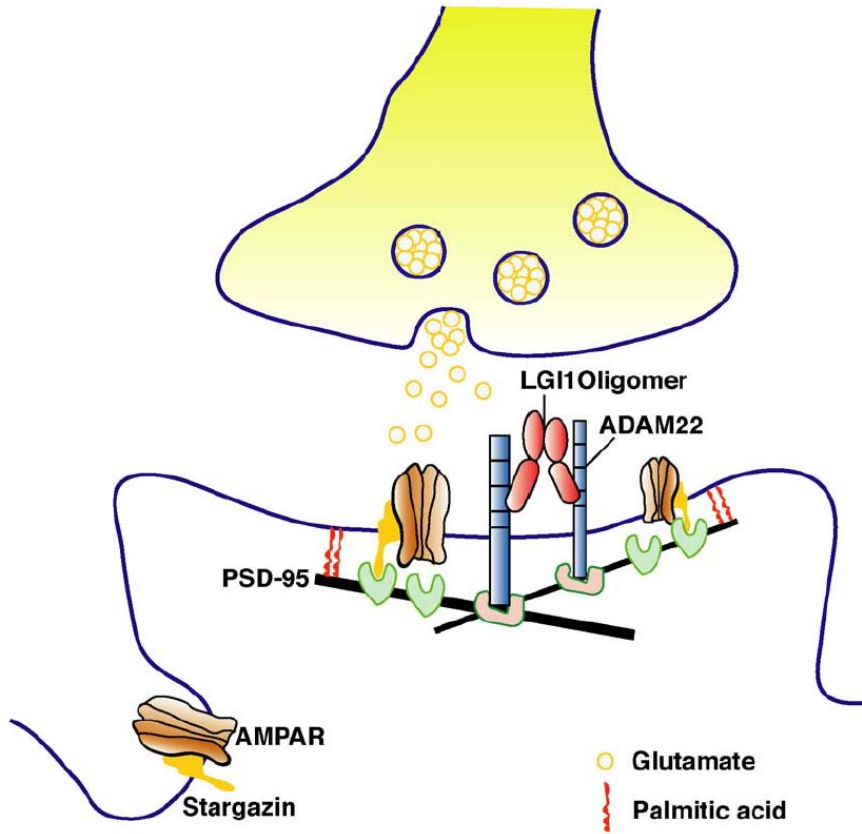


Fig. S9. LGI1 regulates AMPA receptor-mediated synaptic transmission. Secreted LGI1 oligomers may stabilize ADAM22, which is anchored to the postsynaptic complex containing stargazin and AMPA receptors (AMPA). These scaffolding interactions could mediate LGI1 enhancement synaptic transmission.



Chapter 6

Conservation of Glur2-containing AMPA Receptors during Long-Term Potentiation

Introduction

Most fast excitatory synaptic transmission in the brain is mediated by the AMPA subtype of glutamate receptor (AMPA), which is a heterotetramer composed of combinations of four subunits GluR1-4 (Hollmann and Heinemann, 1994). The calcium permeability of AMPARs is critically dependent on GluR2; those containing GluR2 are calcium impermeable and have a linear current-voltage (IV) relationship and those lacking GluR2 (or lacking the edited form of GluR2) are calcium permeable and are strongly inwardly rectifying (Jonas and Burnashev, 1995). Most AMPARs contain edited GluR2, but calcium permeable AMPA receptors have recently received considerable attention because of their postulated role in synaptic plasticity in a variety of brain regions (Liu and Cull-Candy, 2000; Bagal et al., 2005; Bellone and Luscher, 2006; Clem and Barth, 2006; Plant et al., 2006).

It is generally agreed that under basal conditions most, if not all, synaptic AMPARs in CA1 hippocampal pyramidal cells contain GluR2 subunits (but see (Bagal et al., 2005)). However, studies on the role of calcium permeable receptors in LTP are conflicting. Hayashi et al. (Hayashi et al., 2000) found that the IV of AMPAR EPSCs was unchanged when measured 30 minutes after LTP induction, in contrast to those cells artificially expressing GluR1 homomers. These experiments indicated that under normal conditions the increase in the AMPAR EPSC associated with LTP is not mediated by calcium permeable AMPARs more than half an hour after LTP induction. Since the IV of the AMPAR EPSC was not tested at earlier time points, it remained to be determined whether the rapid insertion of calcium permeable AMPARs mediated the increase in the EPSC for the first 30 minutes after the induction of plasticity. Until recently, the only

study that directly tested the role of calcium permeable AMPARs in LTP (Matthies et al., 1992) reported that the polyamine Philanthotoxin 343 (Phtx), which blocks calcium permeable AMPARs, had no effect on LTP when applied immediately after induction (although it could block LTP induction itself when applied before tetanization, probably by non-specifically antagonizing NMDARs (see Supplemental Fig. 1A). However, a recent study (Plant et al., 2006) found evidence for the appearance of rectifying, Phtx-sensitive, AMPAR EPSCs for a brief 25-minute window after LTP induction, not inconsistent with Hayashi et al. In seeming contradiction, another recent report from Bagal et al. (Bagal et al., 2005) presented evidence for an actual loss of synaptic rectifying AMPARs following LTP induction. To understand the role of calcium permeable AMPARs in hippocampal pyramidal cells we conducted several further experiments using the GluR2 knockout mouse as a control for our manipulations. Additionally, we examined the notion that synaptic activity after LTP induction plays a role in the maintenance of synaptic plasticity.

Results

The most rapid and sensitive test for the presence of synaptic calcium permeable AMPARs is to determine the IV relation of the AMPAR EPSC. Thus, we first confirmed that under our recording conditions rectification of synaptic AMPAR currents could be readily observed. Towards this end we compared the rectification of EPSCs in CA1 pyramidal cells in wt ($R2^{+/+}$) and GluR2 knockout ($R2^{-/-}$) mice. Indeed, in all cells tested in the $R2^{-/-}$ background EPSCs were sharply attenuated at positive potentials as compared to currents in $R2^{+/+}$ cells that exhibited nearly linear current-voltage (IV) relationships

(R2^{-/-} RI = 0.12±0.04; n = 5, R2^{+/+} RI = 0.91±0.05; n = 6, p < 0.005) (Fig. 1A). This result verifies that with our internal solution we could easily resolve the insertion of calcium permeable AMPARs to synapses by measuring the IV relation of the AMPAR EPSC. Next, to test if rectification could be observed following LTP induction, we compared the IV relation of the synaptic AMPAR current between a paired and an unpaired pathway (Fig. 1B). Immediately following LTP induction APV (50 μM) was added to the bath to isolate the AMPAR current. Ten minutes after induction the cell was depolarized to +40 mV and then to 0 mV for a three-point measure of rectification (see Methods). In neither the paired nor the unpaired pathway was significant rectification observed (RI LTP path = 0.90±0.04; RI control = 0.94±0.07, n = 24, p = 0.60; Fig. 1C) suggesting that neither pathway expressed calcium permeable AMPA receptors 10 minutes after LTP induction.

To test further for rectifying AMPARs in the earliest stages of LTP expression we conducted a series of LTP experiments where the recorded cell was held at +50 mV for the entire duration of the recording. By recording at positive potentials we could continuously monitor the presence of calcium-permeable AMPA receptors at the synapse as at these potentials such AMPA receptors are nearly completely blocked by internal polyamines. We reasoned that if LTP involved a brief insertion of calcium permeable, rectifying AMPARs that are later replaced with non-rectifying receptors, the time course of LTP at positive potentials should show no increase after induction, but rapidly become potentiated as these receptors are replaced with GluR2-containing AMPARs, (like that in Fig. 1B). To examine the AMPAR current in isolation, APV was applied during the baseline with a local flow pipe, rapidly removed prior to pairing, and then rapidly

reapplied after pairing (see Methods). Under these conditions, even at +50 mV, LTP was apparent immediately after pairing, and the overall time-course of potentiation was not significantly different from experiments where cells were voltage-clamped at negative potentials ($p = 0.65$ at 30 minutes) (Fig. 2A,B; $n = 9$). This result confirms that no detectable calcium permeable receptors are inserted following LTP. To test if an increase in AMPAR currents at positive potentials is evident in the absence of NMDAR blockers, we measured the EPSC at +40 or -60 mV before and after LTP induction, using a slope measurement to minimize the contamination of the NMDAR EPSC at positive potentials. The degree of increase of EPSC slope at negative and positive potentials was similar ($V_{\text{neg}} = 1.98 \pm 0.16$, $V_{\text{pos}} = 1.78 \pm 0.12$; $n = 7$; $p = 0.44$, Fig. 2C).

As an independent test of the idea that calcium permeable receptors are inserted after LTP induction, we used the polyamine toxin Philanthotoxin 433 (Phtx), a potent, use-dependent antagonist of calcium permeable receptors, to assess the presence of such receptors in LTP. First, we tested Phtx on slices from the GluR2 knockout ($R2^{-/-}$) mouse to determine the maximal extent and rate of block that can be expected by applying a given concentration of the antagonist to AMPARs that lack edited GluR2. In the presence of picrotoxin and APV to isolate synaptic AMPARs, 10 μM Phtx reduced the fEPSP in the GluR2 knockout to $58 \pm 2\%$ of its initial value within 25 minutes of application ($n = 5$; test frequency = 0.05 Hz, Fig. 3A). In a second pathway stimulation was stopped during the wash-in of Phtx to assess the use-dependency of block. Upon restarting this pathway the fEPSP was reduced to only $91 \pm 2\%$ of its baseline value, but after 15 minutes of sampling in the presence of Phtx it was reduced to $59 \pm 2\%$ of its initial value, not different from the pathway that was not stopped ($n = 4$, $p = 0.93$).

Unlike its effect on synaptic potentials, even 1 μ M Phtx completely blocked currents in outside-out patches from R2^{-/-} cells when glutamate was bath applied (Supplemental Fig. 1B). The weaker antagonism on synaptic potentials can be explained by the lesser ability of this use-dependent drug to block receptors when they are only briefly opened by synaptic pulses of glutamate. Ten μ M Phtx reduced the whole-cell EPSC in GluR2 knockout cells to 44 \pm 7% of its initial value within 25 minutes of application (n = 4; test frequency = 0.2 Hz, Fig. 3B). The greater degree of block of whole-cell synaptic currents can be attributed to the higher sampling rate used in the whole-cell experiments (Mainen et al., 1998). Phtx also effectively blocked the GluR2-lacking receptors on cerebellar Bergmann glia (see Supplemental Fig. 1C). These experiments confirm that under our conditions Phtx behaved as a specific and effective antagonist of GluR2-lacking receptors, and imposes strict limits on the extent of block that can be expected when applying this drug to synaptic currents mediated by calcium permeable AMPARs. Based on the degree of antagonism by Phtx on R2^{-/-} synapses we suggest that were LTP exclusively mediated by the insertion of calcium permeable AMPARs, Phtx should reduce the potentiation maximally by 50-60%.

To test this we next applied 10 μ M Phtx to wild type slices in which LTP was induced in one of two monitored pathways. Phtx was applied 3 minutes after the LTP induction protocol. In contrast to what would be expected if LTP were mediated by an insertion of calcium permeable AMPARs, Phtx did not affect the tetanized or control pathway (Fig. 3C, note that some heterosynaptic LTD was observed in the untetanized pathway consistent with previous findings (Scanziani et al., 1996)). We repeated this experiment in the whole-cell configuration to test if pairing-induced LTP differs from

tetanus induced LTP with respect to sensitivity to Phtx. Again, Phtx did not affect the paired or unpaired pathway (Fig. 3D). Taken together with the previous experiments on rectification, we find no support for the idea that LTP at the hippocampal CA3-CA1 synapses involves the insertion of calcium permeable AMPARs.

Perhaps a more fundamental question on LTP is whether activity through synaptic AMPARs following LTP induction is required for the maintenance of synaptic plasticity. Plant et al. suggest that calcium signaling through the newly inserted calcium permeable AMPARs following LTP induction may be required to solidify the increase in synaptic strength, serving as a synaptic 'tag.' However, previous studies have shown that LTP can be induced in the presence of the AMPAR antagonist, CNQX, and that following removal of CNQX from the slice, the potentiation becomes apparent (Kauer et al., 1988; Muller et al., 1988). Furthermore, rapidly chelating intracellular calcium immediately following LTP induction has no effect on the magnitude of LTP (Malenka et al., 1992). To test whether AMPAR activity is required for LTP maintenance more directly we conducted two experiments. First, LTP was induced in two pathways, but shortly after induction the test stimulation was stopped in one of the two pathways (Fig. 4A). After 15 minutes stimulation was resumed in the quiescent pathway and a comparison was made between the percent increase between the two pathways. If continuous activity through synaptic AMPARs at potentiated synapses is required to maintain the potentiation, then after restarting stimulation the LTP in the arrested pathway, but not the control pathway, should be abolished. However, after 15 minutes without stimulation the continuously stimulated pathway averaged $165 \pm 7\%$, and the pathway that was stopped averaged $179 \pm 12\%$ ($n = 6$, $p = 0.07$). In addition, no difference was found for the same experiment

on pairing-induced LTP in whole-cell ($n = 5$, S. Panicker and R.N., unpublished observations). This rules out the idea that test stimulation of a pathway is required to maintain LTP. However, spontaneous activity in the LTP pathway could function to maintain the potentiation. To test this we rapidly applied the ionotropic glutamate receptor antagonist, kynureate (1 mM), shortly after LTP induction (Fig. 4B) to completely block activity through synaptic glutamate receptors. Upon wash out of the antagonist the control pathway recovered to close to baseline, but the LTP pathway returned to a potentiated level close to that prior to applying kynureate. These experiments indicate that activity through synaptic receptors is not necessary to maintain LTP.

Discussion

Based on these experiments we conclude that LTP in CA1 does not involve the insertion of calcium permeable AMPARs to synapses. This is in contrast to forms of synaptic plasticity at the parallel fiber-stellate cell synapse (Liu and Cull-Candy, 2000) and synapses on to dopaminergic neurons in the VTA (Bellone and Luscher, 2006) that are reported to involve a switch in AMPAR subunit composition. However, unlike CA1 pyramidal cells, these classes of non-glutamatergic neurons contain appreciable amounts of rectifying receptors in the basal state, affording a readily available source for changing the subunit composition of synaptic AMPARs. It remains to be determined if changes in the subunit composition of AMPARs on CA1 interneurons, some of which do express GluR2-lacking receptors, occurs during LTP.

More importantly, our conclusions do not agree with a recent study that examined the presence of calcium permeable receptors at potentiated synapses in CA1 cells (Plant et al., 2006). It is possible that this study may have arrived a different conclusion because rectification was primarily measured with the NMDAR current intact. Inspection of the traces in Fig. 2C shows that potentiation of the AMPAR EPSC in the mixed AMPA/NMDA EPSC recorded at positive potentials is not obvious without a slope measurement. In fact, using a peak measurement there is a substantial difference in potentiation between EPSCs recorded at negative and positive potentials (% change $V_{\text{neg}} = 1.85 \pm 0.06$, % change $V_{\text{pos}} = 1.09 \pm 0.06$; $n = 7$; $p < 0.0005$). Additionally, we found that simply measuring the EPSC at +40 mV sometimes resulted in some brief potentiation, perhaps due to synaptic NMDAR activation (supplemental Fig. 1D). LTP can be readily induced at potentials up to +60 mV (Perkel and Nicoll, 1993), and single activation of synaptic NMDA receptors can be sufficient to induce LTP (Bagal et al., 2005). In Plant et. al., as it is presented, LTP was induced immediately after sampling at +40 mV, without returning to a negative holding potential to ensure that the baseline had not changed. Thus it is possible that no change of the EPSC was observed at +40 mV after pairing, even with a slope measurement, because the EPSC was already potentiated during the sampling phase. Potentiation may not have been observed in the control pathway because further high-frequency pairing at 0 mV was required to convert the short-term potentiation caused by sampling at +40 mV into a long-lasting potentiation. Despite these possibilities, subtle differences in recording conditions and slice preparation may have given rise to the apparent disparity between our data and that of Plant et. al., although all attempts were made to use identical solutions and age-matched

animals. Nonetheless, the fact that Phtx does not antagonize the extracellularly recorded fEPSP following LTP induction strongly argues that calcium permeable AMPA receptors do not play a significant role in LTP in the most commonly used preparation for studying hippocampal synaptic plasticity.

Figure 1. LTP is not associated with a change in the rectification of synaptic AMPAR currents. **(A)** Average IV plots for synaptic currents in wt ($R2^{+/+}$ n=6) and $R2^{-/-}$ (n=5) pyramidal cells. Top, example traces. Scale bars: 20 ms, 50 pA. **(B)** Summary data in which the IV profile of synaptic currents was measured in a control and a potentiated pathway (n=24). Top, example traces and IV plots; gray, before LTP, black, after. Scale bars: 20 ms, 50 pA. **(C)** Rectification indices for a sample of 24 cells between the control and potentiated pathway. The RI for cells in the $R2^{-/-}$ is included for comparison. In **(A)** mouse brain slices were used; in **(B)** and **(C)** rat slices were used; **(B)** and **(C)** were repeated in mouse slices with no apparent difference and the data were pooled.

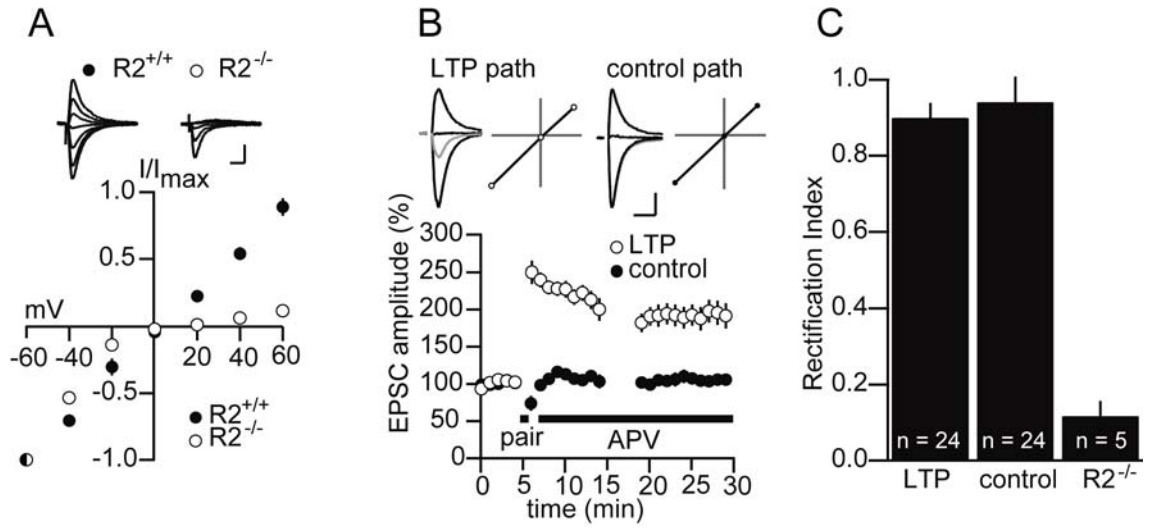


Figure 2. (A) Sample experiment where a cell was voltage-clamped at +50 mV during the entire experiment, except during pairing to 0 mV (black bar). Top, example traces. Scale bars: 20 ms, 80 pA. (B) Pooled data for 9 experiments as in (A). (C) Sets of samples traces of synaptic responses in three different cells before and after LTP at negative and positive potentials in the absence of APV. Traces are presented on two timescales for comparison; black, before LTP, grey, after. Vertical scale bar: 80 pA. Right: averaged EPSC slope change for seven such recordings at negative and positive potentials (n=7, p=0.43). Error bars represent s.e.m. Experiments were conducted in rat brain slices.

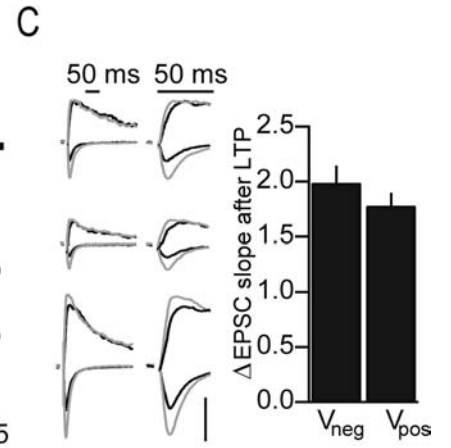
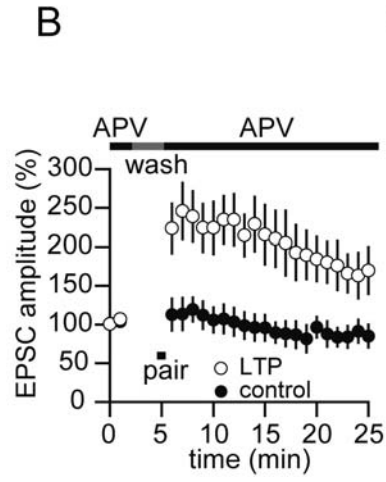
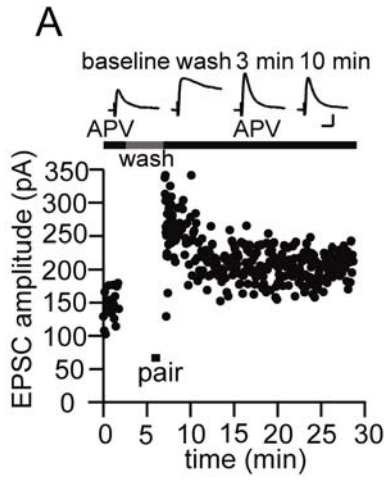


Figure 3. Philanthotoxin 433 does not block synaptic currents after LTP, and LTP does not require synaptic activity to be maintained. **(A)** Summary data for experiments in which 10 μM Phtx was applied to fEPSPs in $\text{R2}^{+/+}$ (n=4) and $\text{R2}^{-/-}$ (n=4) slices. Open triangles indicate the second pathway in experiments on $\text{R2}^{-/-}$ slices (the second pathway for $\text{R2}^{+/+}$ slices has been omitted for clarity). Top, example traces. Scale bars: 10 ms, 0.3 mV. **(B)** Summary data for experiments in which 10 μM Phtx was applied to whole-cell EPSCs in $\text{R2}^{+/+}$ (n=5) and $\text{R2}^{-/-}$ (n=4) slices. Application of 10 μM CNQX at the end of the recording confirmed that the remaining unblocked EPSC was mediated by AMPARs. Top, example traces. Scale bars: 20 ms, 30 pA. **(C)** Summary data for experiments in which 10 μM Phtx (open symbols n=10) or no Phtx (closed symbols n=8) was applied to fEPSPs after the induction of LTP by tetanization in one pathway (circles) but not the second control pathway (triangles). Top, example traces. Scale bars: 10 ms, 0.5 mV. **(D)** Summary data for experiments in which 10 μM Phtx (open symbols n=9) or no Phtx (closed symbols n=8) was applied to whole-cell EPSCs after the induction of LTP by pairing in one pathway (circles) but not the second control pathway (triangles). Top, example traces. Scale bars: 20 ms, 80 pA. All data were collected using mouse brain slices.

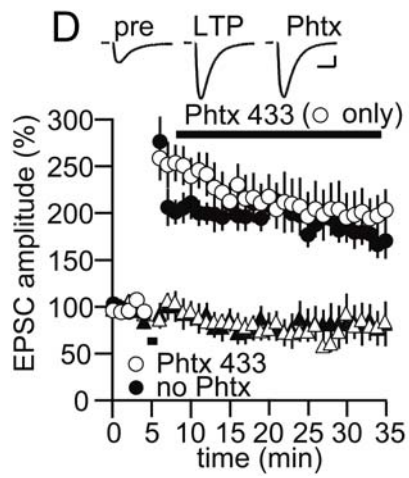
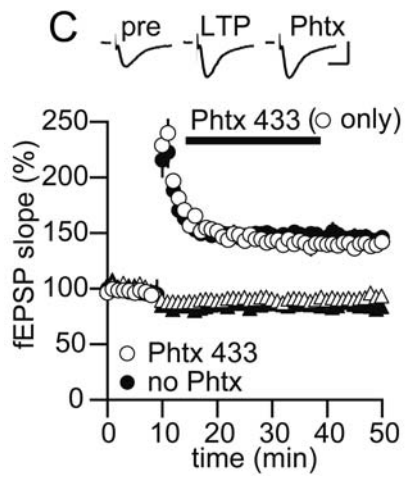
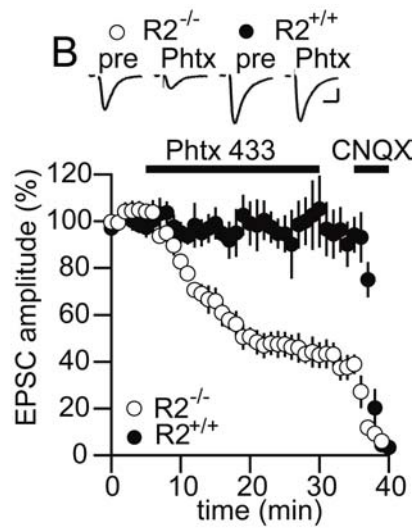
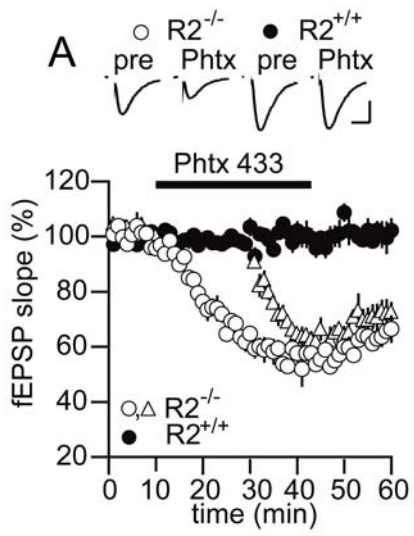
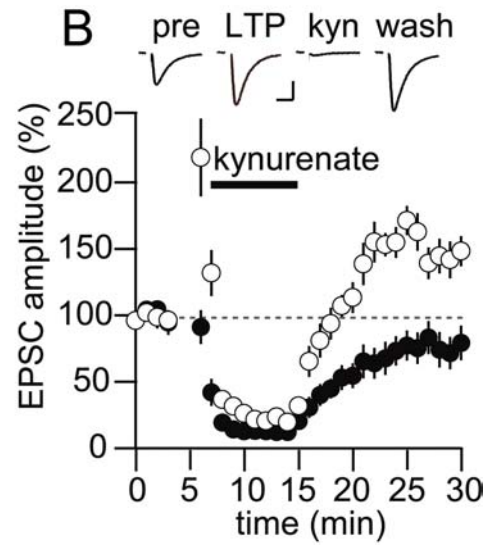
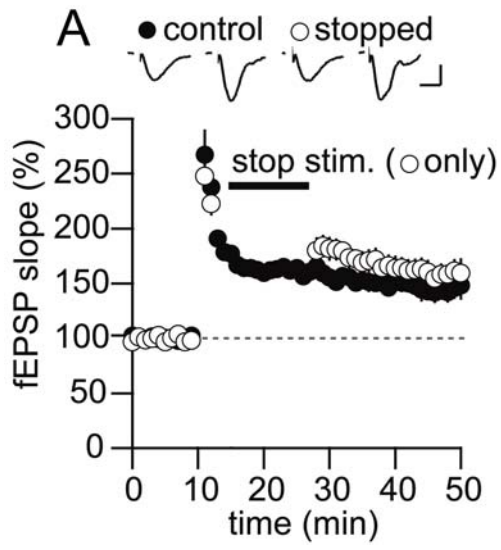
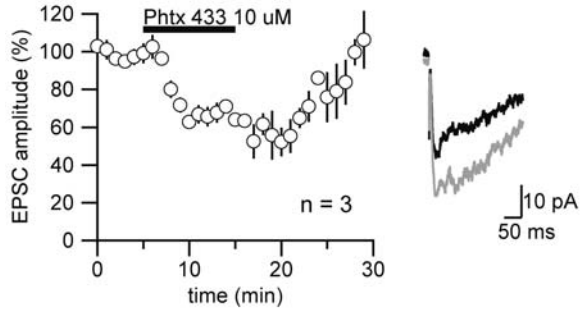


Figure 4. (A) Summary data for experiments in which two pathways were tetanized, but one pathway was stopped for 15 minutes after induction (open symbols). Top, example traces; n=6. Scale bars: 10 ms, 0.3 mV. **(B)**, Summary data for experiments in which kynureinate (1 mM) was rapidly applied for 7 minutes after induction of LTP in one pathway (n=6). Top, example traces. Scale bars: 15 ms, 30 pA. Error bars represent s.e.m. All data were collected using mouse brain slices.

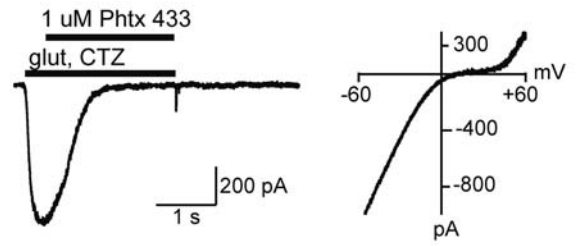


Supplemental Figure 1. Philanthotoxin antagonizes synaptic NMDARs, GluR2-lacking receptors on outside out patches from GluR2^{-/-} cells, and native GluR2-lacking receptors on cerebellar Bergmann Glial cells. **(A)** Summary data for experiments in which 10 μ M Phtx was applied to synaptic NMDAR EPSCs in wt CA1 cells isolated by application of 0 Mg²⁺ and the AMPAR antagonist CNQX. Right, example traces. **(B)** Representative recording showing the effects of 1 μ M Phtx on the glutamate-evoked current in an outside-out patch from a CA1 cell in the R2^{-/-} mouse. CTZ was co-applied to block desensitization. Right, example IV ramp of a R2^{-/-} outside out patch in 10 mM glutamate, 100 μ M cyclothiazide. **(C)** Summary data for experiments in which 10 μ M Phtx was applied to climbing fiber EPSCs in Bergmann glial cells. Right, example traces. Error bars represent s.e.m. **(D)** Example traces from two cells (two pathways each) of AMPAR EPSCs recorded before (gray) and after (black) sampling the EPSC at +40 mV in the absence of APV. Sampling was 10 pulses at 0.2 Hz.

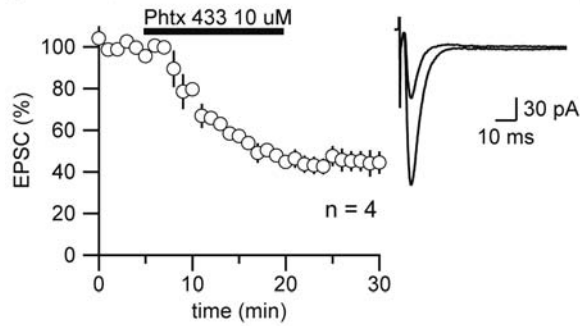
A NMDA EPSCs



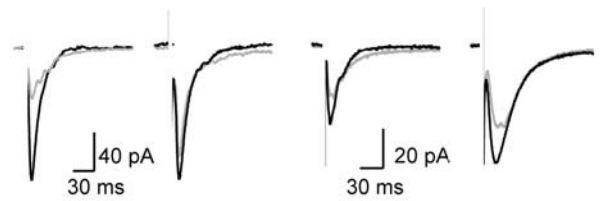
B R2^{-/-} outside-out patches



C Bergmann Glia CF-EPSCs



D AMPA EPSCs before (gray) and after (black) sampling at +40 mV



Chapter 7

Role of NMDA Receptor in synaptic maturation

Introduction

The mechanisms responsible for the precise wiring of neural circuits during brain development are largely unknown. One main challenge is to ascertain how the billions of synapses in the human brain are correctly specified. Based on decades of research, the neural blueprint must have two main components: a sophisticated genetic program and an ability to restructure in response to sensory activity. Much work is now aimed at determining the relative contribution of these two elements at different levels of brain architecture.

In cultured neuronal systems, chronic blockade of synaptic transmission suggests that activity is not required for functional synapses to form (Gomperts et al., 2000; Verhage et al., 2000). Evidence from mutant mice that cannot release synaptic vesicles confirms that ultrastructurally normal synapses can develop in the complete absence of synaptic transmission (Verhage et al., 2000). Thus at the most fundamental levels activity may not be required for brain development. At higher levels of neuronal circuitry, however, many studies have found that blockade of sensory activity influences functional patterning in neocortex (Katz and Shatz, 1996). Some additional work has suggested that spontaneous activity, not correlated with external cues, may also play an important role in wiring neural circuits (Constantine-Paton and Cline, 1998). These results have supported a model wherein a genetic program is mostly responsible for the large-scale patterning of the nervous system embryonically, but that after birth sensory and spontaneous activity determines the fine structure of neural circuits by the proper redistribution of excitatory and inhibitory synapses.

Synaptic plasticity, often studied as long-term potentiation (LTP), is a candidate mechanism for the translation of sensory experience into functional neuronal connectivity. LTP is thought to involve the rapid insertion of AMPA receptors to synapses thereby changing synaptic strength (Hayashi et al., 2000). At early postnatal stages excitatory synapses are few, and the average AMPA receptor content of synapses is low (Hsia et al., 1998). LTP can drive the induction of a functioning synapse by recruiting AMPA receptors to synapses that only contain NMDA receptors, which are functionally silent due to Mg^{2+} -blockade of the NMDA receptor pore at resting potential (Durand et al., 1996). LTP induction itself requires the activation of NMDA receptors by strong or correlated activity (Collingridge et al., 1988; Magee and Johnston, 1997). Two studies have recently taken advantage of electrophysiologically tagged AMPA receptors to suggest that sensory experience *in vivo*, like LTP *in vitro*, delivers AMPA receptors to synapses (Clem and Barth, 2006; Takahashi et al., 2003). Finally, NMDA receptor activity during synaptic plasticity may not only drive synapse maturation by recruitment of AMPA receptors, but may also have a trophic role on neurons by driving gene transcription or by directly influencing the cytoskeleton (Bradley et al., 2006; Matsuzaki et al., 2004).

Thus the most direct test for a role of synaptic plasticity in activity-dependent neural development involves the blockade or ablation of NMDA receptors. In neuronal cultures chronic antagonism of NMDA receptors before and throughout synaptogenesis has been reported to decrease the number of AMPA receptor-containing contacts (Liao et al., 1999; Luthi et al., 2001) and delay the synaptic acquisition of AMPA receptors over time (Zhu and Malinow, 2002). Though these studies are consistent with the idea that

NMDA receptor-dependent LTP is involved in synapse maturation, other *in vitro* studies presented data that NMDA receptor antagonism actually increases synapse number, potentially in a compensatory fashion (Gomperts et al., 2000; Luthi et al., 2001). *In vivo*, pharmacological blockade of NMDA receptors has been found to alter neuronal morphology and inhibit functional remodeling in response to early sensory deprivation (Rocha and Sur, 1995; Singer and Finegold, 1990). Nevertheless, chronic *in vivo* infusion of the NMDA antagonists in some brain regions does not impair the maturation of AMPA receptor-mediated transmission (Colonnese et al., 2003).

Because culture systems may not mimic the natural situation and *in vivo* pharmacological manipulations are difficult to control, genetic ablation of NMDA receptor function by disruption of the essential NMDAR subunit, NR1, has offered the most conclusive evidence on the role of NMDA receptors in synaptic development. The germline NR1 knockout mouse dies perinatally presumably due to respiratory failure, but exhibits grossly normal brain morphology except for abnormalities in somatosensory pathways (Forrest et al., 1994; Li et al., 1994). Additionally, synaptic AMPA currents can be recorded in brainstem neurons and respiratory rhythm recorded *in vitro* is normal in the NR1 knockout (Funk et al., 1997). Thus NMDA receptor activity is not generally required for normal brain architecture at birth, nor is it vital for synaptogenesis in early developing neural structures. Conditional deletion of NR1 in forebrain pyramidal cells from embryonic stages, however, disrupts barrel formation in primary somatosensory cortex (Iwasato et al., 2000), and results in exuberant branching of the projections of thalamic cells, despite that these cells themselves still express functional NMDA receptors (Lee et al., 2005). These findings demonstrate that NMDA receptors must

endogenously influence the development of neocortical circuits, but does not directly assess what effect NR1 deletion has on AMPA receptor transmission. Additionally, global deletion or blockade of NMDA receptors may eliminate any activity-based competition postsynaptic cells engage in to specify neural circuits.

Here we present evidence that NMDA receptors are not required for the developmental recruitment of AMPA receptors to synapses, neither embryonically, nor postnatally. Global deletion of NR1 in forebrain pyramidal cells results in a net increase in synaptic strength, without an increase in synapse number. Postnatal deletion of NR1, in contrast, does not result in a change in quantal strength, but strongly increases synapse number. Reintroduction of NMDA receptor currents in the forebrain NR1 knockout depresses synaptic transmission by a removal of synaptic connections. Thus NMDA receptors limit rather than promote synapse maturation during development.

Results

To test the role of NMDA receptor activity in the developmental recruitment of AMPA receptors to synapses we first examined AMPA-receptor transmission in conditional forebrain knockouts of the essential NMDA receptor subunit, NR1. By breeding the NEX-CRE line, which drives CRE expression from early embryonic stages in all cortical progenitors of pyramidal neurons (Goebbels et al., 2006), with floxed NR1 mice, the NR1 gene could be disrupted in all pyramidal cells well before synaptogenesis. As reported previously in a similar conditional mutant, NEX-CRE;NR1^{fl/fl} mice were viable, but never survived past four weeks of age (Iwasato et al., 2000). Knockout mice could easily be distinguished from littermates by reduced body weight (NR1^{fl/fl} 8.7±1.2 g

n = 8, NEX-CRE;NR1^{fl/fl} = 3.3±0.2 g, n = 10, p = 0.003; Fig. 1g), which was apparent as early as postnatal day 8 (not shown). We first confirmed that deletion of NR1 was successful; whole-cell recording revealed that excitatory synapses completely lacked NMDA receptor-mediated currents, while AMPA receptor EPSCs were intact (n = 9, Fig. 1a). To further quantify the remaining AMPAR-mediated excitatory transmission we compared the input-output relation of fEPSPs in the CA1 region and the size and frequency of quantal events. Inconsistent with the idea that NMDA activity is necessary for the progressive acquisition of AMPA receptors by synapses during development, forebrain NR1 knockout mice exhibited both enhanced field transmission and slightly larger, but not more numerous, mEPSCs (mEPSC amplitude: NR1^{fl/fl} 12.0±0.7 pA, n = 19; NEX-CRE;NR1^{fl/fl} = 15.4±1.0 pA, n = 18, p = 0.026; mEPSC inter-event interval: NR1^{fl/fl} 1.6±0.2 s, n = 19; NEX-CRE;NR1^{fl/fl} = 1.9±0.4 s, n = 18, p = 0.995; Fig 1b,d-f). The paired-pulse ratio of EPSCs, a measure of presynaptic release probability, was unchanged, indicating that the increased synaptic strength was postsynaptic in origin (NR1^{fl/fl} 1.7±0.1, n = 10; NEX-CRE;NR1^{fl/fl} = 1.7±0.2, n = 9, p = 0.93; Fig. 1c). As a control, CA3-CA1 synapses in these mice completely lacked LTP (supplemental Fig. 1). These results establish that when NMDA receptors are globally deleted from excitatory neurons from embryonic stages synapses exhibit a net increase in strength but no change in number despite the total inability to express plasticity.

We also generated a line of NR1 knockouts with NMDA receptors deleted in forebrain interneurons using a Dlx5/6-CRE line (Dlx5/6-CRE;NR1^{fl/fl} mice) (Monory et al., 2006). Though this CRE line only successfully deleted the NR1 gene in a mosaic fashion (16/30), those interneurons lacking NMDA receptors exhibited a slight increase

in quantal size relative to control cells in wild-type littermates, but did not display a change in the frequency of spontaneous events (mEPSC amplitude: NR1^{fl/fl} 10.0±0.4 pA; Dlx5/6-CRE;NR1^{fl/fl} = 11.8±0.8 pA, p = 0.026; mEPSC inter-event interval: NR1^{fl/fl} 1.2±0.3 s; NEX-CRE;NR1^{fl/fl} = 1.5±0.6 s, p = 0.95; supplemental figure 2). This result is consistent with that of the pyramidal cell NR1 deletion and demonstrates that NMDA receptors are dispensable for functional synapse maturation on interneurons as well.

Since global, embryonic deletion of NR1 could mask the effects of removing NMDA receptor activity by eliminating synaptic competition or by engaging compensatory mechanisms, we next asked whether deleting the NMDA receptor postnatally in single cells would uncover a different role of NMDA receptors in synaptogenesis at later stages. Biolistic transfection of organotypic hippocampal slice cultures prepared from P6-P9 NR1^{fl/fl} mice with CRE recombinase and GFP allowed the rigorous comparison of the effects of NMDA receptor deletion on synaptic transmission by utilizing paired, simultaneous whole-cell recording from transfected cells and nearby untransfected controls. 12-17 days following introduction of CRE recombinase NMDA currents were decreased on average by 77±2%, with some cells exhibiting almost no detectable NMDA EPSC, confirming the efficacy of the deletion (Fig 2a, n = 41 pairs, p < 10⁻¹⁰). Surprisingly, AMPA receptor EPSCs increased by 318±35% (Fig 2b, n = 41 pairs, p < 10⁻⁵), resulting in a ~20 fold change in the AMPA/NMDA ratio (AMPA/NMDA ratio: untransfected = 41±9, CRE-transfected = 2±0.2, n = 41; Fig 2c). Analysis of mEPSCs revealed that quantal strength was unchanged, but the frequency of synaptic events more than doubled (mEPSC amplitude: untransfected = 9.6±0.4 pA, n = 16; CRE-transfected = 10.2±0.3 pA, n = 15, p = 0.60; mEPSC inter-event interval:

untransfected = 4.1 ± 0.7 s, $n = 16$, CRE-transfected = 2.0 ± 0.3 s, $n = 15$, $p < 0.005$; Fig. 2d,e). Presynaptic release probability was unaltered as there was no difference in the paired-pulse ratio between control and transfected cells (untransfected = 1.8 ± 0.1 , $n = 13$; CRE-transfected = 1.8 ± 0.1 , $n = 13$, $p = 0.6$; Fig. 2f). As an additional control, CRE expression in slice cultures from wild-type animals was without effect on the AMPA or NMDA EPCSs (AMPA: $p = 0.21$, $n = 14$; NMDA: $p = 0.22$, $n = 14$; supplemental figure 3). These results demonstrate that even postnatally, NMDA receptors are not required for AMPAfication of synapses, but rather, deletion of NMDA receptor function in single cells is sufficient to profoundly enhance the total number of synapses onto a given cell.

The increase in synapses in NR1 deleted cells could result from cell autonomous changes driven by lack of incoming NMDA receptor activity, or by differences in activity relative to unaffected neighboring cells. To test this, we incubated slice cultures from NR1^{fl/fl} mice in NMDA antagonists during transfection with CRE recombinase to eliminate all NMDA receptor function in the slice. We could be sure that the antagonism was successful during the incubation because MK-801 confers irreversible block of the NMDA receptor channel, and no cells incubated in MK-801 exhibited detectable NMDA EPCSs even when the recording solution was free of NMDA receptor antagonists ($n = 12$, Fig. 3c). Blocking all NMDA activity in culture prevented the difference in AMPA EPCSs between CRE-expressing and untransfected cells (paired recording: $n = 17$, $p = 0.4$; mEPSC amplitude: untransfected = 11.4 ± 0.6 pA, $n = 13$; CRE-transfected = 10.6 ± 0.7 pA, $n = 9$, $p = 1.00$; mEPSC inter-event interval: untransfected = 0.9 ± 0.2 s, $n = 13$, CRE-transfected = 0.90 ± 0.2 s, $n = 9$, $p = 0.67$; Fig. 3d,e). However, this was due to

an occlusion of the effects of single-cell deletion, because on its own chronic NMDA receptor antagonism strongly potentiated the number of synapses without affecting quantal strength in control, untransfected cells (mEPSC inter-event interval: control = 4.1 ± 0.7 s, $n = 16$; NMDAR antagonist cocktail = 0.9 ± 0.2 s, $n = 13$, $p < 0.005$; Fig. 3F). We also note that there was no difference in the AMPA EPSC between control and CRE transfected neurons when cells were voltage clamped at +40 mV either, indicating that removal of NMDA receptor activity did not change the GluR2 content of the receptors ($n = 9$, $p = 0.80$, Fig. 3b). These results further suggest that in our system NMDA receptor activity is required normally to limit the extent of synaptogenesis, and that removing NMDA receptor function even in a single cell is sufficient to trigger this process.

As a further test of the influence of NMDA receptor activity on development of synaptic transmission, we re-introduced NR1 to slice cultures from NEX-CRE;NR1^{fl/fl} mice. This allowed single cells to express functional NMDA receptor currents in an environment where all other pyramidal cells are completely devoid of this activity, the functional inverse of CRE introduction to NR1^{fl/fl} slices. Rescue with NR1 restored NMDA receptor mediated EPSCs ($n = 21$ pairs, Fig. 4a), but strongly reduced AMPA-receptor mediated transmission (NR1-GFP-transfected/control = $52 \pm 1\%$, $n = 21$ pairs; Fig. 4b). The reduction was due to an elimination of AMPA-receptor containing synapses because NR1 rescue cells exhibited normal mEPSC amplitude, but a diminished frequency of spontaneous miniature events (mEPSC amplitude: untransfected = 13 ± 2 pA, $n = 9$; NR1-GFP-transfected = 12 ± 1 pA, $n = 9$, $p = 0.72$; mEPSC inter-event interval: untransfected = 3.7 ± 0.9 s, $n = 9$, NR1-GFP-transfected = 9 ± 2 s, $n = 9$, $p < 0.005$; Fig. 4d,e).

Deletion of NR1 or blockade of NMDA receptors with antagonists cannot distinguish whether the crucial function of NMDA receptors on synapse number is mediated by its calcium conductance, which is necessary for induction of plasticity, or its ability to depolarize the postsynaptic membrane. Towards this end we co-transfected NR1^{fl/fl} slice cultures with CRE recombinase and an NR1 pore mutant (N598R) that does not conduct calcium (Barria and Malinow, 2002). This allowed the complete molecular replacement of native NMDA receptors with those that are impermeable to calcium. We could monitor directly the substitution of native receptors with mutants because the pore mutation also confers insensitivity to Mg²⁺ block, and co-transfection linearized the *I-V* relation of the synaptic NMDA receptor EPSC (n = 4, p = 0.02; supplementary figure 5a,c). In co-transfected cells there was no apparent difference in the AMPA EPSC with that of untransfected neighbors, unlike transfection with CRE alone, but more data is need to make firm conclusions (n = 4, supplementary figure 5b).

Taken together, the foregoing data strongly implicates postnatal NMDA receptor activity in limiting the number of functional AMPA-receptor containing contacts neurons make. This contrasts with results obtained from the embryonic forebrain NR1 knockout, which does not exhibit increased synaptogenesis, but greater quantal strength. The difference between these two experiments is two-fold: the time of NR1 excision, and a global versus mosaic deletion. To test these two possibilities, we deleted NR1 in a small number of pyramidal neurons, embryonically, using *in utero* transfection of pyramidal cell progenitors with CRE recombinase. Though we do not have sufficient data yet, simultaneous paired-recording from CRE-transfected cells and neighboring control pyramidal neurons should help resolve this discrepancy.

Though these results define a role for NMDA receptors during embryonic and postnatal development, we wanted to test what effects deletion of NMDA receptor protein had on mature synapses in adult animals. Although most of synaptogenesis occurs during the first few weeks of life, chronic *in vivo* imaging has revealed that some new contacts can be made during adulthood (Trachtenberg et al., 2002). We took advantage of a CA1-specific CRE expressing line that only drives NR1 deletion after 4-5 weeks of age (Fukaya et al., 2003). CA1-NR1 knockout mice completely lack LTP and have deficits in spatial memory (Tsien et al., 1996), but a full characterization of AMPA-receptor mediated transmission in these mutants is lacking. Consistent with the initial study, we found that CA1-NR1KO mice had no changes in the input-output relation of fEPSPs, no alteration in mEPSC amplitude or frequency, and no difference in the paired-pulse ratio (supplemental figure 5). These results establish that NMDA receptors are not required for the maintenance of functional circuitry in the CA1 region. Furthermore they demonstrate that the changes observed in cells with NR1 deletions at early developmental stages were caused by perturbations to the development process, and not to a general effect of removing NMDA receptors on synaptic transmission.

Finally, to test if acute blockade of NMDA receptors is sufficient to induce changes in quantal strength or synapse number, we compared AMPA receptor-mediated quantal events between slices that were incubated in the NMDA antagonist D-APV and control slices. Incubation in NMDA receptor antagonist for two or more hours had no effect on the amplitude or frequency of mEPSCs, indicating that ongoing activity through NMDA receptors in slices does not influence the net strength of AMPA receptor transmission on fast timescales ((mEPSC amplitude: control (TTX only) = 10.0 ± 0.4 pA,

n = 14; APV + TTX incubated = 9.7 ± 0.5 pA, n = 16, p = 0.95; mEPSC inter-event interval: control (TTX only) = 5.0 ± 0.8 s, n = 14, APV + TTX incubated = 5.0 ± 0.8 s, n = 16, p = 0.33; supplemental figure 6).

Discussion

Taken together, our data show that NMDA receptor activity is not required for the functional maturation of synapses in mammalian forebrain neurons. On the contrary, complete, irreversible deletion of NMDA receptor function potentiates AMPA receptor-mediated synaptic transmission. When NMDA receptors are removed embryonically prior to synaptogenesis neurons exhibit an increase in quantal strength, but no change in synapse number. When NR1 deletion occurs postnatally during the period of rapid synaptic proliferation cells instead exhibit a strong increase in total synapse number. Because removal or reintroduction of functional NMDA receptors to single cells is sufficient to trigger these processes, we suggest that intracellular signaling driven through the NMDA receptor allows individual neurons to actively regulate their net synaptic input.

Synapse elimination is a well studied process that seems to be crucial for ultimately specifying neuronal connectivity (Sanes and Lichtman, 1999). One model of neural development, stemming from work at the neuromuscular junction in vertebrates as well as in insects, is that a genetic program drives multiple axons convergently to each target cell and those connections with the highest activity are ultimately stabilized, while less active connections are eliminated (Goda and Davis, 2003). Since deletion of NR1 or incubation of cultured slices with NMDA receptor antagonists strongly increases total

synapse number it is tempting to conclude that the normal role of NMDA receptor activity in developing circuits is to destabilize nascent synapses, promoting their elimination. Thus the primary role of NMDA receptors in activity-dependent neural development may be to consolidate specific circuits by removing extraneous neuronal connectivity. Such an idea is consistent both in vivo pharmacological experiments (Hahm et al., 1991) and the apparent hyper-arborization of thalamic axons in the somatosensory system of forebrain NR1 knockouts (Iwasato et al., 2000).

While NMDA receptors are essential for LTP, some recent results suggest the NMDA-receptor dependent LTD shares similarities with synaptic pruning (Zhou et al., 2004). If, during postnatal development, LTD has a dominating influence over LTP, the net effect of disrupting NMDA-receptor dependent plasticity should be an increase in connectivity or synaptic strength, as was observed with deletion of NR1 in organotypic slice culture or embryonically. Some variant of an NMDA receptor mutant that selectively lacks LTP but retains LTD should further delineate the role of NMDA receptors on AMPA-receptor transmission during development.

An important question is why the deletion of the NR1 gene embryonically as compared to deletion in postnatal slice culture increases AMPA-receptor synaptic transmission but by different mechanisms. It is possible that developing pyramidal cells that have never experienced NMDA receptor activity are not governed by the same genetic program as cells that retain NMDA receptor function through the early stages of synaptogenesis, since activation of NMDA receptors can drive protein synthesis and gene expression (Bradley et al., 2006; Ghosh et al., 1994). Such an alteration may trigger increased AMPA receptor insertion (or decreased AMPA receptor removal) at synapses

while disrupting the cellular machinery that normally translates reductions in NMDA receptor activity into increased synaptogenesis. Regardless of this difference, because the end result of eliminating NMDA receptor function in developing neurons is to increase the net synaptic drive to single cells, it seems rigorous to conclude that activity through NMDA receptors during development limits, rather than promotes, the maturation of excitatory synapses.

Figure 1. Embryonic deletion of NR1 in NEX-CRE;NR1^{fl/fl} mice does not impede the functional maturation of synapses in CA1. **(A)** CA1 pyramidal neurons in NEX-CRE;NR1^{fl/fl} mice exhibit no detectable NMDA EPSCs, though AMPA EPSCs are intact. **(B)** Summary graph of fEPSP input-output relationships in the KO and NR1^{fl/fl} littermates. **(C)** Paired-pulse ratio in CA1 pyramidal cells from KO and control NR1^{fl/fl} littermates. **(D)** Cumulative distribution of mEPSC amplitudes in control and KO animals. **(E)** Cumulative distribution of mEPSC inter-event intervals in control and KO animals. **(F)** mEPSC amplitude is increased in the KO relative to control littermates. **(G)** KO animals have a reduced bodyweight at postnatal day 18. All error bars represent s.e.m.

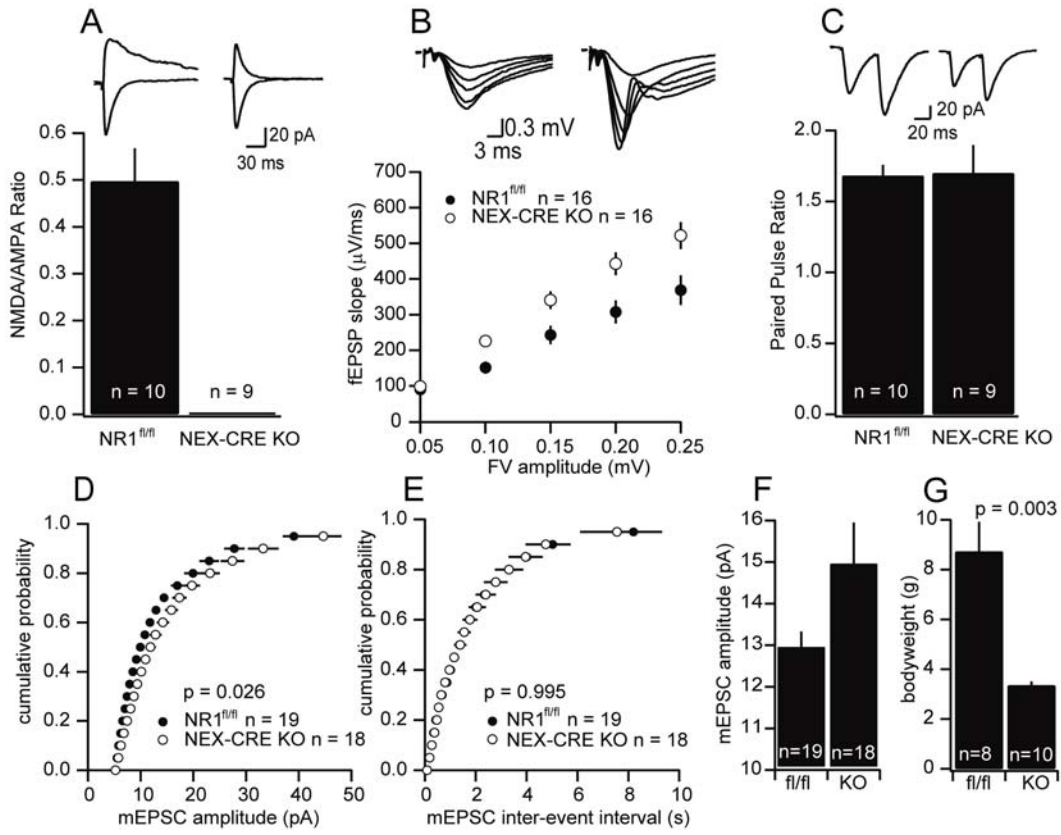


Figure 2. Mosaic deletion of NR1 in organotypic slice culture increases AMPA receptor-mediated synaptic transmission by a large increase in synapse number. **(A)** Summary plot of NMDA EPSCs in simultaneous paired recordings from CRE-transfected and control cells 12-17 days post transfection. Inset: example traces from one pair. Green: CRE-transfected; black: control. **(B)** Summary plot of AMPA EPSCs in simultaneous paired recordings from CRE-transfected and control cells 12-17 days post transfection. **(C)** Average AMPA-NMDA ratios in CRE-transfected and control cells. **(D)** Cumulative distribution of mEPSC amplitudes in control and CRE-transfected cells. Above: example mEPSC trace from a control cell. **(E)** Cumulative distribution of mEPSC inter-event intervals in control and CRE-transfected cells. Above: example mEPSC trace from a CRE-transfected cell. **(F)** No difference in paired-pulse ratio between control and CRE-transfected cells. Error bars represent s.e.m.

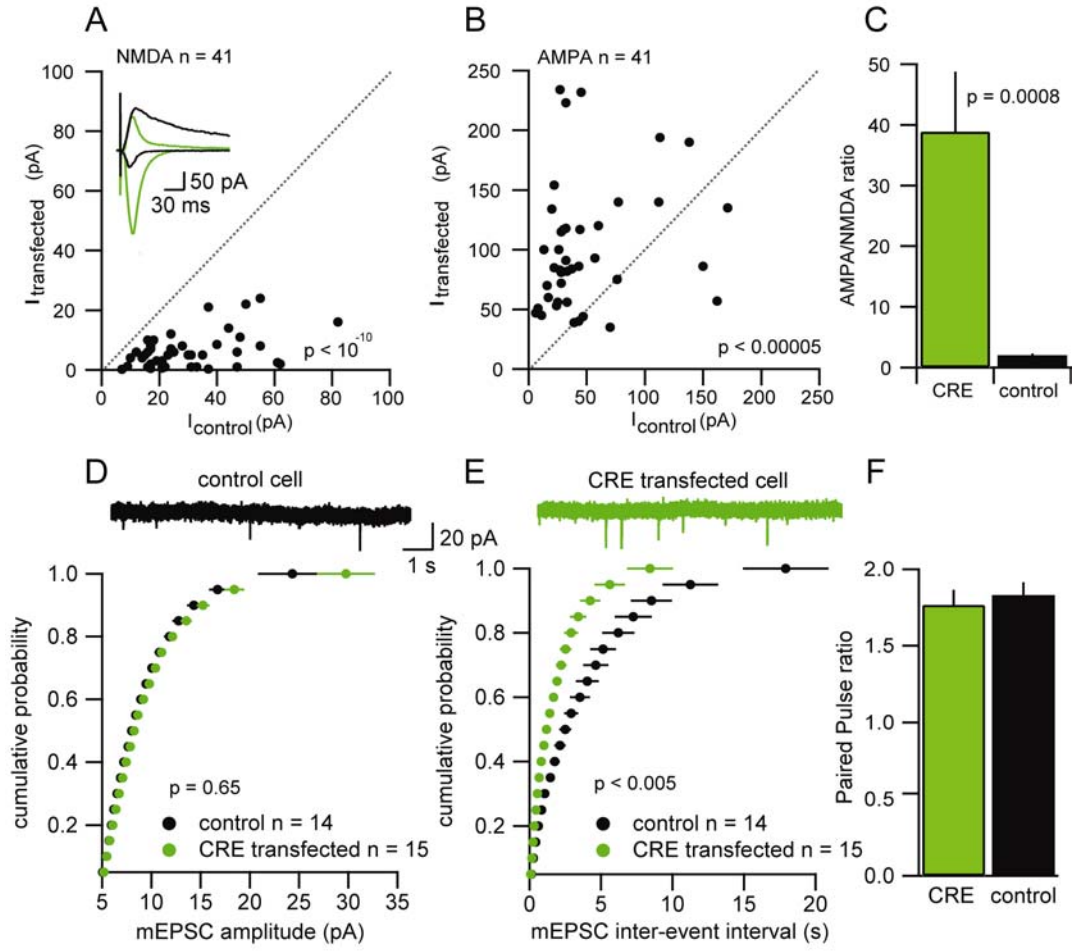


Figure 3. Incubating slice cultures in an NMDA receptor antagonist cocktail occludes the effect of CRE-mediated NR1 deletion. **(A)** Summary plot of AMPA EPSCs at holding potential of -60 mV in simultaneous paired recordings from CRE-transfected and control cells 12-17 days post transfection following incubation in AP-V (100 μ M), CPP (10 μ M), and MK-801 (40 μ M). **(B)** Summary plot of AMPA EPSCs at holding potential of $+40$ mV in simultaneous paired recordings from CRE-transfected and control cells 12-17 days post transfection following incubation in the NMDA receptor antagonist cocktail. **(C)** Example traces from a simultaneous recording of CRE-expressing (green) and control (black) cell incubated in the NMDAR antagonist cocktail. No NMDA receptor antagonists were present in the bath solution, indicating irreversible block by MK-801. **(D)** Cumulative distribution of mEPSC amplitudes in control and CRE-transfected cells after incubation in the NMDAR antagonist cocktail. **(E)** Cumulative distribution of mEPSC inter-event intervals in control and CRE-transfected cells after incubation in the NMDAR antagonist cocktail. **(F)** Cumulative distribution of mEPSC inter-event intervals in control and CRE-transfected cells with and without incubation in the NMDAR antagonist cocktail. Error bars represent s.e.m.

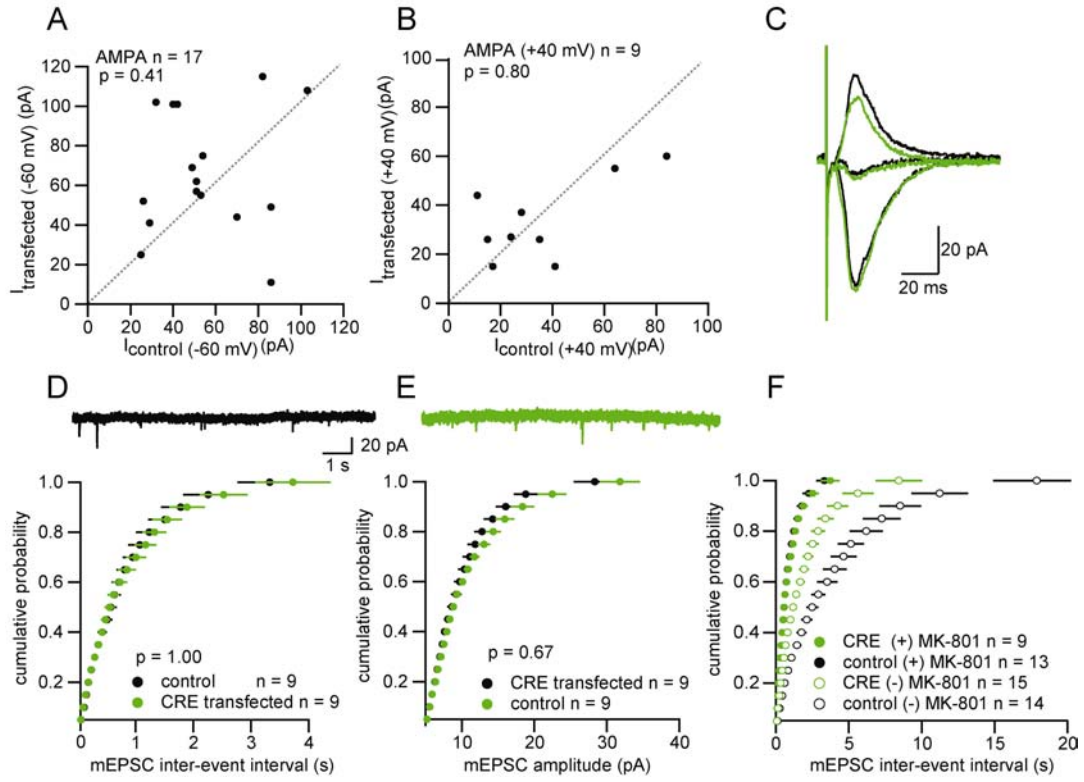
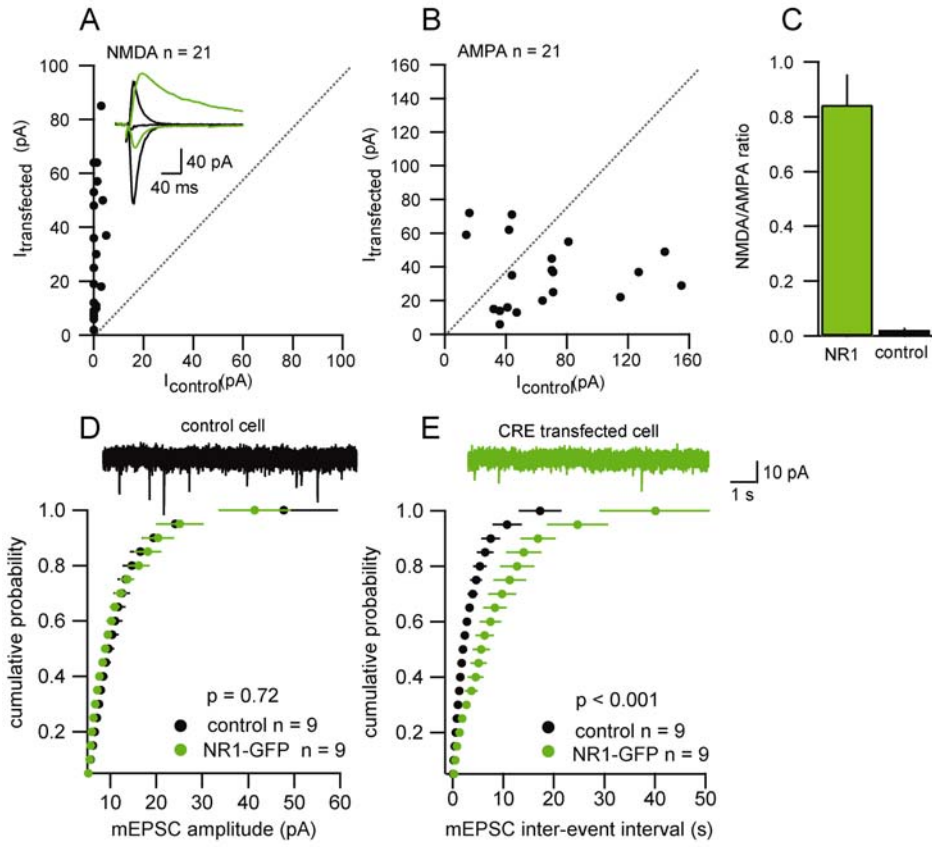
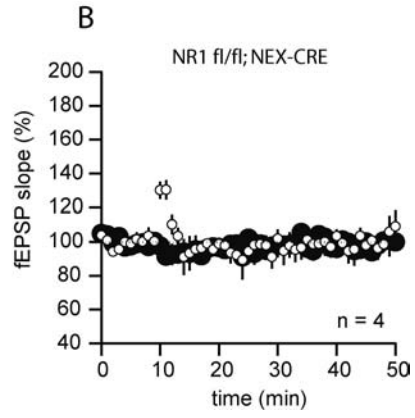
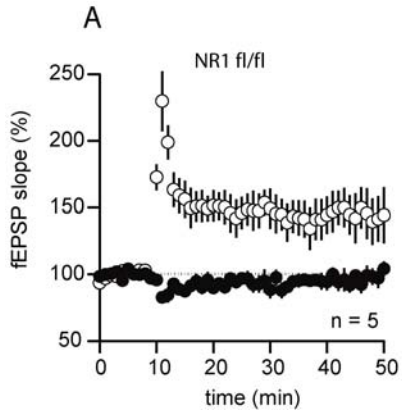


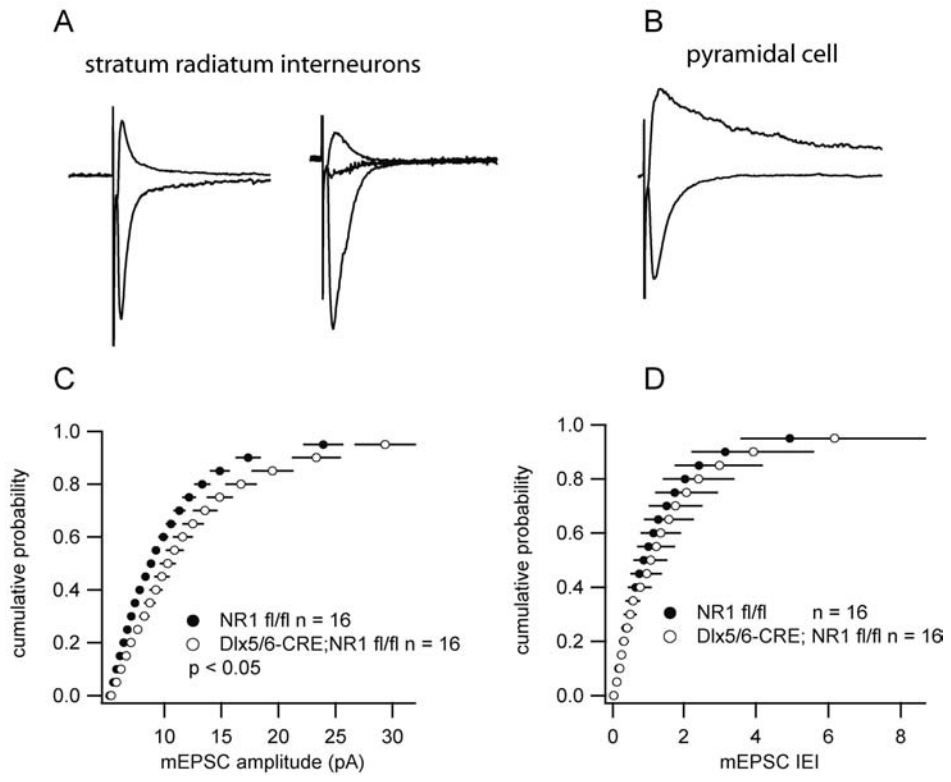
Figure 4. Reintroduction of NR1 to slice cultures from NEX-CRE;NR1^{fl/fl} mice drives a net loss in synapse number. **(A)** Summary plot of NMDA EPSCs at holding potential of +40 mV in simultaneous paired recordings from NR1-GFP-transfected and control forebrain NR1 KO cells 8-10 days post transfection. Insert: example traces from one pair. Green: NR1-GFP-transfected; black: control. **(B)** Summary plot of AMPA EPSCs at holding potential of +40 mV in simultaneous paired recordings from CRE-transfected and control cells 8-10 days post transfection. **(C)** Average NMDA-AMPA ratios in NR1-GFP transfected and control cells. **(D)** Cumulative distribution of mEPSC amplitudes in control and NR1-GFP-transfected cells. Above: example mEPSC trace from a control cell. **(E)** Cumulative distribution of mEPSC inter-event intervals in control and NR1-GFP-transfected cells. Above: example mEPSC trace from a NR1-GFP-transfected cell. Error bars represent s.e.m.



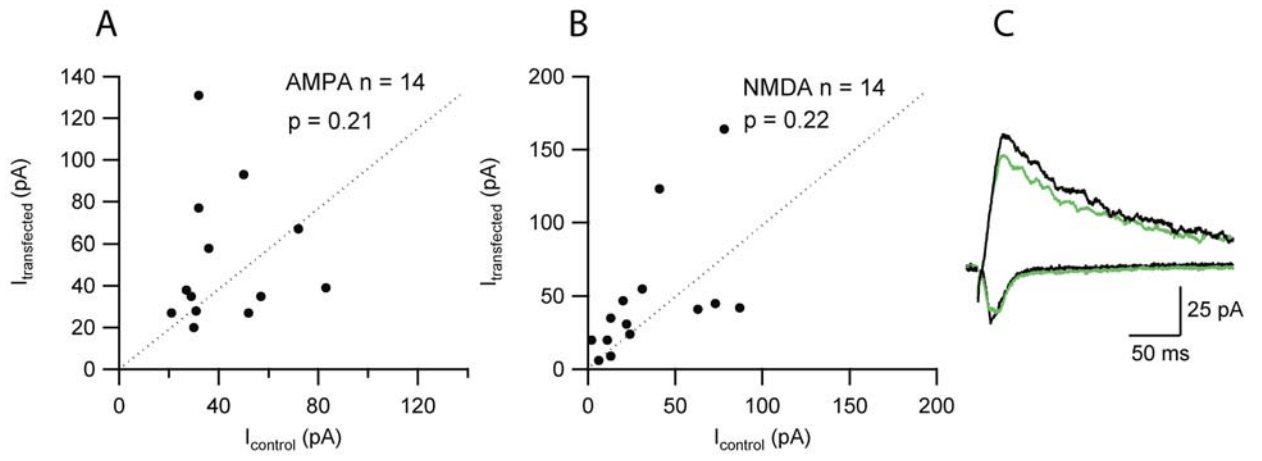
Supplemental Figure 1. LTP and heterosynaptic LTD are absent from NEX-CRE:NR1^{fl/fl} mice. **(A)** Summary graph for LTP induction in slices from NR1^{fl/fl} animals. **(B)** Summary graph for LTP induction in slices from NEX-CRE;NR1^{fl/fl} animals. Error bars represent s.e.m.



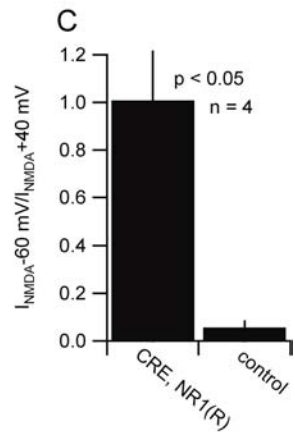
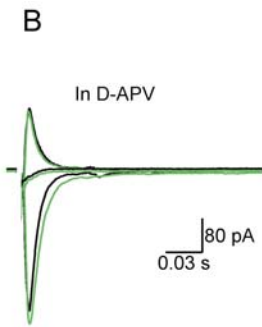
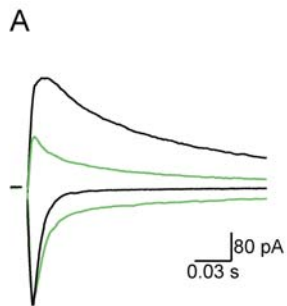
Supplemental Figure 2. Effects of NR1 deletion in forebrain interneurons in Dlx5/6-CRE; NR1^{fl/fl} mice. **(A)** Evoked EPSC traces from two representative cells (at -60 and +40 mV) in the Dlx5/6-CRE;NR1^{fl/fl} mouse. Note the absence of an NMDA EPSC at positive potentials. **(B)** Evoked EPSC traces from a pyramidal cell in the same slice. **(C)** Cumulative distribution of mEPSC amplitudes in control and KO animals. **(D)** Cumulative distribution of mEPSC inter-event intervals in control and KO animals.



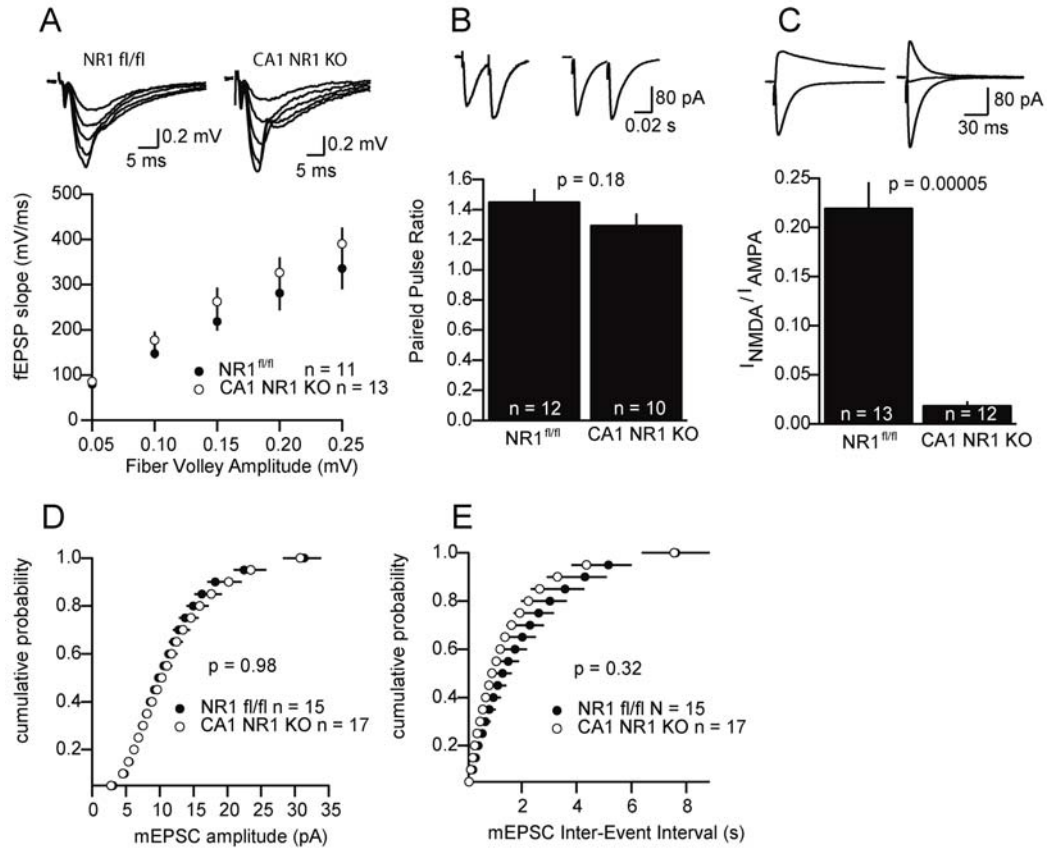
Supplemental Figure 3. CRE-expression in slice cultures from wild-type NR1^{+/+} mice does not affect AMPA or NMDA EPSCs. **(A)** Summary plot of evoked AMPA EPSCs in control and CRE-transfected cells in wild-type slice cultures. **(B)** Summary plot of evoked NMDA EPSCs in control and CRE-transfected cells in wild-type slice cultures. **(C)** Example traces from a simultaneously recorded CRE-transfected (green) and control (black) cell.



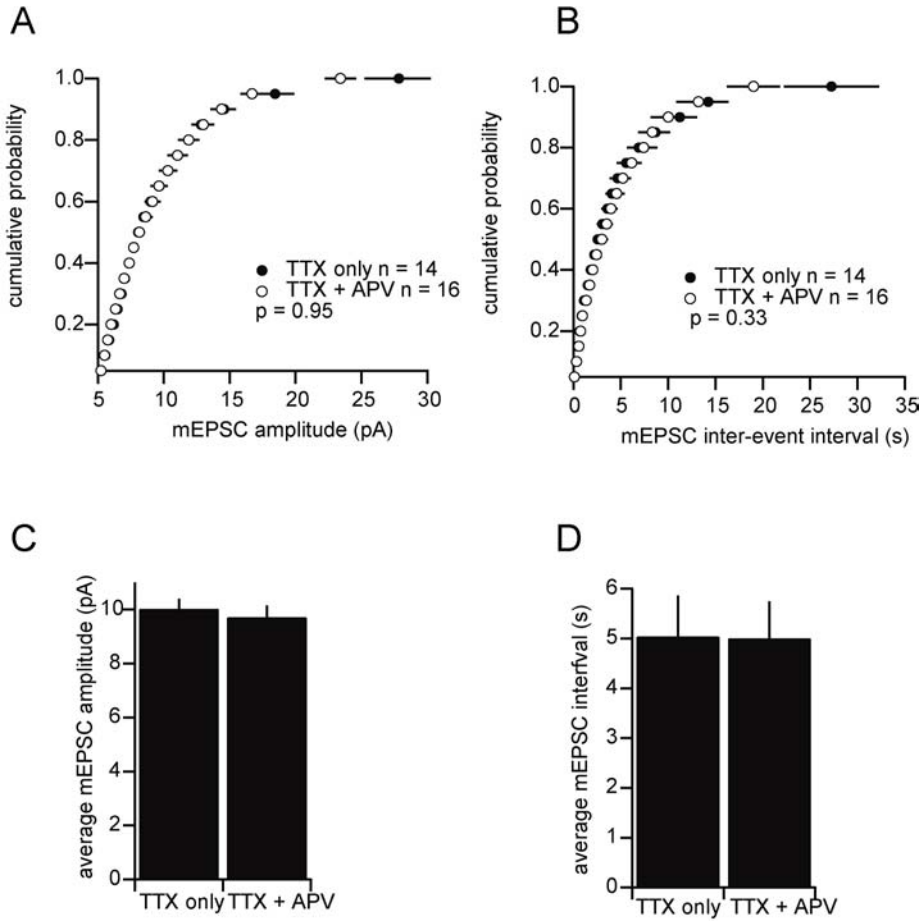
Supplemental Figure 4. Molecular replacement of native NMDA receptors with those containing the pore mutant NR1(R). **(A)** Example traces from a simultaneously recorded CRE; NR1(R)-GFP transfected (green) and control (black) cell. Note the presence of an NMDA EPSC at negative holding potentials. **(B)** Evoked EPSC traces from the same cell as in **(A)** after application of D-APV (50 μ M). **(C)** Summary graph of the ratio of NMDA EPSC at holding potentials of -60 and $+40$ mV in CRE;NR1(R)-GFP and control cells.



Supplemental Figure 5. Normal AMPA receptor-mediated synaptic transmission in T29.1-CRE:NR1^{fl/fl} mice. **(A)** Summary graph for fEPSP input-output relationship in slices from NR1^{fl/fl} and CA1-NR1-KO mice at 8-9 weeks of age. **(B)** No difference in paired-pulse ratio between control and KO animals. **(C)** NMDA EPSCs recorded at positive holding potentials are almost undetectable in slices from KO mice. **(D)** Cumulative distribution of mEPSC amplitudes in control and KO animals. **(E)** Cumulative distribution of mEPSC inter-event intervals in control and KO animals.



Supplemental Figure 6. Acute blockade of NMDA receptors in hippocampal slices does not rapidly affect quantal strength or synapse number. **(A)** Cumulative distribution of mEPSC amplitudes in control slices incubated only in TTX (500 nM) and slices incubated in TTX (500 nM) and D-APV (50 μ M) for 2-5 hours. **(D)** Cumulative distribution of mEPSC inter-event intervals in the same cells.



Chapter 8
General Conclusions

Excitatory glutamatergic transmission in the nervous system requires both action-potential dependent release of glutamate and clustered ionotropic glutamate receptors positioned across from vesicle release sites. The strength of synaptic communication at each contact between axon and dendrite depends on the number of postsynaptic glutamate receptors and their gating properties. A large pool of cycling AMPA receptors may allow for rapid changes in synaptic strength, perhaps supporting the ability of the brain to quickly encode experience and adapt to changes in the environment.

Here I show that synaptic AMPA receptors do not rapidly exchange with receptors in intracellular stores, unlike previously thought. Rather, the complete turnover of synaptic AMPA receptors with a pool inside the cell occurs on the timescale of hours to days. Unlike receptors at synapses though, those lying on the extrasynaptic somatic plasma membrane can exchange with an internal pool in minutes. Furthermore, receptors in the cell surface can move laterally within the membrane at relatively high rates, and may then switch with synaptic receptors without the need for any endocytic/exocytic machinery. Although this data contrasts with previous models, it is consistent with the observed behavior of NMDA, GABA, and nicotinic acetylcholine receptors (Akaaboune et al., 1999; Thomas et al., 2005; Tovar and Westbrook, 2002). Also, since many of the previous studies used biochemical or optical techniques that could not reliably separate between synaptic and extrasynaptic receptors, it is possible that the rapid turnover these studies observed was largely that of extrasynaptic receptors.

Future studies with more advanced inactivation technology should permit the absolute determination of the real time dynamics of AMPA receptors. For instance, two-photon activation of ANQX (or a similar drug with a better two-photon cross-section)

would make it possible to selectively inactivate AMPA receptors at PSDs, or those lying in the perisynaptic domain. Such analysis could absolutely determine the exchange rate of AMPA receptors at synapses under normal conditions, and following the induction of various forms of plasticity.

LTP is thought to rely on membrane insertion of AMPA receptors by exocytosis (Lledo et al., 1998). Since these data show that synaptic receptors do not seem to rapidly cycle through a vesicular pathway, the expression mechanism of LTP is not likely to utilize the biochemical machinery that supports the ongoing cycling of AMPA receptors, as previously proposed (Luscher et al., 1999). However, since ANQX was not useful in brain slices and LTP could not be reliably induced in cultured neurons it remains to be determined if the results obtained using ANQX on dissociated neurons would be the same if it could be utilized in acute brain slices. Nonetheless, a more parsimonious model of LTP involves a privileged pool of internal AMPA receptors on vesicles that are only mobilized following NMDA receptor activity that leads to plasticity. Alternatively, some element of potentiation may be independent of membrane fusion, and instead rely on the recruitment of perisynaptic AMPA receptors already present in the membrane to the PSD.

Stargazin is one of the central molecular players in AMPA receptor trafficking. Nearly all recent work on this protein focused on its potent ability to promote surface and synaptic expression of AMPA receptors (Chen et al., 2000b; Rouach et al., 2005; Schnell et al., 2002b). Since glutamate current was generally used as the assay for surface delivery, it was assumed that stargazin's main role was to facilitate AMPA receptor trafficking. However, an alternative explanation for the increase in surface current

observed when AMPA receptors are co-expressed with stargazin is that their physical interaction enhances the gating properties of the receptor, making the AMPA receptor a more efficient ionotropic channel. The first indication that this could be the case came from the simple result that co-expression of AMPA receptors with stargazin massively potentiated the efficacy of the weak agonist kainate relative to that of glutamate. Since a change in the relative efficacy of two AMPA receptor agonists cannot be explained by a change in trafficking, the only alternative is that stargazin directly alters the biophysical and pharmacological properties of the AMPA receptor causing kainate to become a more efficacious agonist.

This result is supported by additional evidence that stargazin increases the AMPA receptor's affinity for glutamate, decreases its deactivation kinetics when unbinding from glutamate, and even slows and diminishes receptor desensitization when in the continuous presence of agonist. Chimeric analysis of stargazin by domain exchange with the loosely homologous protein, γ -5, which does not interact with AMPA receptors, revealed that stargazin's control over AMPA receptor trafficking and gating relies on completely distinct regions of the protein. While the intracellular c-tail of stargazin is sufficient to drive surface delivery of AMPA receptors, the first extracellular domain is crucially involved in modulating the AMPA receptor's response to glutamate. Though all this work was conducted in a heterologous system, over-expression of mutant stargazin whose first extracellular domain has been switched with that of γ -5 decreased AMPA receptor-mediated synaptic transmission in neurons by accelerating the decay and reducing the peak amplitude of quantal events. This result establishes that a stargazin-

AMPA receptor interaction at the synapse is necessary for the proper response of postsynaptic AMPA receptors to presynaptically released glutamate.

Stargazin is thought to deliver AMPA receptors to synaptic sites by a direct interaction with the postsynaptic scaffolding molecule, PSD-95 (Schnell et al., 2002b). Analysis of PSD-95 protein complexes from brain tissue by mass spectrometry revealed that in addition to stargazin, PSD-95 strongly associates with the transmembrane protein, ADAM22. The same complexes also contained the putative secreted factor Lgi1, which was then shown to bind ADAM22 *in vitro*. Interestingly, both ADAM22 and Lgi1, much like stargazin, are coded for by genes that are closely linked to epilepsy and ataxia in humans or mouse models (Kalachikov et al., 2002a; Sagane et al., 2005b). Subcellular immunohistochemical analysis demonstrated that stargazin, PSD-95, and ADAM22 form a complex at synapses. Additionally, incubating acute hippocampal slices with concentrated Lgi1-containing media could potentiate AMPA-receptor synaptic transmission by increasing quantal amplitude. Lgi1 incubation of cultured neurons increased immunoreactivity for AMPA receptor subunits at synapses, suggesting that the potentiating effects of Lgi1 on transmission work by increasing the number of postsynaptic AMPA receptors. One possible mechanism is that Lgi1 binding to ADAM22 enhances its association with PSD-95, which may facilitate incorporation of extrasynaptic PSD-95-stargazin complexes into the synapse. Though PSD-95 interacts with stargazin through its first two PDZ domains, it binds to ADAM22 through its third, and so a three-way binding is complementary and not exclusive. Future work in Lgi1 and ADAM22 knockouts should elucidate how these proteins influence excitatory transmission.

An interesting point is that another recent report identified Lgi1 as an interacting partner with the putative presynaptic potassium channel, Kv1.4, using a very similar cloning strategy (Schulte et al., 2006b). Co-expression of Lgi1 and Kv1.4 in oocytes potentially altered the gating properties of the potassium channel, and thus it was suggested that Lgi1 could modulate synaptic transmission via a presynaptic mechanism. In our experiments Lgi1 incubation had no effect on the paired pulse ratio of field EPSPs in the CA1 region, though CA3 axon terminals may not express Kv1.1. Complicating these data is that multiple studies have shown that Lgi1 is a secreted protein (Senechal et al., 2005b; Sirerol-Piquer et al., 2006), so it not clear how injection of Lgi1 cRNA into oocytes would alter co-expressed Kv1.4 function, though in principal the oocyte-produced Lgi1 protein could immediately bind to extracellular domains of the Kv1.4 channel following exocytosis.

Incubation of slices with Lgi1 had no effect on LTP, so we argue that the mechanism by which it increases AMPA receptor function must not be shared with that of NMDA-receptor dependent plasticity, though both are thought to drive AMPA receptor insertion to synapses. A recent report proposed that LTP relies on the transient incorporation of GluR2-lacking complexes in the first 20 minutes following LTP induction (Plant et al., 2006), and would thus represent an ultimate description of the expression mechanism of LTP at the canonical CA3-CA1 synapse. Similar reports have suggested that at the cerebellar parallel-fiber to stellate synapses and at glutamatergic synapses on dopaminergic neurons of ventral tegmental area high frequency activity can trigger a subtype switch of synaptic AMPA receptors (Bellone and Luscher, 2005; Liu and Cull-Candy, 2000). These forms of plasticity differ from that proposed for

Schaeffer-collateral synapses in that these cells normally express both calcium-permeable and calcium-impermeable receptors on the plasma membrane, that the plasticity is NMDA receptor independent, and that it involves a removal of GluR2-lacking receptors, not an insertion. Since our own preliminary experiments did not implicate a role for subtype switching of AMPA receptors during hippocampal LTP, we conducted a number of further experiments to rigorously test this intriguing hypothesis.

Using two potent tests for calcium-permeable AMPA receptors, namely, intracellular block by endogenous polyamines and extracellular block by polyamine toxins from wasp venom, we conclusively demonstrated that LTP does not involve the insertion of GluR2-lacking AMPA receptors. We could be sure that these manipulations would have been successful at blocking synaptic calcium-permeable AMPA receptors, despite the lack of block after LTP induction, by using the same tests in the GluR2 knockout mouse. In these mice, AMPA receptor function could be completely shut down by intracellular polyamines at positive holding potentials, and potently and use-dependently inhibited by extracellular application of the drug Philanthotoxin 433 at negative holding potentials. Importantly, LTP could be observed even when voltage clamping pyramidal neurons at positive potentials for the entire duration of an LTP experiment where AMPA receptors lacking GluR2 would normally be blocked by intracellular polyamines. Lastly, we showed that no 'synaptic tag' is necessary to maintain LTP-induced synaptic specific potentiation, because inactivity in a previously potentiated pathway had no effect on the maintenance of the increase in synaptic strength.

We finally sought to determine the extent that LTP-like processes contribute to the functional wiring of neuronal circuits during development. The dramatic increase of functional synapses, particularly those containing AMPA receptors, during the first few postnatal weeks (Hsia et al., 1998) suggests that experience-driven recruitment of AMPA receptors to synapses may represent the mechanism by which the brain restructures in response to environmental stimuli during early ontogeny (Takahashi et al., 2003). Towards this end, we performed temporally and spatially control deletions of NMDA receptor function by introduction of CRE recombinase to the floxed NR1 mouse. Because the NR1 subunit of the NMDA receptor is absolutely essential for functional expression of NMDA receptor current, this manipulation ensures complete and irreversible ablation of all NMDA-receptor dependent processes.

Were LTP-like mechanisms needed for circuit formation, removing NR1 from developing pyramidal neurons should profoundly inhibit synapse maturation, and thus AMPA receptor synaptic current should be strongly reduced in NR1-deleted cells. Inconsistent with this idea, AMPA receptor-mediated synaptic transmission in the pyramidal neuron knockout mouse was actually increased, driven partly by an enhancement of quantal strength. Removing NR1 from interneurons had a similar effect. Global deletion of NR1 well before synaptogenesis could alter the genetic program of neurons making them insensitive to removal of NMDA receptor activity. Thus we then introduced CRE recombinase to neurons in postnatal organotypic slice culture prepared from NR1 floxed mice. In this situation, NR1 deletion again resulted in an increase in AMPA receptor mediated synaptic transmission, but as a result of a strong increase in synapse number, but not of quantal strength. The additional finding that the

reintroduction of NMDA receptor currents to single cells from the forebrain NR1 knockout drives a reduction in synapse number confirms that NMDA receptor function in individual neurons is both necessary and sufficient to negatively regulate net synaptic input.

These results establish that NMDA receptors are not required for the functional maturation of synapses during brain ontogeny. Alternatively, NMDA receptor activity may play a crucial role in experience-driven elimination of synapses in neuronal circuitry during development. This activity-dependent pruning of superfluous connectivity could be essential for the specific wiring of mature neural circuits that allows effective and efficient computation.

Chapter 9

References

- Akaaboune, M., S.M. Culican, S.G. Turney, and J.W. Lichtman. 1999. Rapid and reversible effects of activity on acetylcholine receptor density at the neuromuscular junction in vivo. *Science*. 286:503-7.
- Arikkath, J., and K.P. Campbell. 2003. Auxiliary subunits: essential components of the voltage-gated calcium channel complex. *Curr Opin Neurobiol*. 13:298-307.
- Armstrong, N., and E. Gouaux. 2000a. Mechanisms for activation and antagonism of an AMPA-sensitive glutamate receptor: crystal structures of the GluR2 ligand binding core. *Neuron*. 28:165-81.
- Armstrong, N., and E. Gouaux. 2000b. Mechanisms for activation and antagonism of an AMPA-sensitive glutamate receptor: crystal structures of the GluR2 ligand binding core. *Neuron*. 28:165-81.
- Armstrong, N., Y. Sun, G.Q. Chen, and E. Gouaux. 1998. Structure of a glutamate-receptor ligand-binding core in complex with kainate. *Nature*. 395:913-7.
- Bagal, A.A., J.P. Kao, C.M. Tang, S.M. Thompson. 2005. Long-term potentiation of exogenous glutamate responses at single dendritic spines. *PNAS* 102:14434-14439.
- Banke, T.G., D. Bowie, H. Lee, R.L. Huganir, A. Schousboe, and S.F. Traynelis. 2000. Control of GluR1 AMPA receptor function by cAMP-dependent protein kinase. *J Neurosci*. 20:89-102.
- Barria, A., and R. Malinow. 2002. Subunit-specific NMDA receptor trafficking to synapses. *Neuron*. 35:345-53.

- Barria, A., D. Muller, V. Derkach, L.C. Griffith, and T.R. Soderling. 1997. Regulatory phosphorylation of AMPA-type glutamate receptors by CaM-KII during long-term potentiation. *Science*. 276:2042-5.
- Barry, M.F., and E.B. Ziff. 2002. Receptor trafficking and the plasticity of excitatory synapses. *Curr Opin Neurobiol*. 12:279-86.
- Bellone, C., and C. Luscher. 2005. mGluRs induce a long-term depression in the ventral tegmental area that involves a switch of the subunit composition of AMPA receptors. *Eur J Neurosci*. 21:1280-8.
- Bergles, D.E., and C.E. Jahr. 1998. Glial contribution to glutamate uptake at Schaffer collateral-commissural synapses in the hippocampus. *J Neurosci*. 18:7709-16.
- Birmingham, J.R., Jr., H. Shearin, J. Pennington, J. O'Moore, M. Jaegle, S. Driegen, A. van Zon, A. Darbas, E. Ozkaynak, E.J. Ryu, J. Milbrandt, and D. Meijer. 2006. The claw paw mutation reveals a role for Lgi4 in peripheral nerve development. 76-84 pp.
- Bliss, T.V., and T. Lomo. 1973. Long-lasting potentiation of synaptic transmission in the dentate area of the anaesthetized rabbit following stimulation of the perforant path. *J Physiol*. 232:331-56.
- Borgdorff, A.J., and D. Choquet. 2002. Regulation of AMPA receptor lateral movements. *Nature*. 417:649-53.
- Boulter, J., M. Hollmann, A. O'Shea-Greenfield, M. Hartley, E. Deneris, C. Maron, and S. Heinemann. 1990. Molecular cloning and functional expression of glutamate receptor subunit genes. *Science*. 249:1033-7.

- Bradley, J., S.R. Carter, V.R. Rao, J. Wang, and S. Finkbeiner. 2006. Splice variants of the NR1 subunit differentially induce NMDA receptor-dependent gene expression. *J Neurosci.* 26:1065-76.
- Bredt, D.S., and R.A. Nicoll. 2003. AMPA receptor trafficking at excitatory synapses. *Neuron.* 40:361-79.
- Brose, K., K.S. Bland, K.H. Wang, D. Arnott, W. Henzel, C.S. Goodman, M. Tessier-Lavigne, and T. Kidd. 1999. Slit proteins bind Robo receptors and have an evolutionarily conserved role in repulsive axon guidance. *In Cell.* Vol. 96. 795-806.
- Catterall, W.A. 2000. Structure and regulation of voltage-gated Ca²⁺ channels. *Annu Rev Cell Dev Biol.* 16:521-55.
- Chen, L., S. Bao, X. Qiao, and R.F. Thompson. 1999. Impaired cerebellar synapse maturation in waggler, a mutant mouse with a disrupted neuronal calcium channel gamma subunit. *Proceedings of the National Academy of Sciences of the United States of America.* 96:12132-7.
- Chen, L., D.M. Chetkovich, R.S. Petralia, N.T. Sweeney, Y. Kawasaki, R.J. Wenthold, D.S. Bredt, and R.A. Nicoll. 2000a. Stargazin regulates synaptic targeting of AMPA receptors by two distinct mechanisms. *In Nature.* Vol. 408. 936-943.
- Chen, L., D.M. Chetkovich, R.S. Petralia, N.T. Sweeney, Y. Kawasaki, R.J. Wenthold, D.S. Bredt, and R.A. Nicoll. 2000b. Stargazin regulates synaptic targeting of AMPA receptors by two distinct mechanisms. *Nature.* 408:936-43.

- Chen, L., A. El-Husseini, S. Tomita, D.S. Brecht, and R.A. Nicoll. 2003. Stargazin differentially controls the trafficking of alpha-amino-3-hydroxyl-5-methyl-4-isoxazolepropionate and kainate receptors. *Mol Pharmacol.* 64:703-6.
- Chernova, O.B., R.P. Somerville, and J.K. Cowell. 1998. A novel gene, LGI1, from 10q24 is rearranged and downregulated in malignant brain tumors. *In Oncogene.* Vol. 17. 2873-2881.
- Clem, R.L., and A. Barth. 2006. Pathway-specific trafficking of native AMPARs by in vivo experience. *Neuron.* 49:663-70.
- Clements, J.D., and G.L. Westbrook. 1991. Activation kinetics reveal the number of glutamate and glycine binding sites on the N-methyl-D-aspartate receptor. *Neuron.* 7:605-13.
- Collingridge, G.L., C.E. Herron, and R.A. Lester. 1988. Frequency-dependent N-methyl-D-aspartate receptor-mediated synaptic transmission in rat hippocampus. *J Physiol.* 399:301-12.
- Collingridge, G.L., J.T. Isaac, and Y.T. Wang. 2004. Receptor trafficking and synaptic plasticity. *Nat Rev Neurosci.* 5:952-62.
- Collingridge, G.L., S.J. Kehl, and H. McLennan. 1983. The antagonism of amino acid-induced excitations of rat hippocampal CA1 neurones in vitro. *J Physiol.* 334:19-31.
- Colonnese, M.T., J. Shi, and M. Constantine-Paton. 2003. Chronic NMDA receptor blockade from birth delays the maturation of NMDA currents, but does not affect AMPA/kainate currents. *J Neurophysiol.* 89:57-68.

- Constantine-Paton, M., and H.T. Cline. 1998. LTP and activity-dependent synaptogenesis: the more alike they are, the more different they become. *Curr Opin Neurobiol.* 8:139-48.
- Cottrell, J.R., G.R. Dube, C. Egles, and G. Liu. 2000. Distribution, density, and clustering of functional glutamate receptors before and after synaptogenesis in hippocampal neurons. *J Neurophysiol.* 84:1573-87.
- Derkach, V., A. Barria, and T.R. Soderling. 1999. Ca²⁺/calmodulin-kinase II enhances channel conductance of alpha-amino-3-hydroxy-5-methyl-4-isoxazolepropionate type glutamate receptors. *Proc Natl Acad Sci U S A.* 96:3269-74.
- Dong, H., R.J. O'Brien, E.T. Fung, A.A. Lanahan, P.F. Worley, and R.L. Huganir. 1997. GRIP: a synaptic PDZ domain-containing protein that interacts with AMPA receptors. *Nature.* 386:279-84.
- Durand, G.M., Y. Kovalchuk, and A. Konnerth. 1996. Long-term potentiation and functional synapse induction in developing hippocampus. *Nature.* 381:71-5.
- Eccles, J.C., and W. Rall. 1950. Post-tetanic potentiation of responses of motoneurons. *Nature.* 166:465-6.
- Ehlers, M.D. 2000. Reinsertion or degradation of AMPA receptors determined by activity-dependent endocytic sorting. *Neuron.* 28:511-25.
- El-Husseini, A.E., E. Schnell, D.M. Chetkovich, R.A. Nicoll, and D.S. Brecht. 2000a. PSD-95 involvement in maturation of excitatory synapses. *Science.* 290:1364-8.
- El-Husseini, A.E., E. Schnell, D.M. Chetkovich, R.A. Nicoll, and D.S. Brecht. 2000b. PSD-95 involvement in maturation of excitatory synapses. *In Science.* Vol. 290. 1364-1368.

- Erreger, K., P.E. Chen, D.J. Wyllie, and S.F. Traynelis. 2004. Glutamate receptor gating. *Crit Rev Neurobiol.* 16:187-224.
- Ferrer-Montiel, A.V., and M. Montal. 1996. Pentameric subunit stoichiometry of a neuronal glutamate receptor. *Proc Natl Acad Sci U S A.* 93:2741-4.
- Forrest, D., M. Yuzaki, H.D. Soares, L. Ng, D.C. Luk, M. Sheng, C.L. Stewart, J.I. Morgan, J.A. Connor, and T. Curran. 1994. Targeted disruption of NMDA receptor 1 gene abolishes NMDA response and results in neonatal death. *Neuron.* 13:325-38.
- Fukaya, M., A. Kato, C. Lovett, S. Tonegawa, and M. Watanabe. 2003. Retention of NMDA receptor NR2 subunits in the lumen of endoplasmic reticulum in targeted NR1 knockout mice. *Proc Natl Acad Sci U S A.* 100:4855-60.
- Funk, G.D., S.M. Johnson, J.C. Smith, X.W. Dong, J. Lai, and J.L. Feldman. 1997. Functional respiratory rhythm generating networks in neonatal mice lacking NMDAR1 gene. *J Neurophysiol.* 78:1414-20.
- Funke, L., S. Dakoji, and D.S. Bredt. 2005. Membrane-associated guanylate kinases regulate adhesion and plasticity at cell junctions. *In Annu Rev Biochem.* Vol. 74. 219-245.
- Gardner, S.M., K. Takamiya, J. Xia, J.G. Suh, R. Johnson, S. Yu, and R.L. Huganir. 2005. Calcium-permeable AMPA receptor plasticity is mediated by subunit-specific interactions with PICK1 and NSF. *Neuron.* 45:903-15.
- Geiger, J.R., T. Melcher, D.S. Koh, B. Sakmann, P.H. Seeburg, P. Jonas, and H. Monyer. 1995. Relative abundance of subunit mRNAs determines gating and Ca²⁺

- permeability of AMPA receptors in principal neurons and interneurons in rat CNS. *Neuron*. 15:193-204.
- Ghosh, A., D.D. Ginty, H. Bading, and M.E. Greenberg. 1994. Calcium regulation of gene expression in neuronal cells. *J Neurobiol*. 25:294-303.
- Goda, Y., and G.W. Davis. 2003. Mechanisms of synapse assembly and disassembly. *Neuron*. 40:243-64.
- Goebbels, S., I. Bormuth, U. Bode, O. Hermanson, M.H. Schwab, and K.A. Nave. 2006. Genetic targeting of principal neurons in neocortex and hippocampus of NEX-Cre mice. *Genesis*. 44:611-21.
- Goff, D.C., L. Leahy, I. Berman, T. Posever, L. Herz, A.C. Leon, S.A. Johnson, and G. Lynch. 2001. A placebo-controlled pilot study of the ampakine CX516 added to clozapine in schizophrenia. *J Clin Psychopharmacol*. 21:484-7.
- Gomperts, S.N., R. Carroll, R.C. Malenka, and R.A. Nicoll. 2000. Distinct roles for ionotropic and metabotropic glutamate receptors in the maturation of excitatory synapses. *J Neurosci*. 20:2229-37.
- Gouaux, E. 2004. Structure and function of AMPA receptors. *J Physiol*. 554:249-53.
- Grunfeld, C. 1984. Antibody against the insulin receptor causes disappearance of insulin receptors in 3T3-L1 cells: a possible explanation of antibody-induced insulin resistance. *Proc Natl Acad Sci U S A*. 81:2508-11.
- Hahm, J.O., R.B. Langdon, and M. Sur. 1991. Disruption of retinogeniculate afferent segregation by antagonists to NMDA receptors. *Nature*. 351:568-70.

- Hashimoto, K., M. Fukaya, X. Qiao, K. Sakimura, M. Watanabe, and M. Kano. 1999. Impairment of AMPA receptor function in cerebellar granule cells of ataxic mutant mouse stargazer. *J Neurosci.* 19:6027-36.
- Hayashi, Y., S.H. Shi, J.A. Esteban, A. Piccini, J.C. Poncer, and R. Malinow. 2000. Driving AMPA receptors into synapses by LTP and CaMKII: requirement for GluR1 and PDZ domain interaction. *Science.* 287:2262-7.
- Hollmann, M., J. Boulter, C. Maron, and S. Heinemann. 1994. Molecular biology of glutamate receptors. Potentiation of N-methyl-D-aspartate receptor splice variants by zinc. *Ren Physiol Biochem.* 17:182-3.
- Hollmann, M., A. O'Shea-Greenfield, S.W. Rogers, and S. Heinemann. 1989. Cloning by functional expression of a member of the glutamate receptor family. *Nature.* 342:643-8.
- Honore, T., S.N. Davies, J. Drejer, E.J. Fletcher, P. Jacobsen, D. Lodge, and F.E. Nielsen. 1988. Quinoxalinediones: potent competitive non-NMDA glutamate receptor antagonists. *Science.* 241:701-3.
- Hsia, A.Y., R.C. Malenka, and R.A. Nicoll. 1998. Development of excitatory circuitry in the hippocampus. *J Neurophysiol.* 79:2013-24.
- Isaac, J.T., R.A. Nicoll, and R.C. Malenka. 1995. Evidence for silent synapses: implications for the expression of LTP. *Neuron.* 15:427-34.
- Ito, I., S. Tanabe, A. Kohda, and H. Sugiyama. 1990. Allosteric potentiation of quisqualate receptors by a nootropic drug aniracetam. *J Physiol.* 424:533-43.

- Iwasato, T., A. Datwani, A.M. Wolf, H. Nishiyama, Y. Taguchi, S. Tonegawa, T. Knopfel, R.S. Erzurumlu, and S. Itohara. 2000. Cortex-restricted disruption of NMDAR1 impairs neuronal patterns in the barrel cortex. *Nature*. 406:726-31.
- Jahr, C.E., and C.F. Stevens. 1987. Glutamate activates multiple single channel conductances in hippocampal neurons. *Nature*. 325:522-5.
- Jia, Z., N. Agopyan, P. Miu, Z. Xiong, J. Henderson, R. Gerlai, F.A. Taverna, A. Velumian, J. MacDonald, P. Carlen, W. Abramow-Newerly, and J. Roder. 1996. Enhanced LTP in mice deficient in the AMPA receptor GluR2. *Neuron*. 17:945-56.
- Jin, R., T.G. Banke, M.L. Mayer, S.F. Traynelis, and E. Gouaux. 2003. Structural basis for partial agonist action at ionotropic glutamate receptors. *Nat Neurosci*. 6:803-10.
- Jonas, P. 2000. The Time Course of Signaling at Central Glutamatergic Synapses. *News Physiol Sci*. 15:83-89.
- Jonas, P., and B. Sakmann. 1992. Glutamate receptor channels in isolated patches from CA1 and CA3 pyramidal cells of rat hippocampal slices. *J Physiol*. 455:143-71.
- Kalachikov, S., O. Evgrafov, B. Ross, M. Winawer, C. Barker-Cummings, F. Martinelli Boneschi, C. Choi, P. Morozov, K. Das, E. Teplitskaya, A. Yu, E. Cayanis, G. Penchaszadeh, A.H. Kottmann, T.A. Pedley, W.A. Hauser, R. Ottman, and T.C. Gilliam. 2002a. Mutations in LGI1 cause autosomal-dominant partial epilepsy with auditory features. *Nat Genet*. 30:335-41.
- Kalachikov, S., O. Evgrafov, B. Ross, M. Winawer, C. Barker-Cummings, F. Martinelli Boneschi, C. Choi, P. Morozov, K. Das, E. Teplitskaya, A. Yu, E. Cayanis, G.

- Penchaszadeh, A.H. Kottmann, T.A. Pedley, W.A. Hauser, R. Ottman, and T.C. Gilliam. 2002b. Mutations in LGI1 cause autosomal-dominant partial epilepsy with auditory features. *In Nat Genet.* Vol. 30. 335-341.
- Katz, L.C., and C.J. Shatz. 1996. Synaptic activity and the construction of cortical circuits. *Science.* 274:1133-8.
- Kauer, J.A., R.C. Malenka, and R.A. Nicoll. 1988. A persistent postsynaptic modification mediates long-term potentiation in the hippocampus. *Neuron.* 1:911-7.
- Kennedy, M.B. 2000. Signal-processing machines at the postsynaptic density. *In Science.* Vol. 290. 750-754.
- Kim, E., and M. Sheng. 2004. PDZ domain proteins of synapses. *In Nat Rev Neurosci.* Vol. 5. 771-781.
- Kleckner, N.W., and R. Dingledine. 1989. Selectivity of quinoxalines and kynurenes as antagonists of the glycine site on N-methyl-D-aspartate receptors. *Mol Pharmacol.* 36:430-6.
- Koh, J.Y., M.P. Goldberg, D.M. Hartley, and D.W. Choi. 1990. Non-NMDA receptor-mediated neurotoxicity in cortical culture. *J Neurosci.* 10:693-705.
- Kornau, H.C., L.T. Schenker, M.B. Kennedy, and P.H. Seeburg. 1995. Domain interaction between NMDA receptor subunits and the postsynaptic density protein PSD-95. *Science.* 269:1737-40.
- Lee, H.K., M. Barbarosie, K. Kameyama, M.F. Bear, and R.L. Huganir. 2000. Regulation of distinct AMPA receptor phosphorylation sites during bidirectional synaptic plasticity. *Nature.* 405:955-9.

- Lee, L.J., T. Iwasato, S. Itohara, and R.S. Erzurumlu. 2005. Exuberant thalamocortical axon arborization in cortex-specific NMDAR1 knockout mice. *J Comp Neurol.* 485:280-92.
- Leonard, A.S., M.A. Davare, M.C. Horne, C.C. Garner, and J.W. Hell. 1998. SAP97 is associated with the alpha-amino-3-hydroxy-5-methylisoxazole-4-propionic acid receptor GluR1 subunit. *J Biol Chem.* 273:19518-24.
- Lerma, J. 2006. Kainate receptor physiology. *Curr Opin Pharmacol.* 6:89-97.
- Letts, V.A., R. Felix, G.H. Biddlecome, J. Arikath, C.L. Mahaffey, A. Valenzuela, F.S. Bartlett, 2nd, Y. Mori, K.P. Campbell, and W.N. Frankel. 1998a. The mouse stargazer gene encodes a neuronal Ca²⁺-channel gamma subunit. *In Nat Genet.* Vol. 19. 340-347.
- Letts, V.A., R. Felix, G.H. Biddlecome, J. Arikath, C.L. Mahaffey, A. Valenzuela, F.S. Bartlett, 2nd, Y. Mori, K.P. Campbell, and W.N. Frankel. 1998b. The mouse stargazer gene encodes a neuronal Ca²⁺-channel gamma subunit. *Nature Genetics.* 19:340-7.
- Li, Y., R.S. Erzurumlu, C. Chen, S. Jhaveri, and S. Tonegawa. 1994. Whisker-related neuronal patterns fail to develop in the trigeminal brainstem nuclei of NMDAR1 knockout mice. *Cell.* 76:427-37.
- Liao, D., N.A. Hessler, and R. Malinow. 1995. Activation of postsynaptically silent synapses during pairing-induced LTP in CA1 region of hippocampal slice. *Nature.* 375:400-4.

- Liao, D., X. Zhang, R. O'Brien, M.D. Ehlers, and R.L. Huganir. 1999. Regulation of morphological postsynaptic silent synapses in developing hippocampal neurons. *Nat Neurosci.* 2:37-43.
- Liu, S.Q., and S.G. Cull-Candy. 2000. Synaptic activity at calcium-permeable AMPA receptors induces a switch in receptor subtype. *Nature.* 405:454-8.
- Lledo, P.M., X. Zhang, T.C. Sudhof, R.C. Malenka, and R.A. Nicoll. 1998. Postsynaptic membrane fusion and long-term potentiation. *Science.* 279:399-403.
- Lomeli, H., J. Mosbacher, T. Melcher, T. Hoyer, J.R. Geiger, T. Kuner, H. Monyer, M. Higuchi, A. Bach, and P.H. Seeburg. 1994. Control of kinetic properties of AMPA receptor channels by nuclear RNA editing. *Science.* 266:1709-13.
- Luscher, C., H. Xia, E.C. Beattie, R.C. Carroll, M. von Zastrow, R.C. Malenka, and R.A. Nicoll. 1999. Role of AMPA receptor cycling in synaptic transmission and plasticity. *Neuron.* 24:649-58.
- Luthi, A., R. Chittajallu, F. Duprat, M.J. Palmer, T.A. Benke, F.L. Kidd, J.M. Henley, J.T. Isaac, and G.L. Collingridge. 1999. Hippocampal LTD expression involves a pool of AMPARs regulated by the NSF-GluR2 interaction. *Neuron.* 24:389-99.
- Luthi, A., L. Schwyzer, J.M. Mateos, B.H. Gähwiler, and R.A. McKinney. 2001. NMDA receptor activation limits the number of synaptic connections during hippocampal development. *Nat Neurosci.* 4:1102-7.
- Lynch, G., R. Granger, J. Ambros-Ingerson, C.M. Davis, M. Kessler, and R. Schehr. 1997. Evidence that a positive modulator of AMPA-type glutamate receptors improves delayed recall in aged humans. *Exp Neurol.* 145:89-92.

- Magee, J.C., and D. Johnston. 1997. A synaptically controlled, associative signal for Hebbian plasticity in hippocampal neurons. *Science*. 275:209-13.
- Malenka, R.C., B. Lancaster, R.S. Zucker. 1992. Temporal limits on the rise in postsynaptic calcium required for the induction of long-term potentiation. *Neuron*. 1:121-128.
- Malenka, R.C., and R.A. Nicoll. 1999. Long-term potentiation--a decade of progress? *Science*. 285:1870-4.
- Malinow, R., and R.C. Malenka. 2002. AMPA receptor trafficking and synaptic plasticity. *Annu Rev Neurosci*. 25:103-26.
- Malinow, R., and R.W. Tsien. 1990. Presynaptic enhancement shown by whole-cell recordings of long-term potentiation in hippocampal slices. *Nature*. 346:177-80.
- Mansour, M., N. Nagarajan, R.B. Nehring, J.D. Clements, and C. Rosenmund. 2001. Heteromeric AMPA receptors assemble with a preferred subunit stoichiometry and spatial arrangement. *Neuron*. 32:841-53.
- Matsuzaki, M., N. Honkura, G.C. Ellis-Davies, and H. Kasai. 2004. Structural basis of long-term potentiation in single dendritic spines. *Nature*. 429:761-6.
- Matthies., H., P.T., Brackley, P.N. Usherwood, K.G. Reymann. 1992. Philanthotoxin-343 blocks long-term potentiation in the hippocampus. *Neuroreport*. 3:649-652
- Mayer, M.L., G.L. Westbrook, and P.B. Guthrie. 1984. Voltage-dependent block by Mg²⁺ of NMDA responses in spinal cord neurones. *Nature*. 309:261-3.
- Migaud, M., P. Charlesworth, M. Dempster, L.C. Webster, A.M. Watabe, M. Makhinson, Y. He, M.F. Ramsay, R.G. Morris, J.H. Morrison, T.J. O'Dell, and S.G. Grant.

1998. Enhanced long-term potentiation and impaired learning in mice with mutant postsynaptic density-95 protein. *In Nature*. Vol. 396. 433-439.
- Mitchell, K.J., K.I. Pinson, O.G. Kelly, J. Brennan, J. Zupicich, P. Scherz, P.A. Leighton, L.V. Goodrich, X. Lu, B.J. Avery, P. Tate, K. Dill, E. Pangilinan, P. Wakenight, M. Tessier-Lavigne, and W.C. Skarnes. 2001. Functional analysis of secreted and transmembrane proteins critical to mouse development. *In Nat Genet*. Vol. 28. 241-249.
- Monory, K., F. Massa, M. Egertova, M. Eder, H. Blaudzun, R. Westenbroek, W. Kelsch, W. Jacob, R. Marsch, M. Ekker, J. Long, J.L. Rubenstein, S. Goebbels, K.A. Nave, M. Doring, M. Klugmann, B. Wolfel, H.U. Dodt, W. Zieglgansberger, C.T. Wotjak, K. Mackie, M.R. Elphick, G. Marsicano, and B. Lutz. 2006. The endocannabinoid system controls key epileptogenic circuits in the hippocampus. *Neuron*. 51:455-66.
- Morante-Redolat, J.M., A. Gorostidi-Pagola, S. Piquer-Sirerol, A. Saenz, J.J. Poza, J. Galan, S. Gesk, T. Sarafidou, V.F. Mautner, S. Binelli, E. Staub, B. Hinzmann, L. French, J.F. Prud'homme, D. Passarelli, P. Scannapieco, C.A. Tassinari, G. Avanzini, J.F. Marti-Masso, L. Kluwe, P. Deloukas, N.K. Moschonas, R. Michelucci, R. Siebert, C. Nobile, J. Perez-Tur, and A. Lopez de Munain. 2002. Mutations in the LGI1/Epitempin gene on 10q24 cause autosomal dominant lateral temporal epilepsy. *In Hum Mol Genet*. Vol. 11. 1119-1128.
- Nakanishi, S. 1992. Molecular diversity of glutamate receptors and implications for brain function. *Science*. 258:597-603.

- Nicoll, R.A., and R.C. Malenka. 1999. Expression mechanisms underlying NMDA receptor-dependent long-term potentiation. *Ann N Y Acad Sci.* 868:515-25.
- Nicoll, R.A., S. Tomita, and D.S. Bredt. 2006. Auxiliary subunits assist AMPA-type glutamate receptors. *In Science.* Vol. 311. 1253-1256.
- Novak, U. 2004. ADAM proteins in the brain. *In J. Clin. Neurosci.* Vol. 11. 227-235.
- O'Brien, R.J., D. Xu, R.S. Petralia, O. Steward, R.L. Huganir, and P. Worley. 1999. Synaptic clustering of AMPA receptors by the extracellular immediate-early gene product *Narp*. *Neuron.* 23:309-23.
- O'Neill, M.J., T.K. Murray, K. Whalley, M.A. Ward, C.A. Hicks, S. Woodhouse, D.J. Osborne, and P. Skolnick. 2004. Neurotrophic actions of the novel AMPA receptor potentiator, LY404187, in rodent models of Parkinson's disease. *Eur J Pharmacol.* 486:163-74.
- Osten, P., and E.B. Ziff. 1999. AMPA receptor forms a biochemically functional complex with NSF and alpha- and beta-SNAPs. *Ann N Y Acad Sci.* 868:558-60.
- Park, M., E.C. Penick, J.G. Edwards, J.A. Kauer, and M.D. Ehlers. 2004. Recycling endosomes supply AMPA receptors for LTP. *Science.* 305:1972-5.
- Passafaro, M., V. Piech, and M. Sheng. 2001. Subunit-specific temporal and spatial patterns of AMPA receptor exocytosis in hippocampal neurons. *Nat Neurosci.* 4:917-26.
- Perkel, D.J., R.A. Nicoll. 1993. Evidence for all-or-none neurotransmitter release: implications for long-term potentiation. *J Physiology.* 471:481-500.
- Petersen, C.C., R.C. Malenka, R.A. Nicoll, and J.J. Hopfield. 1998. All-or-none potentiation at CA3-CA1 synapses. *Proc Natl Acad Sci U S A.* 95:4732-7.

- Planells-Cases, R., W. Sun, A.V. Ferrer-Montiel, and M. Montal. 1993. Molecular cloning, functional expression, and pharmacological characterization of an N-methyl-D-aspartate receptor subunit from human brain. *Proc Natl Acad Sci U S A*. 90:5057-61.
- Plant, K., K.A. Pelkey, Z.A. Bortolotto, D. Morita, A. Terashima, C.J. McBain, G.L. Collingridge, and J.T. Isaac. 2006. Transient incorporation of native GluR2-lacking AMPA receptors during hippocampal long-term potentiation. *Nat Neurosci*. 9:602-4.
- Robert, A., and J.R. Howe. 2003. How AMPA receptor desensitization depends on receptor occupancy. *J Neurosci*. 23:847-58.
- Rocha, M., and M. Sur. 1995. Rapid acquisition of dendritic spines by visual thalamic neurons after blockade of N-methyl-D-aspartate receptors. *Proc Natl Acad Sci U S A*. 92:8026-30.
- Rosenmund, C., Y. Stern-Bach, and C.F. Stevens. 1998. The tetrameric structure of a glutamate receptor channel. *Science*. 280:1596-9.
- Rosenmund, C., and C.F. Stevens. 1996. Definition of the readily releasable pool of vesicles at hippocampal synapses. *Neuron*. 16:1197-207.
- Rouach, N., K. Byrd, R.S. Petralia, G.M. Elias, H. Adesnik, S. Tomita, S. Karimzadegan, C. Kealey, D.S. Brecht, and R.A. Nicoll. 2005. TARP gamma-8 controls hippocampal AMPA receptor number, distribution and synaptic plasticity. *Nat Neurosci*. 8:1525-33.

- Sagane, K., K. Hayakawa, J. Kai, T. Hirohashi, E. Takahashi, N. Miyamoto, M. Ino, T. Oki, K. Yamazaki, and T. Nagasu. 2005a. Ataxia and peripheral nerve hypomyelination in ADAM22-deficient mice. *In BMC Neurosci.* Vol. 6. 33.
- Sagane, K., K. Hayakawa, J. Kai, T. Hirohashi, E. Takahashi, N. Miyamoto, M. Ino, T. Oki, K. Yamazaki, and T. Nagasu. 2005b. Ataxia and peripheral nerve hypomyelination in ADAM22-deficient mice. *BMC Neurosci.* 6:33.
- Sanes, J.R., and J.W. Lichtman. 1999. Development of the vertebrate neuromuscular junction. *Annu Rev Neurosci.* 22:389-442.
- Scanziani, M., R.C. Malenka, R.A. Nicoll. 1996. Role of intercellular interactions in heterosynaptic long-term depression. *Nature.* 380:446-450.
- Scheel, H., S. Tomiuk, and K. Hofmann. 2002. A common protein interaction domain links two recently identified epilepsy genes. *In Hum Mol Genet.* Vol. 11. 1757-1762.
- Schnell, E., M. Sizemore, S. Karimzadegan, L. Chen, D.S. Bredt, and R.A. Nicoll. 2002a. Direct interactions between PSD-95 and stargazin control synaptic AMPA receptor number. *In Proc Natl Acad Sci U S A.* Vol. 99. 13902-13907.
- Schnell, E., M. Sizemore, S. Karimzadegan, L. Chen, D.S. Bredt, and R.A. Nicoll. 2002b. Direct interactions between PSD-95 and stargazin control synaptic AMPA receptor number. *Proc Natl Acad Sci U S A.* 99:13902-7.
- Schulte, U., J.O. Thumfart, N. Klocker, C.A. Sailer, W. Bildl, M. Biniossek, D. Dehn, T. Deller, S. Eble, K. Abbass, T. Wangler, H.G. Knaus, and B. Fakler. 2006a. The epilepsy-linked lgi1 protein assembles into presynaptic kv1 channels and inhibits inactivation by kvbeta1. *In Neuron.* Vol. 49. 697-706.

- Schulte, U., J.O. Thumfart, N. Klocker, C.A. Sailer, W. Bildl, M. Biniössek, D. Dehn, T. Deller, S. Eble, K. Abbass, T. Wangler, H.G. Knaus, and B. Fakler. 2006b. The epilepsy-linked Lgi1 protein assembles into presynaptic Kv1 channels and inhibits inactivation by Kvbeta1. *Neuron*. 49:697-706.
- Sekine-Aizawa, Y., and R.L. Huganir. 2004. Imaging of receptor trafficking by using alpha-bungarotoxin-binding-site-tagged receptors. *Proc Natl Acad Sci U S A*. 101:17114-9.
- Senechal, K.R., C. Thaller, and J.L. Noebels. 2005a. ADPEAF mutations reduce levels of secreted LGI1, a putative tumor suppressor protein linked to epilepsy. *In Hum Mol Genet*. Vol. 14. 1613-1620.
- Senechal, K.R., C. Thaller, and J.L. Noebels. 2005b. ADPEAF mutations reduce levels of secreted LGI1, a putative tumor suppressor protein linked to epilepsy. *Hum Mol Genet*. 14:1613-20.
- Sheng, M., and M.J. Kim. 2002. Postsynaptic signaling and plasticity mechanisms. *Science*. 298:776-80.
- Shi, S.H., Y. Hayashi, R.S. Petralia, S.H. Zaman, R.J. Wenthold, K. Svoboda, and R. Malinow. 1999. Rapid spine delivery and redistribution of AMPA receptors after synaptic NMDA receptor activation. *Science*. 284:1811-6.
- Singer, M.A., and L. Finegold. 1990. Interaction of cholesterol with saturated phospholipids: role of the C(17) side chain. *Chem Phys Lipids*. 56:217-22.
- Sirerol-Piquer, M.S., A. Ayerdi-Izquierdo, J.M. Morante-Redolat, V. Herranz-Perez, K. Favell, P.A. Barker, and J. Perez-Tur. 2006. The epilepsy gene LGI1 encodes a secreted glycoprotein that binds to the cell surface. *Hum Mol Genet*. 15:3436-45.

- Skradski, S.L., A.M. Clark, H. Jiang, H.S. White, Y.H. Fu, and L.J. Ptacek. 2001. A novel gene causing a mendelian audiogenic mouse epilepsy. *In Neuron*. Vol. 31. 537-544.
- Smith, T.C., L.Y. Wang, and J.R. Howe. 2000. Heterogeneous conductance levels of native AMPA receptors. *J Neurosci*. 20:2073-85.
- Sommer, B., K. Keinanen, T.A. Verdoorn, W. Wisden, N. Burnashev, A. Herb, M. Kohler, T. Takagi, B. Sakmann, and P.H. Seeburg. 1990. Flip and flop: a cell-specific functional switch in glutamate-operated channels of the CNS. *Science*. 249:1580-5.
- Song, I., and R.L. Huganir. 2002. Regulation of AMPA receptors during synaptic plasticity. *Trends Neurosci*. 25:578-88.
- Srivastava, S., P. Osten, F.S. Vilim, L. Khatri, G. Inman, B. States, C. Daly, S. DeSouza, R. Abagyan, J.G. Valtschanoff, R.J. Weinberg, and E.B. Ziff. 1998. Novel anchorage of GluR2/3 to the postsynaptic density by the AMPA receptor-binding protein ABP. *Neuron*. 21:581-91.
- Staub, E., J. Perez-Tur, R. Siebert, C. Nobile, N.K. Moschonas, P. Deloukas, and B. Hinemann. 2002. The novel EPTP repeat defines a superfamily of proteins implicated in epileptic disorders. *In Trends Biochem Sci*. Vol. 27. 441-444.
- Staubli, U., G. Rogers, and G. Lynch. 1994. Facilitation of glutamate receptors enhances memory. *Proc Natl Acad Sci U S A*. 91:777-81.
- Steinlein, O.K. 2004. Genetic mechanisms that underlie epilepsy. *In Nat Rev Neurosci*. Vol. 5. 400-408.

- Swanson, G.T., S.K. Kamboj, and S.G. Cull-Candy. 1997. Single-channel properties of recombinant AMPA receptors depend on RNA editing, splice variation, and subunit composition. *J Neurosci.* 17:58-69.
- Takahashi, T., K. Svoboda, and R. Malinow. 2003. Experience strengthening transmission by driving AMPA receptors into synapses. *Science.* 299:1585-8.
- Tardin, C., L. Cognet, C. Bats, B. Lounis, and D. Choquet. 2003. Direct imaging of lateral movements of AMPA receptors inside synapses. *Embo J.* 22:4656-65.
- Thomas, P., M. Mortensen, A.M. Hosie, and T.G. Smart. 2005. Dynamic mobility of functional GABAA receptors at inhibitory synapses. *Nat Neurosci.* 8:889-97.
- Tomita, S., H. Adesnik, M. Sekiguchi, W. Zhang, K. Wada, J.R. Howe, R.A. Nicoll, and D.S. Brecht. 2005. Stargazin modulates AMPA receptor gating and trafficking by distinct domains. *In Nature.* Vol. 435. 1052-1058.
- Tomita, S., L. Chen, Y. Kawasaki, R.S. Petralia, R.J. Wenthold, R.A. Nicoll, and D.S. Brecht. 2003. Functional studies and distribution define a family of transmembrane AMPA receptor regulatory proteins. *J Cell Biol.* 161:805-16.
- Tomita, S., M. Fukata, R.A. Nicoll, and D.S. Brecht. 2004. Dynamic interaction of stargazin-like TARPs with cycling AMPA receptors at synapses. *Science.* 303:1508-11.
- Tovar, K.R., and G.L. Westbrook. 2002. Mobile NMDA receptors at hippocampal synapses. *Neuron.* 34:255-64.
- Trachtenberg, J.T., B.E. Chen, G.W. Knott, G. Feng, J.R. Sanes, E. Welker, and K. Svoboda. 2002. Long-term in vivo imaging of experience-dependent synaptic plasticity in adult cortex. *Nature.* 420:788-94.

- Tsien, J.Z., P.T. Huerta, and S. Tonegawa. 1996. The essential role of hippocampal CA1 NMDA receptor-dependent synaptic plasticity in spatial memory. *Cell*. 87:1327-38.
- Verdoorn, T.A., N. Burnashev, H. Monyer, P.H. Seeburg, and B. Sakmann. 1991. Structural determinants of ion flow through recombinant glutamate receptor channels. *Science*. 252:1715-8.
- Verhage, M., A.S. Maia, J.J. Plomp, A.B. Brussaard, J.H. Heeroma, H. Vermeer, R.F. Toonen, R.E. Hammer, T.K. van den Berg, M. Missler, H.J. Geuze, and T.C. Sudhof. 2000. Synaptic assembly of the brain in the absence of neurotransmitter secretion. *Science*. 287:864-9.
- Watkins, J.C., and D.E. Jane. 2006. The glutamate story. *Br J Pharmacol*. 147 Suppl 1:S100-8.
- Weissman, A.M., R.D. Klausner, K. Rao, and J.B. Harford. 1986. Exposure of K562 cells to anti-receptor monoclonal antibody OKT9 results in rapid redistribution and enhanced degradation of the transferrin receptor. *J Cell Biol*. 102:951-8.
- Wentholt, R.J., R.S. Petralia, J. Blahos, II, and A.S. Niedzielski. 1996. Evidence for multiple AMPA receptor complexes in hippocampal CA1/CA2 neurons. *J Neurosci*. 16:1982-9.
- Wyllie, D.J., S.F. Traynelis, and S.G. Cull-Candy. 1993. Evidence for more than one type of non-NMDA receptor in outside-out patches from cerebellar granule cells of the rat. *J Physiol*. 463:193-226.
- Xia, J., X. Zhang, J. Staudinger, and R.L. Huganir. 1999. Clustering of AMPA receptors by the synaptic PDZ domain-containing protein PICK1. *Neuron*. 22:179-87.

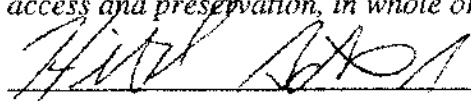
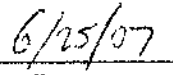
- Yagi, H., Y. Takamura, T. Yoneda, D. Konno, Y. Akagi, K. Yoshida, and M. Sato. 2005. Vlg1 knockout mice show audiogenic seizure susceptibility. *In J Neurochem.* Vol. 92. 191-202.
- Yamazaki, M., T. Ohno-Shosaku, M. Fukaya, M. Kano, M. Watanabe, and K. Sakimura. 2004. A novel action of stargazin as an enhancer of AMPA receptor activity. *Neurosci Res.* 50:369-74.
- Zamanillo, D., R. Sprengel, O. Hvalby, V. Jensen, N. Burnashev, A. Rozov, K.M. Kaiser, H.J. Koster, T. Borchardt, P. Worley, J. Lubke, M. Frotscher, P.H. Kelly, B. Sommer, P. Andersen, P.H. Seeburg, and B. Sakmann. 1999. Importance of AMPA receptors for hippocampal synaptic plasticity but not for spatial learning. *Science.* 284:1805-11.
- Zerangue, N., B. Schwappach, Y.N. Jan, and L.Y. Jan. 1999. A new ER trafficking signal regulates the subunit stoichiometry of plasma membrane K(ATP) channels. *Neuron.* 22:537-48.
- Zheng, Y., J.E. Mellem, P.J. Brockie, D.M. Madsen, and A.V. Maricq. 2004. SOL-1 is a CUB-domain protein required for GLR-1 glutamate receptor function in *C. elegans*. *Nature.* 427:451-7.
- Zhou, Q., K.J. Homma, and M.M. Poo. 2004. Shrinkage of dendritic spines associated with long-term depression of hippocampal synapses. *Neuron.* 44:749-57.
- Zhu, J.J., and R. Malinow. 2002. Acute versus chronic NMDA receptor blockade and synaptic AMPA receptor delivery. *Nat Neurosci.* 5:513-4.

Publishing Agreement

It is the policy of the University to encourage the distribution of all theses and dissertations. Copies of all UCSF theses and dissertations will be routed to the library via the Graduate Division. The library will make all theses and dissertations accessible to the public and will preserve these to the best of their abilities, in perpetuity.

Please sign the following statement:

I hereby grant permission to the Graduate Division of the University of California, San Francisco to release copies of my thesis or dissertation to the Campus Library to provide access and preservation, in whole or in part, in perpetuity.

Author Signature Date